Aus der Klinik für Neurologie mit Experimenteller Neurologie
der Medizinischen Fakultät Charité – Universitätsmedizin Berlin

DISSERTATION

"Metabolic and behavioral characterization of the APP23 mouse model of Alzheimer's disease with regard to early therapeutic lifestyle interventions"

zur Erlangung des akademischen Grades
Doctor of Philosophy (PhD)

vorgelegt der Medizinischen Fakultät
Charité – Universitätsmedizin Berlin

von

Stefanie Schreyer, geb. Beier

Datum der Promotion: 04.03.2022

Table of Content

List of Abbreviations

1 W	Adolescent mice, spending one week in cage condition (study III)
12 W	Young-adult mice, spending twelve weeks in cage condition (study III)
24 W	Adult mice, spending 24 weeks in cage condition (study III)
Aβ	Amyloid β protein
AD	Alzheimer's disease
ADV	Advanced plaque stage (study II)
APP	Amyloid precursor protein
APP23 mice	Transgenic APP23 mice
BPSD	Behavioral and psychological symptoms of dementia
BrdU	5-Bromo-2´-deoxyuridine (study II+III)
CD/NCD	Control diet (study II)/Normal-control diet (study I)
CD+Chia	Control diet supplemented with chia seeds (study II)
EE	Environmental enrichment (study III)
ELISA	Enzyme-linked immunosorbent assay
EPM	Elevated Plus Maze (study II)
eWAT	Epigonadal white adipose tissue
EZM	Elevated Zero Maze (study III)
HFD	High-fat diet (study I)
HSD/SRD	High-sucrose diet (study I)/sucrose-rich diet (study II)
i.p.	Intraperitoneal
ipGTT:	Intraperitoneal glucose tolerance test (study I+II)
LC-MS/MS	Liquid chromatography–mass spectrometry/mass spectrometry (study I)
MWM	Morris Water Maze (study II+III)
NEFA	Non-esterified fatty acids (study I)
ns.	Non-significant
PRE	Pre-plaque stage (study II)
RER	Respiratory exchange ratio (study I)
SRD+Chia	Sucrose-rich diet supplemented with chia seeds (study II)
STD	Standard environment (study III)
T2DM	Type 2 diabetes mellitus
WT mice	Wild type mice

Abstract (English)

The risk of developing Alzheimer's disease (AD) is increased in patients with type 2 diabetes mellitus. Both diseases share several common features, such as glucose intolerance and insulin resistance. As cerebral glucose hypometabolism already appears prior to Amyloid β (Aβ) plaque development, alterations in glucose metabolism are hypothesized to play a causal role during AD development. Moreover, weight loss is prevalently observed in AD patients, correlating with disease progression and mortality. As no curative therapy of AD exists, there is an urgent need of new therapeutic approaches. Lifestyle interventions, such as specific dietary regimens or physical activity, are subjects to numerous animal and clinical studies. However, underlying mechanisms of their beneficial effects often remain elusive. This thesis comprises three studies, investigating metabolic and behavioral features of a murine AD model with emphasis on the role of glucose metabolism in AD development and potential reasons for AD-related body weight changes. Moreover, the therapeutic potential of dietary supplementation with chia seeds as a modulator of glucose tolerance was examined as well as preventive and therapeutic effects of environmental enrichment (EE). APP23 mice, showing a genetically induced Aβ pathology, served as animal model. The present studies reveal that the lower body weight of APP23 mice compared to wild type (WT) mice results from hyperactivity, increased metabolic rate, and impaired energy balance, and already emerges long before plaque development. Proteome analyses additionally suggest an implication of altered mitochondrial function, going beyond the brain. Peripheral glucose tolerance was intact in younger APP23 mice. In contrast, aged APP23 mice were more vulnerable to diet-induced metabolic stress than WT mice, depicted by deteriorated glucose tolerance. APP23 mice displayed deficits in spatial learning and flexible memory prior to plaque pathology. Cognitive performance was improved by both chia supplementation and EE. The effect of chia seeds is suggested to result from a mild amelioration of glucose tolerance together with a mild reduction of corticosterone and proinflammatory cytokine levels. The effect of EE might have been mediated by enhanced adult hippocampal neurogenesis – the generation of new neurons to serve as an "neurogenic reserve" crucial for neuronal plasticity – and the promotion of microglia recruitment, which are involved in Aβ clearance. Bearing in mind rising incidences of both AD and type 2 diabetes mellitus, the basic research conducted during this thesis contributes to the urgently needed understanding of the metabolic component of AD and provides valuable approaches for further clinical research.

Abstract (German)

Das Risiko an der Alzheimer Krankheit (AD) zu erkranken, ist bei von Typ-2-Diabetes mellitus (T2DM) Betroffenen erhöht. Beide Krankheiten weisen gemeinsame Charakteristika wie Glukoseintoleranz und Insulinresistenz auf. Bereits vor der Bildung von β-Amyloid (Aβ) Plaques treten Veränderungen im Glukosestoffwechsel des Hirns auf. Daher könnten diese Veränderungen mitursächlich für AD sein. Bei AD-Erkrankten wird häufig ein Gewichtsverlust beobachtet, der mit dem Voranschreiten der Erkrankung und der Mortalität korreliert. Da AD bisher unheilbar ist, werden dringend neue therapeutische Ansätze benötigt. Lebensstilinterventionen wie bestimmte Ernährungsparadigmen oder ein aktiver Lebensstil sind Gegenstand zahlreicher tierexperimenteller und klinischer Studien. Häufig bleiben jedoch die zugrundeliegenden Mechanismen ihrer Auswirkungen ungeklärt. Diese Arbeit umfasst drei Studien, in denen Stoffwechsel- und Verhaltensmerkmale des APP23-Mausmodells für AD analysiert wurden, welches eine genetisch induzierte Aβ Pathologie aufweist. Dabei standen insbesondere die Rolle des Glukosestoffwechsels bei der Entwicklung von AD sowie mögliche Gründe für eine AD-bedingte Veränderung des Körpergewichts im Fokus. Zudem wurden das therapeutische Potenzial einer Nahrungsergänzung mit Chia-Samen, welche die Glukosetoleranz beeinflussen können, sowie einer reizreichen Umgebung untersucht. Die Ergebnisse zeigen, dass ein im Vergleich zum Wildtyp niedrigeres Körpergewicht der APP23-Mäuse auf Hyperaktivität, einer erhöhten Stoffwechselrate und einer dysfunktionalen Energie-Homöostase beruht und bereits lange vor der Plaque-Entwicklung auftritt. Proteom-Analysen deuten auf eine systemische Beeinträchtigung der Mitochondrien-Funktionalität hin. Während die periphere Glukosetoleranz bei jüngeren APP23-Mäusen intakt war, waren ältere APP23-Mäuse anfälliger für eine Verschlechterung der Glukosetoleranz aufgrund von metabolischem Stress als der Wildtyp. APP23-Mäuse wiesen bereits vor der Plaquebildung kognitive Defizite auf. Diese wurden sowohl durch die Gabe von Chia-Samen als auch durch eine reizreiche Umgebung verbessert. Der Effekt von Chia-Samen beruhte vermutlich auf der moderaten Verbesserung der Glukosetoleranz kombiniert mit der moderaten Senkung des Kortikosteron- und des proinflammatorischen Zytokinspiegels. Der Effekt einer reizreichen Umgebung wurde vermutlich durch eine Förderung der adulten hippokampalen Neurogenese, der im Rahmen von neuronaler Plastizität erforderlichen Bildung neuer Neurone, und der vermehrten Rekrutierung von Mikroglia zum Abbau von Aβ induziert. Angesichts der zunehmenden Inzidenz von AD und T2DM trägt die in dieser Arbeit durchgeführte Grundlagenforschung zum dringend erforderlichen Verständnis der Stoffwechselkomponente von AD bei und bietet wertvolle Ansätze für die weitere klinische Forschung.

1. Introduction

Globally, more than 50 million patients are affected by dementia, with Alzheimer's disease (AD) being the most prevalent cause (1). Due to demographic changes, the number of AD patients is increasing, causing substantial socio-economic costs (2,3). Proceeding dementia is a key symptom of AD, representing a severe burden for patients and their environment (2,4). As more than 100 years of research failed to decode the underlying mechanisms of AD, no curative therapies are available yet (5). Existing symptomatic treatment can only slow down AD progression, hence application at an early stage is crucial (3). However, early diagnosis of AD is challenging due to a lack of reliable disease markers (3). Therefore, basic research is of utmost importance to shed light on its causative mechanisms, to identify diagnostic markers and new targets for drug development.

AD is characterized by extracellular plaques of aggregated amyloid β (Aβ) protein, intracellular tangles of hyperphosphorylated tau, neuroinflammation, as well as progressive synaptic and neuronal loss (4). These neuropathological alterations cause progressive cognitive decline (4). Adult hippocampal neurogenesis, a process likely involved in the maintenance of structural neuronal plasticity (6), is differentially altered during AD progression (7). Evidence suggests that impaired neurogenesis might contribute to cognitive symptoms, whereas enhanced neurogenesis might reflect a compensatory mechanism to neuronal loss (7). In the majority of cases, AD is accompanied by a variety of symptoms such as agitation, aggressive behavior and depression – summarized under the term 'behavioral and psychological symptoms of dementia' (BPSD) (8). 30-40% of patients additionally suffer from advancing involuntary weight loss (9).

The amyloid cascade hypothesis, suggesting the accumulation of Aβ and its aggregation into plaques as the central mechanism of AD pathogenesis (10), has long been the main focus of AD research. Though, reducing Aβ burden has failed to significantly improve cognitive symptoms of AD in numerous clinical trials (11). Consequently, different pathogenic causes have been considered recently, such as implications of glucose metabolism. Alterations in cerebral glucose metabolism, namely reduced cerebral glucose tolerance and insulin sensitivity (12), already occur years before cognitive symptoms emerge (13). Those alterations are strikingly similar to type 2 diabetes mellitus (T2DM), a known risk factor of AD (14). Additionally, frequently observed changes of body weight might play a role in AD pathogenesis (15). This weight loss progresses with advancing AD stage and results in increased mortality rates (9). Interestingly, a low body weight in old age is suggested to predict AD onset (16). Contrary, obesity in midlife is also associated with an increased risk of developing AD (14), underlining the complexity of metabolic alterations and the importance of investigating their implication in AD development.

Lifestyle interventions might provide a useful tool in the prevention of AD and in therapeutic support (17). A healthy lifestyle, such as nutritional practices, physical and cognitive activity, reduces the risk of developing AD (18). Although numerous studies have addressed this issue, there is a lack of concise data revealing the underlying reasons. The influence of diet might be attributed to specific macro- or micronutrients, such as polyunsaturated fatty acids and antioxidants (19). Bearing in mind the risks of obesity and T2DM with regard to AD (14), the positive effect of nutrition might also be related to glucose metabolism. Chia seeds have been reported to positively influence obesity and T2DM by improving glucose tolerance and reducing adiposity (20,21). They also contain high amounts of polyunsaturated fatty acids (22), which are thought to exert beneficial effects on cognitive abilities (23). Physical activity as well as a stimulating environment and a social lifestyle, summarized under the term 'environmental enrichment', have been shown to reduce the risk of developing AD and to slow down disease progression (24,25). However, the underlying mechanisms remain elusive. It is suggested that this beneficial effect might arise from stimulation of adult hippocampal neurogenesis (26).

This thesis investigates the implications of glucose metabolism and energy balance in the pathogenesis of AD to elucidate its relevance in disease development. Moreover, lifestyle interventions are examined as potential preventive and therapeutic options. In this context, three studies were conducted in the murine APP23 disease model. Transgenic APP23 mice overexpress the amyloid precursor protein (APP), resulting in an AD-like plaque pathology in the brain accompanied by cognitive impairment. The objective of study I was the metabolic phenotyping of APP23 mice to explore potential reasons for their lower body weight compared to wild type littermates, which matches the lower body weight frequently observed in AD patients. Mice were additionally challenged with obesogenic diets, rich in sucrose or fat, to investigate the impact of different fuel sources and metabolic stress. The aim of study II was the investigation of the causal relationship between glucose metabolism and AD development. Here, mice were metabolically stressed with a sucrose-rich diet and behavioral and cognitive performance were evaluated. Furthermore, the therapeutic potential of chia seeds as a promising modulator of glucose metabolism was investigated with regard to metabolic and cognitive features. Study III focussed on alterations of adult hippocampal neurogenesis as a potential neuropathological correlate to cognitive decline. Moreover, the occurrence of BPSD in pre-plaque APP23 mice was examined with regard to a potential use as early diagnostic marker. At last, the preventive potential of environmental enrichment as a stimulator of adult hippocampal neurogenesis was analyzed.

2. Methods

2.1. Animals

All experiments conducted in living animals were approved by the Landesamt für Gesundheit und Soziales, Berlin (Germany) and were executed in agreement with the European Council Directive of 22 September 2010 (10/63/EU) as well as with ARRIVE guidelines (27).

In all studies, female transgenic APP23 mice, bred on a C57BL6/J background, and female age-matched wild type littermates (study I and II) or non-transgenic C57BL6/J mice (study III) were used (WT mice). Genotyping was performed by PCR of ear punches using primers against human APP. In APP23 mice, the human APP_{751} transgene containing the Swedish double mutation is overexpressed in brain tissue under the Thy-1 promotor, leading to a deposition of Aβ plaques starting around six months of age (28). Mice were group-housed in a temperature- and humidity-controlled animal facility with a 12 h light/dark-cycle and *ad libitum* access to food and water. Mice were randomly allocated to experimental groups. The experimenter was blinded regarding the experimental condition. Animal numbers varied between eight and fifteen mice per genotype and experimental group and can be found in Fig. 1 of (29), Fig. 1 of (30), and Fig. 1 of (31).

2.2. Lifestyle interventions

2.2.1. Diets

As described in 2.3, mice of study I and II received different diets obtained from Research Diets. In study I, a normal-control diet (NCD), a high-sucrose diet (HSD), and a high-fat diet (HFD) were applied. NCD and HSD provided 60% of energy from carbohydrates (long-chained corn starch in NCD and short-chained sucrose in HSD), whereas HFD provided 60% of energy from fat. Protein (17-20%) and total energy content (4.2-5.2 kcal/g) were similar in all diets. In study II, the same control diet (CD) and sucrose-rich diet (SRD) were used complemented by a chia seed-supplemented version (milled; Onset Worldwide) of each diet (CD+Chia and SRD+Chia), providing the same nutritional values as the respective diets without chia seeds. Detailed composition of diets can be found in Suppl. Tab. S1 and S2 of (30) and Suppl. Tab. S1 of (31).

2.2.2. Environmental and social enrichment

Within study III, environmental enrichment (EE) was applied, combined with a social component. Compared to standard (STD) cages (42 cm x 27 cm x 15 cm), EE cages were larger (74 cm x 74 cm x 30 cm) and equipped with additional plastic tubes, boxes and houses of variable shapes, which were frequently rearranged. To increase social interactions, up to ten animals were housed in one EE cage instead of up to five animals per STD cage.

2.3. *In vivo* study design

2.3.1. Study I

Four to six weeks old APP23 and WT mice received either NCD, HSD, or HFD for a duration of 20 weeks. Weekly, food intake and body weight were documented. Every four weeks, body composition was analyzed using nuclear magnetic resonance spectroscopy and blood was collected to monitor plasma insulin levels. Activity, respiration, and energy expenditure were measured by indirect calorimetry at baseline (week 0), and after 12 and 20 weeks of dietary interventions. Furthermore, glucose tolerance upon acute glucose challenge was analyzed in intraperitoneal glucose tolerance tests (ipGTT) after 12 and 20 weeks of diet. Mice were sacrificed after 20 weeks of dietary interventions and tissues were collected to analyze organ weight, adipocyte size, hepatic steatosis, different blood parameters as well as proteomic profiles of brain and liver. A scheme of the experimental design can be found in Fig. 1 of (31).

2.3.2. Study II

APP23 and WT mice in a pre-plaque stage (PRE; 4-6 weeks old) and an advanced-plaque stage (ADV; 28-32 weeks old) received either CD or SRD for a pre-treatment duration of 12 weeks. Subsequently, each dietary group was split into a control group continuing their original diet (CD+CD or SRD+SRD) and into a therapeutic group receiving a chia seed-supplemented version of their original diet (CD+Chia or SRD+Chia). Body weight of mice was monitored on a weekly basis. Acute glucose handling was analyzed at the end of pre-treatment in week 12 and at the end of therapy in week 20 using an ipGTT. 5-Bromo-2´-deoxyuridine (BrdU) was administered in week 16 for examination of adult hippocampal neurogenesis. Anxiety, motor coordination and cognitive performance were analyzed at the end of the therapeutic period. After sacrifice, brain tissue was collected to investigate Aβ plaque load, neuroinflammation, and adult hippocampal neurogenesis. A scheme of the experimental design can be found in Fig. 1 of (30).

2.3.3. Study III

Five weeks old APP23 and WT mice were allocated to STD or EE conditions for a duration of one week (adolescent, 1 W), twelve weeks (young-adult, 12 W), or 24 weeks (adult, 24 W). Subsequently, anxiety, anhedonia, motor coordination, and cognitive performance were analyzed using a set of behavioral tests. BrdU was applied four weeks (adolescent: three weeks) prior to sacrifice to later investigate adult hippocampal neurogenesis. In the end, mice were sacrificed and brains were collected to analyze Aβ plaque load, microglia abundance, and adult hippocampal neurogenesis. A scheme of the experimental design can be found in Fig. 1 of (29).

2.4. Metabolic tests

All metabolic tests took place in the morning and after habituation of mice to a quiet experimental room. Mice were extensively accustomed to handling prior to metabolic testing.

2.4.1. Glucose tolerance test

To analyze glucose homeostasis upon acute glucose challenge, ipGTTs were conducted after 12 and 20 weeks of dietary intervention in studies I and II. Prior to ipGTT, mice were placed in single cages and fasted for 6 hours starting at the beginning of the light phase. After application of local analgesia (lidocaine/prilocaine salve), a small incision of the tail tip was performed. Glucose levels were analyzed in duplicates of blood drops obtained from the distal tail vein using a commercially available blood glucose meter (Contour Next, Bayer) before (0 min), 15, 30, 60, and 120 min after i.p. injection of glucose solution (2 mg/kg body weight). In study I, additional blood was collected at 0 min for analysis of fasted plasma insulin levels (see 2.7.3.1.).

2.4.2. Nuclear magnetic resonance spectroscopy

Nuclear magnetic resonance spectroscopy was performed monthly in study I to longitudinally assess the body composition of mice. For this purpose, mice were placed within a Minispec LF50 (Bruker), which analyzed fat mass and fat-free (i.e. lean) mass.

2.4.3. Indirect calorimetry

To investigate respiration, energy expenditure, and activity, mice in study I were analyzed in a LabMaster System (TSE). For this purpose, mice were placed for a duration of 48 h in hermetic single cages connected to external gas tanks and to the LabMaster software. Data were collected and analyzed for a 36 h period (one light and two dark phases) after a 12 h adaption period (one light phase). In intervals of 30 min, O_2 consumption and CO_2 production were measured by gas sensors, before cages were flooded with a set gas mixture to replace the used air. The respiratory exchange ratio (RER) was calculated as the ratio from O_2 consumption and CO_2 production. Activity of mice was measured via the interruption of multiple infrared beams running through each cage. From respiratory and activity data, the energy expenditure was calculated, which was later corrected for lean mass according to (32).

2.5. Behavioral tests

All behavioral tests were carried out in the morning and after acclimatization of mice to the experimental room. Mice were always handled by the same experimenter (within each study) and extensively habituated to handling prior to behavioral testing. Behavioral testing equipment was cleaned with 70% ethanol between trials (except for the Morris Water Maze).

2.5.1. Elevated Plus Maze and Elevated Zero Maze

The Elevated Plus Maze (EPM, study II) and the Elevated Zero Maze (EZM, study III) were performed to investigate anxiety based on mice's natural avoidance of open spaces. Both mazes consisted of an elevated runway (plus-shaped for EPM, round for EZM) with two open sections (no walls) and two closed sections (with walls). Mice were placed in the neutral centre region facing a closed section (EPM) or in one of the closed sections (EZM). Mice freely explored the maze for a duration of 5 min. The time spent in the open and closed sections was recorded with TSE VideoMot 3D Classic Version 8.02 (study II) or Biobserve Viewer Software (study III).

2.5.2. Sucrose Preference Test

The Sucrose Preference Test was carried out in study III to detect anhedonia, a main characteristic of depression, here represented by a decreased interest in sugared water. For this purpose, mice were placed in pairs of two in a cage equipped with two identical drinking bottles. During the 24 h habituation phase, mice were presented two bottles filled with 5% sucrose solution for 12 h, followed by two bottles filled with regular water for the subsequent 12 h. During the 24 h test period, mice could choose between one bottle filled with 5% sucrose solution and one bottle filled with regular water. The amount of ingested liquid was analyzed by weighing the bottles before and after presentation. Sucrose preference was calculated according to the following formula:

$$Sucrose\ Preference\ [\%] = \frac{\text{ingested sucrose solution}}{(\text{ingested sucrose solution} + \text{ingested regular water})}\ x\ 100^{24}$$

2.5.3. Rotarod Performance Test

The Rotarod Performance Test was conducted in studies II and III as described in (29,30) to assess motor coordination and fatigue resistance. Mice were placed on an elevated accelerating (5 to 40 rpm) rotating rod, where they had to balance for a maximum time of 5 min per trial. The latency to drop off the rod was automatically recorded with TSE-ROD Version 4.0 (study II) or TSE RotaRod Version 4.1.7 (study III). On training days (day 1-2), four trials each were conducted with an inter-trial-interval of 15-30 min. On the test day (day 3), three trials were performed. The latency to fall off the rod was averaged across these trials.

2.5.4. Morris Water Maze

The Morris Water Maze (MWM) was performed in studies II and III according to a well-established protocol to investigate hippocampus-dependent spatial learning and flexible memory (33). A circular pool with a diameter of 1.2 m, virtually divided into four quadrants, was filled with opaque water. Different geometric shapes were placed on the wall above each quadrant. A circular escape platform was positioned in the middle of one quadrant, 1 cm below the water

surface. A reversal learning paradigm was applied: The escape platform remained within the same quadrant during the acquisition phase (day 1-3) and was relocated into the opposite quadrant during the reversal learning phase (day 4-5). Mice performed six trials per day with a maximum length of 2 min. The inter-trial-interval was 30-45 min. Mice were guided to the escape platform by the experimenter's hand, if they were unable to detect its location within the duration of the trial. Each trial ended with a 10 sec long stay on the platform. The starting position within the MWM alternated each day. A graphical description of the MWM paradigm is given in Fig. 1c, d of (30). Swimming trajectories of mice were recorded with TSE VideoMot 2 Version 5.68 (study II) or Biobserve Viewer Software (study III). Matlab R2011b was used to further process swim trajectory data into presence probability maps (heatmaps) and to additionally analyze search strategies in study III.

2.6. Administration of 5-Bromo-2´-deoxyuridine and blood withdrawal

BrdU, an analog of thymidine, is incorporated into the DNA of proliferating cells (34). Its presence can be visualized with antibodies. In studies II and III, BrdU was i.p. injected four weeks before sacrifice, thus serving as a marker for cell survival of newborn cells. In study I, blood was drawn from *Vena Facialis* monthly. Blood serum was stored at -80°C for later analysis of insulin levels.

2.7. Post-mortem analyses

In all three studies, mice were sacrificed after deep anesthesia with ketamine/xylazine. In study II, mice were fasted for 6 h beforehand as described in 2.4.1. In studies I and II, a final blood withdrawal from *Vena Facialis* (study I) or *Inferior Vena Cava* (study II) was performed prior to or after laparotomy, respectively. Subsequently, thoracotomy and a transcardial perfusion with phosphate-buffered saline (PBS) was conducted. In study I, whole brain, liver, and epigonadal white adipose tissue (eWAT) were removed from all animals. Brain and parts of the liver and eWAT were snap-frozen and stored at -80°C. The remaining parts of the liver and eWAT were stored in 4% paraformaldehyde (PFA) at 4°C. In study II, the hippocampi of one half of animals were dissected from whole brains, snap-frozen and stored at -80°C. In the other half of mice within study II and in all mice of study III, perfusion with PBS was followed by perfusion with PFA. Whole brains were removed, post-fixated at 4°C in PFA for 24 h, dehydrated at 4°C in sucrose solution for 48 h and finally deep-frozen.

2.7.1. Tissue processing

In studies II and III, post-fixated whole brains were cut into 40 µm coronal slices using a cryostat (Leica). Slices were collected and stored in cryoprotectant solution at -20°C. In study I, post-

fixated liver tissue was cut into 5 µm sections using a cryostat (Leica). Post-fixated eWAT was paraffin-embedded and cut into 5 µm slices using a microtome (Thermo Scientific). Liver and eWAT sections were mounted on object slides and stored at -20°C (liver) or room temperature (eWAT).

2.7.2. Immunohistochemistry and immunofluorescence

2.7.2.1. Analysis of hepatic steatosis and adipocyte size

In study I, the degree of hepatic steatosis was analyzed represented by the amount of fat incorporated into liver tissue. Mounted liver slices were treated with Oil Red O. The percentage area coverage was calculated using ImageJ V1.52a. To investigate adipocyte size in study I, mounted eWAT slices were incubated with hematoxylin, followed by incubation with eosin Y. Cell size was measured using ImageJ V1.52a.

2.7.2.2. Analysis of plaque load

Aβ plaque load was determined in a one-in-twelve series of brain sections with fluorescent pentameric oligothiophene (pFTAA) in study II and with Congo Red in study III.

In study II, free-floating brain sections were incubated with pFTAA and subsequently counter-stained with 4′,6-diamidino-2-phenylindole (DAPI). pFTAA-positive plaques were imaged using a fluorescent microscope (Leica). The percentage area coverage within hippocampi and cortices was measured using ImageJ V1.52a.

In study III, mounted brain slices were at first incubated with haemalaun. This was followed by incubation with alcoholic sodium chloride (NaCl) including sodium hydroxide (NaOH) and by incubation with alcoholic NaCl excluding NaOH. Finally, slices were incubated with Congo Red. The number of Congo Red-positive plaques was determined using a light microscope (Olympus).

2.7.2.3. Analysis of microglia and macrophages

In studies II and III, microglia and macrophages were quantified as a correlate for neuroinflammation. A one-in-twelve series (study II) and a one-in-six series (study III) of free-floating brain slices were pre-treated with hydrogen peroxide (H_2O_2) and blocked with donkey serum, followed by overnight incubation with a primary antibody against ionized calcium-binding adapter molecule 1 (Iba1) – a microglia/macrophage marker. Tissue was then treated for 2 h with a biotinylated secondary antibody, followed by incubation with streptavidin-biotin complex. Results were visualized with diaminobenzidine(DAB)-nickel staining. Iba1-positive cells in the hippocampus were stereologically extrapolated via Stereo Investigator (MBF Bioscience) (study II) or counted and extrapolated using ImageJ V1.52a (study III).

2.7.2.4. Analysis of adult hippocampal neurogenesis

Adult hippocampal neurogenesis was investigated in studies II and III. A one-in-six-series of free-floating brain slices was treated as described in 2.7.2.3. with an additional pre-treatment step with hydrochloric acid (HCl) for BrdU-staining only. Primary antibodies against BrdU as a marker for survival of newborn cells (studies II and III) or doublecortin (DCX) as a marker for immature neurons (study II) were applied. BrdU- and DCX-positive cells were counted using a light microscope (Zeiss). In study III, an additional triple fluorescent staining against BrdU, DCX, and neuronal nuclei (NeuN), a marker for mature neurons, was performed to analyze the developmental stage of newborn cells. For this purpose, a one-in-six-series of free-floating brain sections was pre-treated with HCl, followed by an overnight incubation with primary antibodies against BrdU, DCX, and NeuN. Subsequently, tissue was incubated with fluorescent secondary antibodies for 4 h. The co-expression of BrdU/DCX, BrdU/NeuN, or BrdU/DCX/NeuN was analyzed in a total of 50 BrdU-positive cells per animal using a confocal microscope (Leica).

2.7.3. Biochemical analyses

2.7.3.1. Analysis of insulin and corticosterone levels

Insulin levels were analyzed via enzyme-linked immunosorbent assay (ELISA). In study I, insulin was measured in serum, monthly obtained from fed mice, and in plasma obtained from fasted mice at the baseline time-point of both ipGTTs. In study II, insulin was measured in plasma obtained from fasted mice during sacrifice. Serum or plasma samples were analyzed in duplicates using the Mouse Insulin ELISA kit. Additionally, corticosterone levels were investigated in plasma obtained during sacrifice of fed (study I) or fasted (study II) mice. Samples were measured in duplicates using the Corticosterone ELISA kit (for human, rat and mouse).

2.7.3.2. Analysis of free fatty acids and triglycerides

In study I, triglycerides were quantified in liver tissue. For this purpose, liver tissue was saponificated in alcoholic potassium hydroxide (KOH) and magnesium chloride ($MgCl_2$). After centrifugation, the supernatant was analyzed in duplicates using the Triglycerides FS 10’ kit. Additionally, non-esterified fatty acids (NEFA) were measured in plasma duplicates obtained during sacrifice using the NEFA-HR(2) Assay.

2.7.3.3. Proteome analyses by mass spectrometry

In study I, proteome analyses were conducted in snap-frozen brain and liver tissue using a two-column liquid chromatography–mass spectrometry/mass spectrometry (LC-MS/MS). Tissue was suspended, homogenized and processed as previously described (35–37). Further details are given

in (31). Proteome data were processed with MaxQuant software V1.6.0.1 (brain) or DIA-NN software V1.7.12 (liver) (38,39). Results were then searched against the mouse UniProt database for annotation.

2.7.3.4. Analysis of inflammatory cytokines

In study II, inflammatory cytokines were quantified in snap-frozen hippocampal tissue. Hippocampi were sheared in suspension with radioimmunoprecipitation assay (RIPA) buffer and protease inhibitor. After centrifugation, the protein concentration of the supernatant was analyzed using the Pierce™ BCA Protein Assay Kit. Proinflammatory cytokine quantification was performed in duplicates using the V-PLEX Plus Proinflammatory Panel1 Mouse Kit and subsequently normalized for total protein concentration.

2.8. Statistical analyses

In all studies, data was visualized as 25^{th} to 75^{th} percentile boxes with median and whiskers from minimum to maximum (including individual data points as scatter in studies I and II) or as mean with standard deviation using GraphPad Prism V8.4.2 (studies I and II) or V7 (study III). No data was excluded. In all studies, a p-value of ≤ 0.05 was considered significant.

In all studies, Shapiro-Wilks and Levene's test were applied using IBM SPSS Statistics V25 (studies I and II) or V23 (study III) to analyze distribution and variance of data. If assumptions for parametric testing were violated, R packages (R V3.6.3) nparcomp and nparLD were used to conduct Tukey-type nonparametric multiple contrast test in case of independent data or nonparametric ANOVA-type statistics in case of repeated measures (40,41). Here, the effect of the factors genotype (g), diet (d), and time (t) was investigated. If data met assumptions for parametric testing, two-way or repeated measures ANOVA with Tukey post-hoc test was performed in study I investigating the factors genotype (g), diet (d) (and time (t) where applicable) using GraphPad Prism. Likewise, three-way or repeated measures ANOVA for the factors genotype (g), cage condition (c), and duration (d) (and time (t) where applicable) with Bonferroni post-hoc was conducted in study III. In study I, energy expenditure data were analyzed with ANCOVA according to (32) to correct for effects of lean mass/body weight. In study I, mass spectrometry data were processed (filtering, imputation of missing values, contrast analysis) using R packages car, DEP and clusterProfiler. MATLAB R2012a optimization toolbox was used to generate Volcano plots and heatmaps, and to perform gene set enrichment analyses. Metabolic capacities were computed with MATLAB R2012a using an established kinetic model, which was calibrated with proteome profiles (42,43).

Table 1: List of materials used in all three studies

		Substance / Reagent	Abbreviation / Formula	Company	Concentration / Dilution / Dose
Diets		Normal-control diet (study I) / Control diet (study II)	NCD / CD	Research Diets	4.15 kcal/g
		Control diet supplemented with Chia seeds	CD+Chia	Research Diets	4.15 kcal/g
		High-sucrose diet (study I) / Sucrose-rich diet (study II)	HSD / SRD	Research Diets	4.28 kcal/g
		Sucrose-rich diet supplemented with Chia seeds	SRD+Chia	Research Diets	4.28 kcal/g
		High-fat diet	HFD	Research Diets	5.2 kcal/g
		Chia seeds (milled)	-	Onset Worldwide	286 g/kg diet
Immunohistochemistry and Immunofluorescence	Antibodies	5-Bromo-2´-deoxyuridine antibody (rat)	anti-BrdU	Biozol	1:500
		Doublecortin antibody (guinea pig) (study II) / Doublecortin antibody (goat) (study III)	anti-DCX	Merck Millipore / Santa Cruz Biotechnology	1:1000 / 1:100
		Ionized calcium-binding adapter molecule 1 antibody (rabbit)	anti-Iba1	Fujifilm Wako Chemicals Europe	1:500
		Neuronal nuclei antibody (mouse)	anti-NeuN	Merck Millipore	1:1000
		mouse Alexa 488 antibody (goat)	-	Invitrogen	1:1000
		goat Alexa 647 antibody (donkey)	-	Invitrogen	1:300
		rat/guinea pig/rabbit Biotin-SP-conjugated antibodies (goat/donkey)	-	Dianova	1:250
		rat Rhodamine X antibody (goat)	-	Dianova	1:250
	Dyes	4′,6-Diamidino-2-phenylindole	DAPI	Thermo Scientific	1:2000
		3,3'-Diaminobenzidine	DAB	Sigma-Aldrich	25 µg/ml
		Eosin Y	-	Carl Roth	0.5%
		Fluorescent pentameric oligothiophene	pFTAA	Sigma-Aldrich	20 µg/ml
		Mayer's hematoxylin	-	Merck Millipore	undiluted
		Oil Red O	ORO	Carl Roth	0.0072 mM
	Kits / Others	Donkey serum	-	Merck Millipore	300µl/ml PBS
		Hydrochloric acid	HCl	Merck Millipore	2 M
		Hydrogen peroxide	H2O2	Carl Roth	0.6%
		Nickel chloride	NiCl	Sigma-Aldrich	400 µg/ml
		Vectastain® ABC Elite kit	ABC	Vector Laboratories	9 µl/ml
Biochemical Analyses	Kits	Corticosterone ELISA kit (for human, rat and mouse)	-	IBL International	-
		Mouse Insulin ELISA kit	-	Mercodia	-
		NEFA-HR(2) Assay	-	Fujifilm Wako Chemicals Europe	-
		Pierce™ BCA protein assay kit	-	Thermo Scientific	-
		Triglycerides FS 10' kit	-	Diagnostic Systems	-
		V-PLEX Plus Proinflammatory Panel1 Mouse Kit	-	Meso Scale Discovery	-
	Proteomics Accessories / Others	cOmplete™ Mini Protease Inhibitor Cocktail	Protease inhibitor	Roche	1 tablet/10 ml
		Magnesium chloride	MgCl2	Sigma-Aldrich	1 M
		Potassium hydroxide	KOH	VWR	30%
		Radioimmunoprecipitation assay buffer	RIPA buffer	Abcam	1:10
		Sodium dodecyl sulphate	SDS	Thermo Scientific	1%
		Ammonium bicarbonate	ABC	Sigma-Aldrich	100 mM
		Protease inhibitor cocktail	PIC	Sigma-Aldrich	1.25x
		Formic acid	CH_2O_2	Thermo Scientific	0.1%
		Acetonitrile	C_2H_3N	Carl Roth	80%
Drugs / Others	Drugs	Emla Creme (Lidocaine/Prilocaine)	-	AstraZeneca	25 mg/g + 25 mg/g
		Ketamine	-	Inresa Arzneimittel	50 mg/ml, 300 mg/kg
		Xylazine	-	CP-Pharma	20 mg/ml, 20 mg/kg
	Others	5-Bromo-2´-deoxyuridine	BrdU	Sigma-Aldrich	10 mg/ml, 50 mg/kg
		2-Methylbutane	C15H12	Sigma-Aldrich	undiluted
		Paraformaldehyde	PFA	Sigma-Aldrich	40 g/l
		Phosphate-buffered saline	PBS	Carl Roth	0.1 M
		Sucrose (for Sucrose Preference Test or for tissue dehydration)	C6H12O6	Carl Roth	50 g/l or 300 g/l

3. Results

3.1. Study I: APP23 mice were less affected by obesogenic diets and showed increased activity, respiration, and energy expenditure

APP23 mice displayed a significantly lower body weight compared to WT mice across the whole study period ($F(1.00,52.55)=30.25$, $p<0.001$), without showing differences in body length. A body weight difference of 8% ($p=0.001$) was already present at baseline, remaining similar during 20 weeks of NCD and HSD (both ns.) but rising to 15% during HFD ($p=0.008$). At baseline, this difference was caused exclusively by a 10% lower lean mass in APP23 mice ($p<0.001$). After 20 weeks, an additive effect of lower lean mass ($p=0.087$ in HFD-fed mice) and up to 37% lower fat mass ($p=0.007$ in HFD-fed mice) was observed. Food intake of APP23 mice was constant across all diets, whereas WT mice ingested more food during HSD and HFD compared to NCD. Moreover, APP23 mice showed up to 40% smaller adipocytes compared to WT mice, most prominently during HFD ($p=0.015$), although eWAT weight did not differ between genotypes. In accordance with lower liver weight, APP23 livers contained smaller and less lipid droplets during HSD ($p=0.009$) and HFD (<0.001) as well as lower levels of hepatic triglycerides during HFD ($p<0.001$). After both 12 and 20 weeks, ipGTT revealed superior glucose tolerance in APP23 mice (week 12: $F(1.000,49.541)=3.764$, $p=0.052$; week 20: $F(1.000,41.614)=4.183$, $p=0.041$), becoming particularly evident in HFD-fed APP23 mice showing up to 32% lower glucose levels. Indirect calorimetry uncovered an increase in O_2 consumption by up to 22% (baseline: $p<0.001$; week 12: NCD – $p=0.030$, HSD – $p=0.013$, HFD – $p=0.002$; week 20: NCD – $p=0.013$, HSD – $p=0.057$, HFD – $p<0.001$) and an elevation in CO_2 production by up to 14% in APP23 mice (baseline: $p<0.001$; week 12: NCD – $p<0.001$, HFD – $p=0.003$; week 20: NCD – $p=0.018$, HFD – $p<0.001$) at any time-point regardless of diet. CO_2 consumption in HFD-fed mice was reduced by up to 22% compared to NCD and HSD (week 12: NCD vs. HFD – $p=0.051$ (WT)/$p=0.003$ (APP23), HSD vs. HFD – $p<0.001$ (WT and APP23 each)). Energy expenditure was elevated up to 11% in APP23 mice of all dietary groups (baseline: $F(1,58)=15.488$, $p<0.001$; week 12: $F(1,63)=51.102$, $p<0.001$; week 20: $F(1,65)=21.948$, $p<0.001$; all corrected for lean mass and pooled across dietary groups). Accordingly, APP23 mice displayed up to 84% higher locomotor activity (baseline: $p=0.009$; week 12: NCD – $p=0.016$, HFD – $p=0.061$; week 20: NCD – $p=0.010$, HFD – $p=0.007$). However, HFD reduced activity by up to 60% compared to NCD and HSD (week 12: NCD vs. HFD – $p=0.016$ (APP23), HSD vs. HFD – $p=0.004$ (WT); week 20: NCD vs. HFD – $p<0.001$ (WT)/$p=0.001$ (APP23), HSD vs. HFD – $p=0.007$ (WT)/$p=0.002$ (APP23)). Proteome analyses revealed that several proteins implicated in mitochondrial function, oxidative

phosphorylation, β-oxidation, and metabolic stress were differentially regulated in APP23 livers. In APP23 brains, this effect occurred to a lesser extent together with a differential regulation of proteins required for signal transduction, neuronal plasticity, and synaptic function.

Altogether, the early body weight difference of APP23 mice could not be compensated for during the dietary intervention. It was initially caused by lower lean mass and later further promoted by lower fat mass. APP23 mice were resilient against diet-induced hepatic weight gain, triglyceride build-up and adipocyte hypertrophy. Diet-induced glucose intolerance was less evident in APP23 mice, although no differences in glucose tolerance were observed during NCD. APP23 mice showed increased respiration, energy expenditure, and locomotor activity. Proteome analyses pointed towards altered mitochondrial function in APP23 mice.

3.2. Study II: Chia seeds moderately improved spatial learning deficits in APP23 mice accompanied by a mild amelioration of glucose tolerance and a mild reduction of corticosterone and proinflammatory cytokine levels

During the acquisition phase, PRE and ADV APP23 mice swam up to 46% longer distances in the MWM to detect the escape platform compared to WT mice (PRE: $F(1,78.596)=21.148$, $p<0.001$; ADV: $F(1,84.952)=25.685$, $p<0.001$). Chia seeds reduced the covered distance of APP23 mice almost to WT-level on the last day of acquisition in both age groups, however not significantly. In ADV APP23 mice, chia supplementation even resulted in a superior performance compared to CD+CD ($p=0.078$). SRD+SRD induced a 14% reduction of the covered distance compared to CD+CD in ADV APP23 mice ($p=0.068$). Heatmaps revealed that the distance reduction due to both chia supplementation and SRD was also reflected in more directed swim patterns. During the reversal learning phase, APP23 mice of both age groups covered up to 30% longer distances than WT mice (PRE: $F(1,82.512)=12.035$, $p<0.001$; ADV: $F(1,89.701)=10.169$, $p<0.001$). Chia seeds had no effect on the MWM performance within the reversal leaning phase, whereas SRD+SRD improved the performance by up to 51% on the last day of reversal learning in both PRE ($p<0.001$) and ADV APP23 mice ($p=0.048$). Again, more targeted swim patterns were observed in the heatmaps due to SRD. Glucose tolerance of CD-fed APP23 mice was similar to WT mice in the PRE group but inferior to WT mice in the ADV group ($p=0.001$). 12 weeks of SRD-pre-treatment did not alter glucose tolerance in PRE APP23 and WT mice. However, ADV APP23 mice showed a 21% impaired glucose tolerance after 12 weeks of SRD-pre-treatment ($p=0.015$). In the PRE group, additional 8 weeks of SRD started to deteriorate glucose tolerance in WT mice by up to 35% (SRD+SRD: $p=0.027$, SRD+Chia: $p=0.008$), but did not affect APP23 mice. Chia supplementation did not influence glucose tolerance in the PRE group. In contrast, chia seed

supplementation of both CD and SRD resulted in up to 18% inferior glucose tolerance in both genotypes of the ADV group, however not significant. Moreover, ADV APP23 mice displayed about 2.5-fold elevated corticosterone levels compared to WT mice (CD+CD WT vs. APP23: p=0.033). Chia seeds reduced corticosterone levels by 51% (ns.) in ADV APP23 mice. Aβ plaque load and the number of microglia were not affected by any diet, but were increased in ADV APP23 mice compared to PRE APP23 mice. In both age groups, proinflammatory cytokine levels in the hippocampus were similar between genotypes. In the PRE group, SRD+SRD increased proinflammatory cytokine levels by up to 86% in both genotypes, but more prominent in APP23 mice (TNF-α: WT CD+Chia vs. SRD+SRD, p=0.008, APP23 SRD+SRD vs. SRD+Chia, p=0.049; IL-1β: APP23 SRD+SRD vs. SRD+Chia, p=0.040; IL-6: WT CD+CD/CD+Chia vs. SRD+SRD, p=0.048/p=0.027, APP23 SRD+SRD vs. SRD+Chia, p=0.047). However, chia seeds completely reversed this effect by reducing proinflammatory cytokines to CD-comparable levels or even lower. Proinflammatory cytokine levels in the ADV group were not affected by any diet.

To sum up, chia seeds but also SRD improved impaired spatial learning in APP23 mice, more prominently in ADV mice. Impaired cognitive flexibility in both age groups was not affected by chia seeds but ameliorated by SRD. ADV APP23 mice displayed superior glucose tolerance compared to WT mice during CD, but were earlier affected by SRD-mediated deterioration of glucose tolerance. Chia supplementation mildly improved glucose tolerance in aged mice of both genotypes and mildly reduce elevated corticosterone levels in ADV APP23 mice. Aβ plaque load and microglia abundance were not altered by any diet, whereas SRD-induced elevation of pro-inflammatory cytokine levels in the PRE group was completely reversed by chia supplementation.

3.3. Study III: Pre-plaque APP23 mice showed early signs of BPSD, cognitive deficits, and altered adult hippocampal neurogenesis, all of which partially alleviated by EE

APP23 mice of any age were less anxious compared to WT mice, represented by spending more time in the open quadrants of the EZM (p<0.001). EE did not affect anxiety behavior in WT mice, but further reduced anxiety in APP23 mice, regardless of age (1 W: p=0.009; 12 W and 24 W: p<0.001). The significantly higher consumption of sweetened water compared to pure water (p<0.001) was neither influenced by age, genotype, nor EE. No differences in motor coordination were observed in any group. During the acquisition phase of the MWM task, APP23 mice of all age groups covered longer distances to the escape platform than age-matched WT mice (p<0.001). EE reduced the covered distances of WT mice during the acquisition phase (p=0.002), whereas APP23 mice did not benefit from EE. During the reversal learning phase, APP23 mice covered longer distances than WT mice, regardless of age (p<0.001). However, EE resulted in a reduction

of covered distances in young-adult (p=0.001) and adult APP23 mice (p=0.056) as well as in WT mice of all age groups (1 W/12 W: p<0.001; 24 W: p=0.045). Corresponding to their inferior performance, APP23 mice applied significantly less spatial search strategies to detect the escape platform compared to WT mice (p<0.001). EE increased the use of spatial search strategies in both genotypes (WT: p=0.003; APP23: p=0.015), with a greater effect in APP23 mice (p=0.007). Aβ plaque load was only observed in adult APP23 mice and was not influenced by cage condition. The abundance of newborn neuronal precursor cells (BrdU-/DCX-positive cells) in the dentate gyrus in adolescent APP23 and WT mice outnumbered any other age group (1 W vs. 12 W: p<0.001; 1 W vs. 24 W: p<0.001). Adolescent APP23 mice produced more neuronal precursor cells than WT mice (p<0.001). EE elevated the number of neuronal precursor cells in adolescent APP23 mice (p<0.001), but had no effect in age-matched WT mice. A similar quantity of newborn mature neurons (BrdU-/NeuN-positive cells) in the dentate gyrus was observed in all age groups and genotypes. EE increased the number of mature neurons in adolescent WT mice (p<0.001) but not in age-matched APP23 mice. Contrary, young-adult APP23 mice displayed increased numbers of mature neurons due to EE (p<0.001) but not age-matched WT mice. Microglia abundance was increased in APP23 mice compared to WT mice (p=0.002). Microglia numbers were elevated by EE (p=0.012).

Altogether, APP23 mice of all age groups showed impaired spatial learning and flexible memory, accompanied by a favour of non-spatial over spatial search strategies. Although EE could only reduce the covered distance of APP23 mice during the reversal learning phase, it generally increased the use of spatial strategies. Adolescent APP23 mice showed elevated numbers of newborn neuronal precursor cells in the dentate gyrus, which were further increased by EE. However, the abundance of newborn mature neurons was similar between genotypes but still positively affected by EE. Microglia were more frequently observed in APP23 mice and their number was increased by EE.

4. Discussion

This thesis investigated metabolic and behavioral features of the APP23 mouse model for AD with a focus on the implications of glucose metabolism in AD pathogenesis and on the therapeutic potential of early lifestyle interventions. For this purpose, three animal studies were conducted. In study I, body composition and distinct metabolic characteristics of pre-plaque APP23 mice were monitored while challenged with obesogenic diets. In study II, metabolically stressed PRE and ADV APP23 mice underwent a dietary therapy with chia supplementation. Here, cognitive

abilities, glucose tolerance, and inflammatory parameters were key aspects of the investigations. In study III, the suitability of BPSD as early diagnostic markers was examined in adolescent, young-adult, and adult APP23 mice and early treatment with EE was applied. Analyses focused on cognitive performance and potential neuropathological correlates, namely adult hippocampal neurogenesis and neuroinflammation.

4.1. Potential causes of lower body weight in APP23 mice

Decoding the underlying mechanisms of lower body weight in APP23 mice is of clinical importance, as it corresponds to lower body weight frequently observed in AD patients due to pre-clinical weight loss (44), often leading to a life-threatening disease aggravation (9). Study I revealed that lower body weight of APP23 mice mainly came from lower lean mass, a phenomenon also detected in AD patients (45). In HFD-fed APP23 mice, a lower fat mass additionally contributed to lower body weight, which has been similarly observed in other murine AD models (46). Food intake was altered in APP23 mice, such as they consumed equal amounts of each diet, whereas WT mice increased their ingested amount of food from NCD to HSD to HFD. Usually, mice adapt their food intake according to a ratio of low protein to high carbohydrates (47). This adaption seems to occur in WT but not in APP23 mice. Moreover, increased energy expenditure and activity of APP23 mice were not, as expected (48), compensated for with higher food intake. Together, this suggests an impaired energy balance, which is mediated by hypothalamic leptin signalling (49). Dysfunctional hypothalamic leptin signalling has been previously observed in different AD mouse models (50), thus representing an interesting target of future analyses. Moreover, study I revealed increased O_2 consumption and elevated CO_2 production, accompanied by higher energy expenditure and locomotor activity of APP23 mice compared to WT mice. These observations are corroborated by observations in other murine AD models (50) and potentially are main reasons for lower body weight. Interestingly, activity and CO_2 production were reduced in HFD-fed mice of both genotypes, whereas energy expenditure and O_2 production were not affected by diet. This strongly suggests that additionally to hyperactivity an elevated resting metabolic rate may have led to higher energy expenditure in APP23 mice. Hence, future studies should address the question of elevated resting metabolic rate in AD patients as a potential underlying mechanism of involuntary weight loss, as existing studies are outdated revealing inconclusive results (51–54).

4.2. Metabolic phenotype of APP23 mice with emphasis on glucose tolerance

In accordance with lower body weight and in line with literature (46), APP23 mice in study I displayed a lesser degree of hepatic steatosis, lower hepatic triglyceride levels, as well as smaller adipocytes, especially during HFD. Moreover, HFD-fed APP23 mice showed lower insulin levels

towards the end of the dietary intervention as well as superior glucose tolerance upon acute glucose challenge compared to WT mice, which has been reported previously (46). In addition, study II revealed superior glucose tolerance in ADV APP23 mice even during CD. However, there is also literature contradicting these results, reporting higher insulin levels and impaired glucose tolerance in HFD-fed AD mice (55). Potentially, these conflicting observations result from differences in peripheral Aβ levels, as there is evidence that they promote dysfunctional glucose metabolism (56). The generally low plasma Aβ levels in APP23 mice (57) may therefore represent a downside of this model with regard to the investigation of peripheral AD-related metabolic alterations. Moreover, low peripheral Aβ levels together with lower body weight – a key regulator of glycemic control (58) – might contribute to APP23 mice being less prone to a metabolic syndrome-like phenotype. However, ADV APP23 mice were earlier affected by a SRD-induced deterioration of glucose tolerance than WT mice. As mentioned above, similar observations have been made in HFD-fed AD mouse models (55). These data indicate that the increasing abundance of cerebral Aβ with advancing age, in combination with metabolic stress, might also contribute to glucose intolerance, for example mediated by Aβ-induced impairment of hypothalamic insulin signalling (59). Additionally, proteome analyses in study I suggest that mitochondrial function might be altered in liver and brain of APP23 mice. This is especially interesting regarding hypotheses about a potential key role of mitochondria in the development of AD (60). Notably, oxidative stress and altered mitochondrial pathways have been previously observed in APP23 brains (61). Beyond that, the results of this thesis indicate a general implication of mitochondria in AD not only limited to the brain.

4.3. Therapeutic potential of chia supplementation in APP23 mice

Confirming previous observations (29,62), PRE APP23 mice already showed deficits in spatial learning and cognitive flexibility. Given the very low Aβ deposition at this age, this observation further supports the hypothesis of Aβ not being the sole driver of AD-related cognitive decline. Chia supplementation lead to a moderate enhancement of spatial learning, more prominently in ADV APP23 mice. Only two previous studies analyzed a potential cognitive effect of chia seeds in AD models, observing either no effect (63) or even an aggravation of cognitive deficits (64). However, in none of the used models AD-like pathology was induced by Aβ-overexpression. Hence, they might not mimic AD-related glycemic alterations, which seem to be dependent on Aβ (56). Chia-induced improvement of spatial learning might be caused by a combination of the following observations: Chia seeds mildly ameliorated glucose tolerance in ADV APP23 mice and there is evidence of glucose tolerance being associated with cognitive performance (65).

Moreover, chia seeds mildly reduced corticosterone levels in ADV APP23 mice, which similarly have been shown to impact cognitive abilities (66). Additionally, chia supplementation exerted a beneficial impact on proinflammatory cytokine levels in PRE APP23 mice. Evidence suggests a link between neuroinflammation and cognitive function (67). Finally, chia seeds are a rich source of polyunsaturated fatty acids (22). These are thought to improve cognitive performance via several mechanisms such as enhanced long-term potentiation, neuroprotection and increased synaptogenesis (23). Notably, chia seeds had no effect on cognitive flexibility. Bearing in mind that reversal learning requires a high degree of functional plasticity (e.g. to inhibit the memory of the old platform position, to memorize the new platform position, or with regard to motivational aspects) (68), the mentioned beneficial aspects of chia seeds might not be sufficient in our AD model, as functional plasticity is potentially impaired (69). Unexpectedly, SRD ameliorated spatial as well as reversal learning. Contradicting the present results, previous studies have revealed cognitive impairment induced by SRD or similar energy-rich diets (70,71). However, since these studies have typically compared high-caloric diets to conventional diets, the results may represent the effect of high calorie intake rather than the effect of sugar. Calorie intake is suggested to modulate several aspects of brain function, such as adult hippocampal neurogenesis (72). In contrast, the SRD used in the present study was isocaloric to the CD. Moreover, the notably leaner APP23 mice might have profited from the supply of short-chain carbohydrates as a fast energy source, potentially enhancing cognitive capacities.

4.4. BPSD and cognitive performance in APP23 mice

Study III revealed reduced anxiety in APP23 mice compared to WT mice across all ages, hence before deposition of Aβ plaques. This observation is consistent with findings in similar murine AD models (73). Although anxiety in AD patients is usually increased but not decreased (74), the observed decreased anxiety of APP23 mice can be seen as an aberration from the physiological state, which is typically anxious for mice and not anxious for humans. Hence, anxiety behavior of APP23 mice indeed models early AD-related alterations of anxiety (74). In contrast, APP23 mice showed no signs of depressive behavior during the sucrose preference test. This is in line with literature (75) and should generally be assessed in the light of the challenge regarding animal models of depression (76). In summary, APP23 mice partially reflect BPSD with the present symptoms occurring very early in disease development, hence potentially contributing to early diagnosis. Spatial learning was impaired in APP23 mice. Interestingly, although adolescent and young-adult APP23 mice performed inferior to WT mice in the beginning of the acquisition phase, they were able to catch up with the performance of their WT littermates on the last day of

acquisition. In contrast, adult APP23 mice covered longer distances than WT mice across the entire acquisition phase. As previous studies obtained similar results (77), these data suggest that deficits in spatial learning already occur before plaque onset in APP23 mice and can only be compensated for with training in early disease stages. During reversal learning, APP23 mice of all ages performed inferior compared to WT mice. This finding promotes the above suggested theory of reversal learning being even more challenging for APP23 mice, potentially due to a lack of functional plasticity (69). The observation of a less frequent use of spatial search strategies in all age groups of APP23 mice has been previously made in other AD mouse models (78), strongly indicating a beginning impairment of cognitive function.

4.5. Therapeutic effect of EE and its potential neuropathological correlates

Unexpectedly, EE failed to improve spatial learning in APP23 mice during the acquisition phase. This contradicts previous studies, which have shown beneficial effects of EE on the cognitive performance of APP23 mice (79,80). Although there is overwhelming evidence of a positive impact of EE on cognitive performance, one study using a similar AD mouse model could not show an effect of EE on MWM performance either (81). Interestingly, the mentioned studies observing a positive effect of EE have applied 7-10 days of acquisition phase in the MWM task. In contrast, the study showing no effect of EE has applied a 3-day acquisition phase, such as in this thesis. Thus, the EE-induced amelioration of spatial learning might be dependent on the training intensity. In line with previous studies (82), EE ameliorated the performance of APP23 mice during the reversal learning phase, although only young-adult and adult APP23 mice profited by EE. This suggests that the short exposure to EE within the adolescent group might be insufficient to exert its positive influence. Additionally, EE increased the use of the more efficient spatial search strategies during both acquisition and reversal learning phase. Altogether, this indicates that the positive impact of EE on the use of more efficient search strategies seems to develop already quite early, whereas the transition of more efficient search strategies into shorter swim paths might be dependent on training intensity. Adult hippocampal neurogenesis was investigated as a potential neuropathological correlate of cognitive impairment and of the effect of EE, as it is suggested to be crucial in building a neurogenic reserve, important for neuronal plasticity (83). We observed increased abundance of neuronal precursor cells in adolescent APP23 mice compared to WT mice, indicating a compensatory mechanism to early disease manifestations (7). Interestingly, this was further promoted by EE, suggesting a potential mechanism for the beneficial effect of EE on cognitive performance (7). In young-adult APP23 mice the effect of EE shifted from increased neuronal precursor abundance to increased numbers of mature neurons.

Those mature neurons probably integrate into the neuronal network, hence providing larger capacities for complex tasks such as reversal learning (83). Moreover, microglia abundance was elevated in APP23 mice and further increased by EE. Neuroinflammation in early disease stages is thought to be protective, as microglia increase the clearance of Aβ, whereas neuroinflammation in later disease stages is potentially detrimental due to the prolonged release of proinflammatory factors and neurotoxins (84). As the observed age groups of APP23 mice represent early disease stages, the EE-mediated increase in microglia abundance might contribute to the beneficial effect of EE on cognitive performance.

4.6. Limitations

The conclusions drawn from the APP23 mouse model regarding underlying mechanisms might be limited, as the pathology of this model is naturally caused by the genetic overexpression of APP. Moreover, amyloidosis, as observed in this model, does not fully reflect AD neuropathology. However, due to the complexity and the multitude of open questions regarding AD etiology, there are no animal models available, which fully mimic the disease or accurately model its development. Among the existing models, the APP23 mouse is a well-characterized animal model, facilitating the integration of the present data into literature. Another caveat of this thesis could be the gender bias. All studies were conducted in female mice, since females are more prone to develop AD (85). The underlying reasons for the overrepresentation of women among AD patients remain elusive, hence a focus on gender differences is important. However, the usage of female mice might increase variation within study data due to a potential interference of the estrous cycle with analyzed parameters. Thus, the estrous cycle of female mice should be monitored in future experiments and similar investigations should be conducted in male mice to reveal potential differences.

4.7. Conclusions and future directions

This thesis extensively analyzed metabolic and behavioral features of the APP23 mouse model with emphasis on implications of body weight regulation and glucose metabolism as well as the therapeutic potential of lifestyle interventions in AD. The following conclusions can be drawn from the present thesis: (1) Pre-plaque APP23 mice show hyperactivity, increased metabolic rate, and impaired energy balance, resulting in lower body weight and accompanied by strong signs of systemic mitochondrial dysfunction; (2) Peripheral glucose metabolism of younger APP23 mice is unaltered or even superior to WT mice, but aged APP23 mice are more vulnerable to metabolic stress; (3) Cognitive impairment of APP23 mice occurs prior to plaque onset; (4) Cognitive deficits of APP23 mice are ameliorated by chia supplementation, potentially due to an additive

effect of improved glucose tolerance and reduced corticosterone and proinflammatory cytokine levels; (5) EE positively affects the cognitive performance of APP23 mice possibly via the enhancement of adult hippocampal neurogenesis and the elevation of microglia abundance. These data are of clinical relevance as the metabolic component of AD is coming more and more into focus recently and accessory symptoms of AD such as weight loss strongly correlate with mortality rate. Therefore, the underlying mechanisms of the observed metabolic alterations should be addressed in future studies, for example by investigating hypothalamic leptin signalling as a regulator of energy balance or the role of mitochondria in AD pathogenesis. Moreover, clinical investigations are of utmost importance to analyze, whether those functional changes also occur in AD patients and to compile adequate strategies for the prevention of fatal involuntary weight loss. While no curative therapies exist, lifestyle interventions are useful and easy implementable therapeutic approaches. Hence, a balanced diet, supplemented with chia seeds, and an active and socially enriched lifestyle might contribute to prevention or slowdown of AD pathology as well as amelioration of cognitive symptoms, such as demonstrated in the APP23 mouse model during the present studies.

5. References

1. Patterson C. World Alzheimer Report 2018. Alzheimer's Dis Int. 2018;
2. Alzheimer's Association. 2020 Alzheimer's disease facts and figures. Alzheimer's Dement. 2020;16(3):391–460.
3. Guest FL, Rahmoune H, Guest PC. Early Diagnosis and Targeted Treatment Strategy for Improved Therapeutic Outcomes in Alzheimer's Disease. In: Guest PC, editor. Reviews on New Drug Targets in Age-Related Disorders [Internet]. Cham: Springer International Publishing; 2020. p. 175–91. Available from: https://doi.org/10.1007/978-3-030-42667-5_8
4. Serrano-Pozo A, Frosch MP, Masliah E, Hyman BT. Neuropathological alterations in Alzheimer disease. Cold Spring Harb Perspect Med. 2011;1–24.
5. Mangialasche F, Solomon A, Winblad B, Mecocci P, Kivipelto M. Alzheimer's disease: clinical trials and drug development. Lancet Neurol [Internet]. 2010 Jul 1;9(7):702–16. Available from: https://doi.org/10.1016/S1474-4422(10)70119-8
6. Toda T, Gage FH. Review: adult neurogenesis contributes to hippocampal plasticity. Cell Tissue Res. 2018;373(3):693–709.
7. Mu Y, Gage FH. Adult hippocampal neurogenesis and its role in Alzheimer's disease. Mol Neurodegener. 2011;6(1):1–9.
8. Cerejeira J, Lagarto L, Mukaetova-Ladinska EB. Behavioral and psychological symptoms of dementia. Front Neurol. 2012;3:1–21.
9. Gillette-Guyonnet S, Abellan van Kan G, Alix S, Andrieu S, Belmin J, Berrut G, Bonnefoy M, Brocker P, Constans T, Ferry M, Ghisolfi-Marque A, Girard L, Gonthier R, Guerin O, Hervy M-P, Jouanny P, Laurain M-C, Lechowksi L, Nourhashemi F, Raynaud-Simon A, Ritz P, Roche J, Rolland Y, Salva T, Vellas B. IANA (International Academy on Nutrition and Aging) Expert group: Weight loss and Alzheimer's disease. J Nutr Health Aging. 2007;11(1).
10. Hardy JA, Higgins GA. Alzheimer's disease: The amyloid cascade hypothesis. Science (80-). 1992;256(5054):184–5.
11. Foroutan N, Hopkins RB, Tarride J-E, Florez ID, Levine M. Safety and efficacy of active and passive immunotherapy in mild-to-moderate Alzheimer's disease : A systematic review and network meta-analysis. Clin Invest Med. 2019;42(1):53–65.
12. Baglietto-Vargas D, Shi J, Yaeger DM, Ager R, LaFerla FM. Diabetes and Alzheimer's disease crosstalk.

Neurosci Biobehav Rev. 2016;64:272–87.
13. Calsolaro V, Edison P. Alterations in Glucose Metabolism in Alzheimer's Disease. Recent Pat Endocr Metab Immune Drug Discov. 2016;(10):31–9.
14. Profenno LA, Porsteinsson AP, Faraone S V. Meta-Analysis of Alzheimer's Disease Risk with Obesity, Diabetes, and Related Disorders. Biol Psychiatry [Internet]. 2010;67(6):505–12. Available from: http://dx.doi.org/10.1016/j.biopsych.2009.02.013
15. Sergi G, De Rui M, Coin A, Inelmen EM, Manzato E. Weight loss and Alzheimer's disease: Temporal and aetiologic connections. Proc Nutr Soc. 2013;72(1):160–5.
16. Cova I, Clerici F, Rossi A, Cucumo V, Ghiretti R, Maggiore L, Pomati S, Galimberti D, Scarpini E, Mariani C, Caracciolo B. Weight loss predicts progression of mild cognitive impairment to Alzheimer's disease. PLoS One. 2016;11(3):1–12.
17. Kivipelto M, Mangialasche F, Ngandu T. Lifestyle interventions to prevent cognitive impairment, dementia and Alzheimer disease. Nat Rev Neurol [Internet]. 2018;14(11):653–66. Available from: http://dx.doi.org/10.1038/s41582-018-0070-3
18. Dhana K, Evans DA, Rajan KB, Bennett DA, Morris MC. Healthy lifestyle and the risk of Alzheimer dementia: Findings from 2 longitudinal studies. Neurology. 2020;95(4).
19. Yusufov M, Weyandt LL, Piryatinsky I. Alzheimer's disease and diet: a systematic review. Int J Neurosci. 2017;127(2):161–75.
20. Chicco AG, D'Alessandro ME, Hein GJ, Oliva ME, Lombardo YB. Dietary chia seed (Salvia hispanica L.) rich in alpha-linolenic acid improves adiposity and normalises hypertriacylglycerolaemia and insulin resistance in dyslipaemic rats. Br J Nutr. 2009;101(1):41–50.
21. Ullah R, Nadeem M, Khalique A, Imran M, Mehmood S, Javid A, Hussain J. Nutritional and therapeutic perspectives of chia (Salvia hispanica L.): a review. Vol. 53, J Food Sci Technol. 2016. p. 1750–8.
22. Ayerza R. Oil content and fatty acid composition of chia (Salvia hispanica L.) from five northwestern locations in Argentina. J Am Oil Chem Soc. 1995;72(9):1079–81.
23. Dyall SC. Long-chain omega-3 fatty acids and the brain: a review of the independent and shared effects of EPA, DPA and DHA. Front Aging Neurosci. 2015;7.
24. Cui MY, Lin Y, Sheng JY, Zhang X, Cui RJ. Exercise intervention associated with cognitive improvement in Alzheimer's disease. Neural Plast. 2018;2018.
25. Scarmeas N, Levy G, Tang MX, Manly J, Stern Y. Influence of leisure activity on the incidence of Alzheimer's disease. Neurology. 2001;57(12):2236–42.
26. Fabel K, Wolf SA, Ehninger D, Babu H, Leal-Galicia P, Kempermann G. Additive effects of physical exercise and environmental enrichment on adult hippocampal neurogenesis in mice. Front Neurosci. 2009;3:1–7.
27. Kilkenny C, Browne WJ, Cuthill IC, Emerson M, Altman DG. Improving bioscience research reporting: The ARRIVE guidelines for reporting animal research. PLoS Biol. 2010;8(6):6–10.
28. Sturchler-Pierrat C, Abramowski D, Duke M, Wiederhold KH, Mistl C, Rothacher S, Ledermann B, Bürki K, Frey P, Paganetti PA, Waridel C, Calhoun ME, Jucker M, Probst A, Staufenbiel M, Sommer B. Two amyloid precursor protein transgenic mouse models with Alzheimer disease-like pathology. Proc Natl Acad Sci U S A. 1997;94(24):13287–92.
29. Pfeffer A, Munder T, Schreyer S, Klein C, Rasińska J, Winter Y, Steiner B. Behavioral and psychological symptoms of dementia (BPSD) and impaired cognition reflect unsuccessful neuronal compensation in the pre-plaque stage and serve as early markers for Alzheimer's disease in the APP23 mouse model. Behav Brain Res. 2018;347:300–13.
30. Schreyer S, Klein C, Pfeffer A, Rasińska J, Stahn L, Knuth K, Abuelnor B, Panzel AEC, Rex A, Koch S, Hemmati-Sadeghi S, Steiner B. Chia seeds as a potential cognitive booster in the APP23 Alzheimer's disease model. Sci Rep. 2020;10(1):1–16.
31. Schreyer S, Berndt N, Eckstein J, Mülleder M, Hemmati-Sadeghi S, Klein C, Abuelnor B, Panzel A, Meierhofer D, Spranger J, Steiner B, Brachs S. Dietary-challenged mice with Alzheimer-like pathology show increased energy expenditure and reduced adipocyte hypertrophy and steatosis. Aging (Albany NY). 2021;13.
32. Tschöp MH, Speakman JR, Arch JRS, Auwerx J, Brüning JC, Chan L, Eckel RH, Farese R V., Galgani JE, Hambly C, Herman MA, Horvath TL, Kahn BB, Kozma SC, Maratos-Flier E, Müller TD, Münzberg H, Pfluger PT, Plum L, Reitman ML, Rahmouni K, Shulman GI, Thomas G, Kahn CR, Ravussin E. A guide to analysis of mouse energy metabolism. Nat Methods. 2012;9(1):57–63.
33. Garthe A, Behr J, Kempermann G. Adult-generated hippocampal neurons allow the flexible use of spatially precise learning strategies. PLoS One. 2009;4(5).
34. Miller MW, Nowakowski RS. Use of bromodeoxyuridine-immunohistochemistry to examine the proliferation, migration and time of origin of cells in the central nervous system. Brain Res. 1988;457(1):44–52.
35. Guo J, Bertalan G, Meierhofer D, Klein C, Schreyer S, Steiner B, Wang S, Vieira R, Infante-duarte C, Koch S, Boehm-Sturm P, Braun J, Sack I. Brain maturation is associated with increasing tissue stiffness and

decreasing tissue fluidity. Acta Biomater. 2019;99:433–42.
36. Gielisch I, Meierhofer D. Metabolome and proteome profiling of complex I deficiency induced by rotenone. J Proteome Res. 2015;14(1):224–35.
37. Müller T, Kalxdorf M, Longuespée R, Kazdal DN, Stenzinger A, Krijgsveld J. Automated sample preparation with SP3 for low-input clinical proteomics. Mol Syst Biol. 2020;16.
38. Cox J, Mann M. MaxQuant enables high peptide identification rates, individualized p.p.b.-range mass accuracies and proteome-wide protein quantification. Nat Biotechnol. 2008;26(12):1367–72.
39. Demichev V, Messner CB, Vernardis SI, Lilley KS, Ralser M. DIA-NN : neural networks and interference correction enable deep proteome coverage in high throughput. Nat Methods. 2020;17:41–4.
40. Konietschke F, Placzek M, Schaarschmidt F, Hothorn LA. nparcomp: An R software package for nonparametric multiple comparisons and simultaneous confidence intervals. J Stat Softw. 2015;64(9):1–17.
41. Noguchi K, Gel YR, Brunner E, Konietschke F. nparLD : An R Software Package for the Nonparametric Analysis of Longitudinal Data in Factorial Experiments . J Stat Softw. 2012;50(12).
42. Berndt N, Kann O, Holzhütter H. Physiology-based kinetic modeling of neuronal energy metabolism unravels the molecular basis of NAD (P) H fl uorescence transients. 2015;(0315741):1494–506.
43. Berndt N, Bulik S, Wallach I, Wünsch T, König M, Stockmann M, Meierhofer D, Holzhütter H-G. HEPATOKIN1 is a biochemistry-based model of liver metabolism for applications in medicine and pharmacology. Nat Commun. 2018;
44. Stewart R, Masaki K, Xue Q-L, Peila R, Petrovitch H, White LR, Launer LJ. A 32-Year Prospective Study of Change in Body Weight and Incident Dementia. Arch Neurol. 2005;62:55–60.
45. Buffa R, Mereu E, Putzu P, Mereu RM, Marini E. Lower lean mass and higher percent fat mass in patients with Alzheimer's disease. Exp Gerontol. 2014;58:30–3.
46. Lin B, Hasegawa Y, Takane K, Koibuchi N, Cao C, Kim-Mitsuyama S. High-fat-diet intake enhances cerebral amyloid angiopathy and cognitive impairment in a mouse model of alzheimer's disease, independently of metabolic disorders. J Am Heart Assoc. 2016;5(6):1–16.
47. Solon-Biet SM, McMahon AC, Ballard JWO, Ruohonen K, Wu LE, Cogger VC, Warren A, Huang X, Pichaud N, Melvin RG, Gokarn R, Khalil M, Turner N, Cooney GJ, Sinclair DA, Raubenheimer D, Le Couteur DG, Simpson SJ. The ratio of macronutrients, not caloric intake, dictates cardiometabolic health, aging, and longevity in ad libitum-fed mice. Cell Metab. 2014;19(3):418–30.
48. Drenowatz C. Reciprocal Compensation to Changes in Dietary Intake and Energy Expenditure within the Concept of Energy Balance. Adv Nutr. 2015;6:592–9.
49. Abdalla MMI. Central and peripheral control of food intake. Endocr Regul. 2017;51(1):52–70.
50. Ishii M, Wang G, Racchumi G, Dyke JP, Iadecola C. Transgenic mice overexpressing amyloid precursor protein exhibit early metabolic deficits and a pathologically low leptin state associated with hypothalamic dysfunction in arcuate neuropeptide y neurons. J Neurosci. 2014;34(27):9096–106.
51. Wolf-Klein GP, Silverstone FA, Lansey SC, Tesi D, Ciampaglia C, O'Donnell M, Galkowski J, Jaeger A, Wallenstein S, Leleiko NS. Energy requirements in Alzheimer's disease patients. Nutrition. 1995;11(3):264–8.
52. Dvorak R V., Poehlman ET. Appendicular skeletal muscle mass, physical activity, and cognitive status in patients with Alzheimer's disease. Neurology. 1998;51(5):1386–90.
53. Niskanen L, Piirainen M, Koljonen M, Uusitupa M. Resting energy expenditure in relation to energy intake in patients with Alzheimer's disease, multi-infarct dementia and in control women. Age Ageing. 1993;22(2):132–7.
54. Poehlman ET, Toth MJ, Goran MI, Carpenter WH, Newhouse P, Rosen CJ. Daily energy expenditure in free-living non-institutionalized Alzheimer's patients: A doubly labeled water study. Neurology. 1997;48(4):997–1002.
55. Walker JM, Dixit S, Saulsberry AC, May JM, Harrison FE. Reversal of high fat diet-induced obesity improves glucose tolerance, inflammatory response, β-amyloid accumulation and cognitive decline in the APP/PSEN1 mouse model of Alzheimer's disease. Neurobiol Dis. 2017;100:87–98.
56. Wijesekara N, Gonçalves RA, De Felice FG, Fraser PE. Impaired peripheral glucose homeostasis and Alzheimer's disease. Neuropharmacology. 2018;136:172–81.
57. Kuo Y, Beach TG, Sue LI, Scott S, Layne KJ, Kokjohn TA, Kalback WM, Luehrs DC, Vishnivetskaya TA, Abramowski D, Staufenbiel M, Weller RO, Roher AE. The Evolution of Aß Peptide Burden in the APP23 Transgenic Mice: Implications for Aß Deposition in Alzheimer Disease. Mol Med. 2001;7(9):609–18.
58. Guess ND. Dietary interventions for the prevention of type 2 diabetes in high-risk groups: Current state of evidence and future research needs. Nutrients. 2018;10(9).
59. Jiménez-Palomares M, Ramos-Rodríguez JJ, López-Acosta JF, Pacheco-Herrero M, Lechuga-Sancho AM, Perdomo G, García-Alloza M, Cózar-Castellano I. Increased Aβ production prompts the onset of glucose intolerance and insulin resistance. Am J Physiol - Endocrinol Metab. 2012;302(11):1373–80.
60. Albensi BC. Dysfunction of mitochondria: Implications for Alzheimer's disease [Internet]. 1st ed. Vol. 145,

International Review of Neurobiology. Elsevier Inc.; 2019. 13–27 p. Available from: http://dx.doi.org/10.1016/bs.irn.2019.03.001
61. Hartl D, Schuldt V, Forler S, Zabel C, Klose J, Rohe M. Presymptomatic alterations in energy metabolism and oxidative stress in the APP23 mouse model of Alzheimer disease. J Proteome Res. 2012;11(6):3295–304.
62. Van Dam D, Hooge RD, Staufenbiel M, Van Ginneken C, Meir F Van, De Deyn PP. Age-dependent cognitive decline in the APP23 model precedes amyloid deposition. Eur J Neurosci. 2003;17:388–96.
63. Rui Y, Lv M, Chang J, Xu J, Qin L, Wan Z. Chia seed does not improve cognitive impairment in SAMP8 mice fed with high fat diet. Nutrients. 2018;10(8).
64. Bilgic Y, Demir EA, Bilgic N, Dogan H, Tutuk O, Tumer C. Detrimental effects of chia (Salvia hispanica L.) seeds on learning and memory in aluminium chloride-induced experimental Alzheimer's disease. Acta Neurobiol Exp. 2018;(78):322–31.
65. Kerti L, Witte V, Winkler A, Grittner U, Rujescu D, Flöel A. Higher glucose levels associated with lower memory and reduced hippocampal microstructure. Neurology. 2014;83(1):102.
66. Gray JD, Kogan JF, Marrocco J, McEwen BS. Genomic and epigenomic mechanisms of glucocorticoids in the brain. Nat Rev Endocrinol. 2017;13(11):661–73.
67. Passamonti XL, Tsvetanov XKA, Jones PS, Arnold R, Borchert RJ, Mak E, Su L, O' Brien JT, Rowe XJB. Neuroinflammation and Functional Connectivity in Alzheimer's Disease: Interactive Influences on Cognitive Performance. J Neurosci. 2019;39(36):7218–26.
68. Izquierdo A, Brigman JL, Radke AK, Rudebeck PH, Holmes A. The neural basis of reversal learning: An updated perspective. Neuroscience. 2017;345:12–26.
69. Styr B, Slutsky I. Imbalance between firing homeostasis and synaptic plasticity drives early-phase Alzheimer's disease. Nat Neurosci. 2018;21(4):463–73.
70. Molteni R, Barnard RJ, Ying Z, Roberts CK, Gómez-Pinilla F. A high-fat, refined sugar diet reduces hippocampal brain-derived neurotrophic factor, neuronal plasticity, and learning. Neuroscience. 2002;112(4):803–14.
71. Kanoski SE, Meisel RL, Mullins AJ, Davidson TL. The effects of energy-rich diets on discrimination reversal learning and on BDNF in the hippocampus and prefrontal cortex of the rat. Behav Brain Res. 2007;182(1):57–66.
72. Morgan AH, Andrews ZB, Davies JS. Less is more: Caloric regulation of neurogenesis and adult brain function. J Neuroendocrinol. 2017;29(10):1–11.
73. Yuk DY, Lee YK, Nam SY, Yun YW, Hwang DY, Choi DY, Oh KW, Hong JT. Reduced anxiety in the mice expressing mutant (N141I) presenilin 2. J Neurosci Res. 2009;87(2):522–31.
74. Johansson M, Stomrud E, Lindberg O, Westman E, Johansson PM, van Westen D, Mattson N, Hansson O. Apathy and anxiety are early markers of Alzheimer's disease. Neurobiol Aging. 2020;85:74–82.
75. Vloeberghs E, Van Dam D, Franck F, Staufenbiel M, De Deyn PP. Mood and male sexual behaviour in the APP23 model of Alzheimer's disease. Behav Brain Res. 2007;
76. Planchez B, Surget A, Belzung C. Animal models of major depression: drawbacks and challenges. J Neural Transm [Internet]. 2019;126(11):1383–408. Available from: https://doi.org/10.1007/s00702-019-02084-y
77. Van Dam D, D'Hooge R, Staufenbiel M, Van Ginneken C, Van Meir F, De Deyn PP. Age-dependent cognitive decline in the APP23 model precedes amyloid deposition. Eur J Neurosci. 2003;17(2):388–96.
78. Brody DL, Holtzman DM. Morris water maze search strategy analysis in PDAPP mice before and after experimental traumatic brain injury. Exp Neurol. 2006;197(2):330–40.
79. Wolf SA, Kronenberg G, Lehmann K, Blankenship A, Overall R, Staufenbiel M, Kempermann G. Cognitive and Physical Activity Differently Modulate Disease Progression in the Amyloid Precursor Protein (APP)-23 Model of Alzheimer's Disease. Biol Psychiatry. 2006;60(12):1314–23.
80. Polito L, Chierchia A, Tunesi M, Bouybayoune I, Kehoe PG, Albani D, Forloni G. Environmental enrichment lessens cognitive decline in APP23 mice without affecting brain sirtuin expression. J Alzheimer's Dis. 2014;42(3):851–64.
81. Hüttenrauch M, Walter S, Kaufmann M, Weggen S, Wirths O. Limited Effects of Prolonged Environmental Enrichment on the Pathology of 5XFAD Mice. Mol Neurobiol. 2017;54(8):6542–55.
82. Jankowsky JL, Melnikova T, Fadale DJ, Xu GM, Slunt HH, Gonzales V, Younkin LH, Younkin SG, Borchelt DR, Savonenko A V. Environmental Enrichment Mitigates Cognitive Deficits in a Mouse Model of Alzheimer ' s Disease. 2005;25(21):5217–24.
83. Kempermann G. The neurogenic reserve hypothesis: what is adult hippocampal neurogenesis good for? Trends Neurosci. 2008;31(4):163–9.
84. Webers A, Heneka MT, Gleeson PA. The role of innate immune responses and neuroinflammation in amyloid accumulation and progression of Alzheimer's disease. Immunol Cell Biol. 2020;98(1):28–41.
85. Pike CJ. Sex and the development of Alzheimer's disease. J Neurosci Res. 2017;95(1–2):671–80.

Statutory Declaration (Eidesstattliche Erklärung)

„Ich, Stefanie Schreyer (geb. Beier), versichere an Eides statt durch meine eigenhändige Unterschrift, dass ich die vorgelegte Dissertation mit dem Thema: *„Metabolic and behavioral characterization of the APP23 mouse model of Alzheimer's disease with regard to early therapeutic lifestyle interventions"* selbstständig und ohne nicht offengelegte Hilfe Dritter verfasst und keine anderen als die angegebenen Quellen und Hilfsmittel genutzt habe.
Alle Stellen, die wörtlich oder dem Sinne nach auf Publikationen oder Vorträgen anderer Autoren/innen beruhen, sind als solche in korrekter Zitierung kenntlich gemacht. Die Abschnitte zu Methodik (insbesondere praktische Arbeiten, Laborbestimmungen, statistische Aufarbeitung) und Resultaten (insbesondere Abbildungen, Graphiken und Tabellen) werden von mir verantwortet.

Ich versichere ferner, dass ich die in Zusammenarbeit mit anderen Personen generierten Daten, Datenauswertungen und Schlussfolgerungen korrekt gekennzeichnet und meinen eigenen Beitrag sowie die Beiträge anderer Personen korrekt kenntlich gemacht habe (siehe Anteilserklärung). Texte oder Textteile, die gemeinsam mit anderen erstellt oder verwendet wurden, habe ich korrekt kenntlich gemacht.

Meine Anteile an etwaigen Publikationen zu dieser Dissertation entsprechen denen, die in der untenstehenden gemeinsamen Erklärung mit dem/der Erstbetreuer/in, angegeben sind. Für sämtliche im Rahmen der Dissertation entstandenen Publikationen wurden die Richtlinien des ICMJE (International Committee of Medical Journal Editors; www.icmje.og) zur Autorenschaft eingehalten. Ich erkläre ferner, dass ich mich zur Einhaltung der Satzung der Charité – Universitätsmedizin Berlin zur Sicherung Guter Wissenschaftlicher Praxis verpflichte.

Weiterhin versichere ich, dass ich diese Dissertation weder in gleicher noch in ähnlicher Form bereits an einer anderen Fakultät eingereicht habe.

Die Bedeutung dieser eidesstattlichen Versicherung und die strafrechtlichen Folgen einer unwahren eidesstattlichen Versicherung (§§156, 161 des Strafgesetzbuches) sind mir bekannt und bewusst."

Datum Unterschrift

Declaration of contribution to the selected publications (Anteilserklärung)

Stefanie Schreyer (geb. Beier) had the following share in the publications listed below:

Publication 1:

Schreyer, S., Berndt, N., Eckstein, J., Mülleder, M., Hemmati-Sadeghi, S., Klein, C., Abuelnor, B., Panzel, A., Meierhofer, D., Spranger, J., Steiner, B. & Brachs, S. Dietary-challenged mice with Alzheimer-like pathology show increased energy expenditure and reduced adipocyte hypertrophy and steatosis. Aging, 2021.

Impact Factor 4.831 (2020 Journal Citation Report)

Contribution in detail: Together with S. Brachs, I developed the study design and created Fig 1. I was the main experimenter of the animal study, performing body weight and composition measurements (data for Fig. 2), glucose tolerance tests (data for Fig. 5), and indirect calorimetry (data for Fig. 6) with technical assistance from the lab of S. Brachs. With assistance from B. Abuelnor and A. Panzel, I conducted biochemical analyses of insulin and corticosterone levels (data for Fig. 4). I prepared the tissue and conducted histological analyses including imaging of eWAT and liver tissue (data for Fig. 3). I performed statistical analyses of data occurring in Fig. 2 to Fig. 6 including the design of the mentioned figures. I wrote the entire manuscript with exception of the methods part about mass spectrometry, which was written by N. Berndt, J. Eckstein, M. Mülleder and D. Meierhofer. Together with S. Brachs, I intensely revised the manuscript according to reviewers' comments.

Publication 2:

Schreyer, S., Klein, C., Pfeffer, A., Rasińska, J., Stahn, L., Knuth, K., Abuelnor, B., Panzel, A. E. C., Rex, A., Koch, S., Hemmati-Sadeghi, S. & Steiner, B. Chia seeds as a potential cognitive booster in the APP23 Alzheimer's disease model. Scientific Reports, 2020.

Impact Factor 3.998 (2020 Journal Citation Report)

Contribution in detail: Together with C. Klein and B. Steiner, I developed the study design and created Fig 1. I was the main experimenter of the animal study, performing anxiety testing (data for Suppl. Fig. 8), motor coordination testing (data for Suppl. Fig. 9), cognitive testing (data for Fig. 2, Fig. 3, Suppl. Fig. 3), glucose tolerance tests (data for Fig. 4), and body weight measurements (data for Suppl. Fig. 7), assisted by students of the Steiner lab, in case of two experimenters were needed (e.g. for cognitive testing). With assistance of K. Knuth, B. Abuelnor,

and A. Panzel, I prepared brain tissue and conducted histological analyses including imaging of brain tissue (data for Fig. 6a-d, Suppl. Fig. 6) as well as biochemical analyses of insulin and corticosterone levels (data for Fig. 5). I performed statistical analyses of data occurring in Fig. 2 to Fig. 6 including the design of the mentioned figures. I wrote the entire manuscript supported by S. Hemmati-Sadeghi and C. Klein. I corresponded with the editor and the reviewers and extensively revised the manuscript including the performance of additional biochemical analyses of hippocampal tissue (data for Fig. 6-j).

Publication 3:

Pfeffer, A., Munder, T., **Schreyer, S.**, Klein, C., Rasińska, J., Winter, Y., & Steiner, B. Behavioral and psychological symptoms of dementia (BPSD) and impaired cognition reflect unsuccessful neuronal compensation in the pre-plaque stage and serve as early markers for Alzheimer's disease in the APP23 mouse model. Behavioral Brain Research, 2018.

Impact Factor 2.770 (2018 Journal Citation Report)

Contribution in detail: I assisted in the performance of cognitive tests and sucrose preference tests (data for Tab. 1, Fig. 3). I assisted in brain tissue processing and contributed to histological stainings and cell counting (data for Fig. 5); I designed Fig. 1. I critically revised the manuscript.

_____

Signature, date and stamp of the supervising University teacher

_____

Signature of the doctoral candidate

Version of Record – Study I

Research Paper

Dietary-challenged mice with Alzheimer-like pathology show increased energy expenditure and reduced adipocyte hypertrophy and steatosis

Stefanie Schreyer[1], Nikolaus Berndt[2], Johannes Eckstein[3], Michael Mülleder[4], Shabnam Hemmati-Sadeghi[1], Charlotte Klein[1], Basim Abuelnor[1], Alina Panzel[1], David Meierhofer[5], Joachim Spranger[6,7], Barbara Steiner[1,*], Sebastian Brachs[6,7,*]

[1]Department of Neurology, Charité – Universitätsmedizin Berlin, Corporate Member of Freie Universität Berlin and Humboldt-Universität zu Berlin, Berlin 10117, Germany
[2]Institute for Imaging Science and Computational Modelling in Cardiovascular Medicine, Charité – Universitätsmedizin Berlin, Corporate member of Freie Universität Berlin and Humboldt-Universität zu Berlin, Berlin 13353, Germany
[3]Institute of Biochemistry, Charité – Universitätsmedizin Berlin, Corporate Member of Freie Universität Berlin and Humboldt-Universität zu Berlin, Berlin 10117, Germany
[4]Core Facility High Throughput Mass Spectrometry, Charité – Universitätsmedizin Berlin, Corporate Member of Freie Universität Berlin and Humboldt-Universität zu Berlin, Berlin 10117, Germany
[5]Max Planck Institute for Molecular Genetics, Berlin 14195, Germany
[6]Department of Endocrinology and Metabolism, Charité – Universitätsmedizin Berlin, Corporate Member of Freie Universität Berlin and Humboldt-Universität zu Berlin, Berlin 10117, Germany
[7]DZHK (German Centre for Cardiovascular Research), Partner Site Berlin, Berlin, Germany
*Equal contribution

Correspondence to: Sebastian Brachs; **email:** sebastian.brachs@charite.de
Keywords: Alzheimer's disease, diet-induced obesity, hypertrophy, energy expenditure, steatosis
Received: February 17, 2021 **Accepted:** March 27, 2021 **Published:** April 16, 2021

ABSTRACT

Alzheimer's disease (AD) is frequently accompanied by progressing weight loss, correlating with mortality. Counter-intuitively, weight loss in old age might predict AD onset but obesity in midlife increases AD risk. Furthermore, AD is associated with diabetes-like alterations in glucose metabolism. Here, we investigated metabolic features of amyloid precursor protein overexpressing APP23 female mice modeling AD upon long-term challenge with high-sucrose (HSD) or high-fat diet (HFD). Compared to wild type littermates (WT), APP23 females were less prone to mild HSD-induced and considerable HFD-induced glucose tolerance deterioration, despite unaltered glucose tolerance during normal-control diet. Indirect calorimetry revealed increased energy expenditure and hyperactivity in APP23 females. Dietary interventions, especially HFD, had weaker effects on lean and fat mass gain, steatosis and adipocyte hypertrophy of APP23 than WT mice, as shown by ^{1}H-magnetic-resonance-spectroscopy, histological and biochemical analyses. Proteome analysis revealed differentially regulated expression of mitochondrial proteins in APP23 livers and brains. In conclusion, hyperactivity, increased metabolic rate, and global mitochondrial dysfunction potentially add up to the development of AD-related body weight changes in APP23 females, becoming especially evident during diet-induced metabolic challenge. These findings emphasize the importance of translating this metabolic phenotyping into human research to decode the metabolic component in AD pathogenesis.

INTRODUCTION

To date, Alzheimer's disease (AD) cannot be cured and its underlying mechanisms remain elusive [1]. Early diagnosis of AD – a crucial requirement for the application of existing symptomatic treatment – is complicated due to its multifaceted pathology and a variety of accessory symptoms, which are partially not well understood [2]. Thus, basic research focusing on these symptoms might provide important insights into pathological mechanisms leading to new approaches for diagnosis and therapy.

Worldwide, about 50 million patients suffer from AD, the most common neurodegenerative disease [3]. Brains affected by AD are characterized by extracellular amyloid-beta (Aβ) aggregates, intracellular neurofibrillary tangles of hyperphosphorylated tau, and progressive neurodegeneration [4, 5]. Synapse and neuronal loss ultimately result in dementia [6]. For decades, AD research focused on Aβ – cleaved from the amyloid precursor protein (APP) – and its aggregation into plaques as disease etiology [7]. Nevertheless, decreasing Aβ burden using antibodies has failed to significantly improve patients' condition [8]. Thus, alternative causes came into the spotlight: Epidemiologic studies identified metabolic dysfunctions such as insulin resistance and glucose insensitivity as risk factors, potentially involved in AD pathology [9, 10]. These shared features lead to the suggestion that AD might represent brain-specific diabetes [11]. However, the exact mechanisms linking both pathologies remain unknown.

Counter-intuitively, both obesity in midlife and low body weight in old age increase the risk of developing AD [12, 13]. However, at least 30-40% of patients suffer from AD-related involuntary weight loss, aggravating as AD progresses leading to poorer health, reduced quality of life, and increased mortality [14]. Since weight loss already occurs years before the onset of clinical AD symptoms, body weight changes in old age might represent early AD manifestations potentially contributing to early diagnosis [15, 16].

Weight loss occurs with negative energy balance, i.e. lower energy intake than energy expenditure [17]. Reasons for negative energy balance might be reduced energy intake, e.g. due to reduced food intake or malabsorption [18], hypermetabolism originating from elevated resting energy expenditure, e.g. increased thermogenesis, or elevated total energy expenditure, e.g. increased physical activity [18]. Previous body weight analyses in AD patients remained inconclusive, requiring further research to elucidate underlying mechanisms of AD-related weight loss.

Here, we investigate early AD-related metabolism and body weight changes challenging the APP-overexpressing APP23 mouse model [19] with different diets before Aβ-plaque development to extensively characterize its metabolic features and the impact of different fuel sources. Thereby, we aim to gain insights into underlying mechanisms of AD-related metabolic and body weight changes, which might provide valuable information for early diagnosis or therapeutic approaches.

RESULTS

APP23 mice showed lower body weight due to lower fat and lean mass

To investigate the impact of APP overexpression on metabolism, APP23 and WT mice were challenged with normal-control (NCD), high-sucrose (HSD) or high-fat diet (HFD) for 20 weeks (Figure 1A, 1B). Across the experiment, all groups significantly gained body weight ($F(4.04,52.55)=484.37$, $p<0.001$; Figure 2A). However, APP23 mice showed a significantly lower body weight ($F(1.00,52.55)=30.25$, $p<0.001$). The effect of diet ($F(1.90,52.55)=63.47$, $p<0.001$) was most prominent in HFD (up to 41% higher body weight compared to NCD/HSD), while HSD had virtually no effect. At baseline, body weight of APP23 mice was 8% lower compared to WT mice ($p=0.001$; Figure 2B). This body weight difference remained constant until week 20 in NCD- and HSD-fed mice (NCD: 6%, n.s.; HSD: 7%, n.s.; Figure 2C). After 20 weeks of dietary intervention, HFD elevated body weight up to 85% in WT mice and up to 68% in APP23 mice (both $p<0.001$), while HSD had no effect on body weight. The body weight difference between genotypes rose to 15% in HFD-fed mice ($p=0.008$).

Lean mass was 10% lower in APP23 mice at baseline (week 0, $p<0.001$; Figure 2D). After 20 weeks of dietary intervention, lean mass was up to 7% lower in NCD- and HSD-fed APP23 mice, however not significant, and 8% lower in HFD-fed APP23 mice ($p=0.087$; Figure 2E). While HSD did not affect lean mass, HFD significantly increased lean mass in both genotypes but more prominently in WT mice (HFD WT vs. NCD/HSD WT, both $p<0.001$; HFD APP23 vs. NCD/HSD APP23, both $p\leq0.005$). Fat mass was equal between genotypes at baseline (week 0; Figure 2F). While 20 weeks of HSD had almost no effect on fat mass, HFD significantly elevated fat mass in both genotypes ($p<0.001$; Figure 2G). Fat mass was 37% lower in HFD-fed APP23 mice ($p=0.007$) and up to 10% lower during NCD and HSD, however not significant. Lower body weight did not originate from a smaller growth as body length was almost identical in

young adult APP23 and WT mice (Figure 2H). Notably, food intake gradually increased in WT mice from NCD to HSD to HFD (NCD WT vs. HFD WT, p<0.001), whereas it remained constant between diets in APP23 mice resulting in a significantly lower HFD intake compared to WT mice (p<0.001; Figure 2I).

In summary, APP23 mice showed lower body weight due to both lower fat and lean mass. The difference in lean mass was already present at baseline, whereas the difference in fat mass occurred only at the end of dietary intervention. APP23 mice could not catch up for this body weight difference due to a similar body weight gain.

Diet-induced adipocyte hypertrophy and steatosis were extenuated in APP23 mice

To further examine body composition changes, tissues were analyzed upon sacrifice. Epigonadal white adipose tissue (eWAT) weight was similar between genotypes and only elevated by HFD (5-fold, vs. NCD/HSD each p<0.001; Figure 3A). Liver weight was also similar during NCD and elevated by HFD (e.g. NCD APP23 vs. HFD APP23, p<0.001) but 45% (p=0.002) and 20% (n.s.) lower in HSD- and HFD-fed APP23 mice (Figure 3B). Adipocyte size was analyzed in hematoxylin/eosin-stained eWAT (Figure 3C, 3D). APP23 mice displayed 20% (NCD, n.s.) to 40% (HSD, n.s.; HFD, p=0.015) smaller adipocytes than WT mice. In contrast to unaffected eWAT weight, HSD increased adipocyte size 2.3-fold (n.s.). HFD rose adipocyte size compared to NCD (7.3-fold, NCD WT/APP23 vs. HFD WT/APP23, both p<0.001) and HSD (3.1-fold, HSD WT vs. HFD WT, p<0.001; HSD APP23 vs. HFD APP23, p=0.010). Moreover, hepatic fat content (i.e. liver steatosis) was analyzed by Oil Red O staining and triglyceride quantification (Figure 3E–3G). During NCD, lipid droplet size and amount was similar, while HSD- and HFD-fed APP23 mice embodied less and smaller droplets than WT mice (HSD: 4.5-fold, p=0.009; HFD: 2-fold, p<0.001; Figure 3E, 3F). According to increasing liver weight, lipid droplet size and amount gradually rose from NCD to HFD, specifically prominent in WT mice (NCD vs. HSD: 11-fold, p=0.002; HSD vs. HFD: 2-fold, p<0.001). Furthermore, hepatic triglycerides were similar between genotypes and diets during NCD and HSD (Figure 3G). In contrast, HFD-fed WT mice showed up to 9.2-fold elevated hepatic triglycerides compared to NCD- and HSD-fed mice of both genotypes (p<0.001), whereas triglycerides in HFD-fed APP23 mice were only increased by 3.4-fold (n.s.). Thus, during HFD hepatic triglycerides were 2.3-fold higher in WT mice compared to APP23 mice (p<0.001).

A

Weeks	0	1	2	3	4	5	6	7	8	9	10	11	12	13	14	15	16	17	18	19	20
Procedures	BW NMR LM BL	BW *Diet Start*	BW	BW	BW NMR BL	BW	BW	BW	BW NMR BL	BW	BW	BW	BW NMR LM BL GTT	BW	BW	BW	BW NMR BL	BW	BW	BW	BW NMR LM BL GTT

B

Genotype	n	Diet	Total Energy [kcal/g]	Carbohydrates [% kcal] (% Sucrose|% Corn starch)	Fat [% kcal]	Protein [% kcal]
WT	15	NCD	4.2	60 (2|80)	23	17
APP23	9					
WT	10	HSD	4.3	60 (96|0)	23	17
APP23	14					
WT	10	HFD	5.2	20 (34|0)	60	20
APP23	10					

Figure 1. Experimental design and nutritional values of diets. (**A**) Experimental procedures: In week 0, baseline measurements of body composition (NMR) and indirect calorimetry (LM) were conducted, as well as the first blood withdrawal (BL). Diets were fed from week 1 to 20. Body weight was assessed weekly. Monthly, NMR and BL were performed. In week 12 and 20, mice additionally underwent LM measurements and glucose tolerance tests (GTT). (**B**) Group layout and diet composition: 4-6-week old transgenic APP23 and WT mice were assigned to either normal-control diet (NCD), high-sucrose diet (HSD) or high-fat diet (HFD). Shown n numbers represent animal numbers for all measurements in living animals and in the animals' blood.

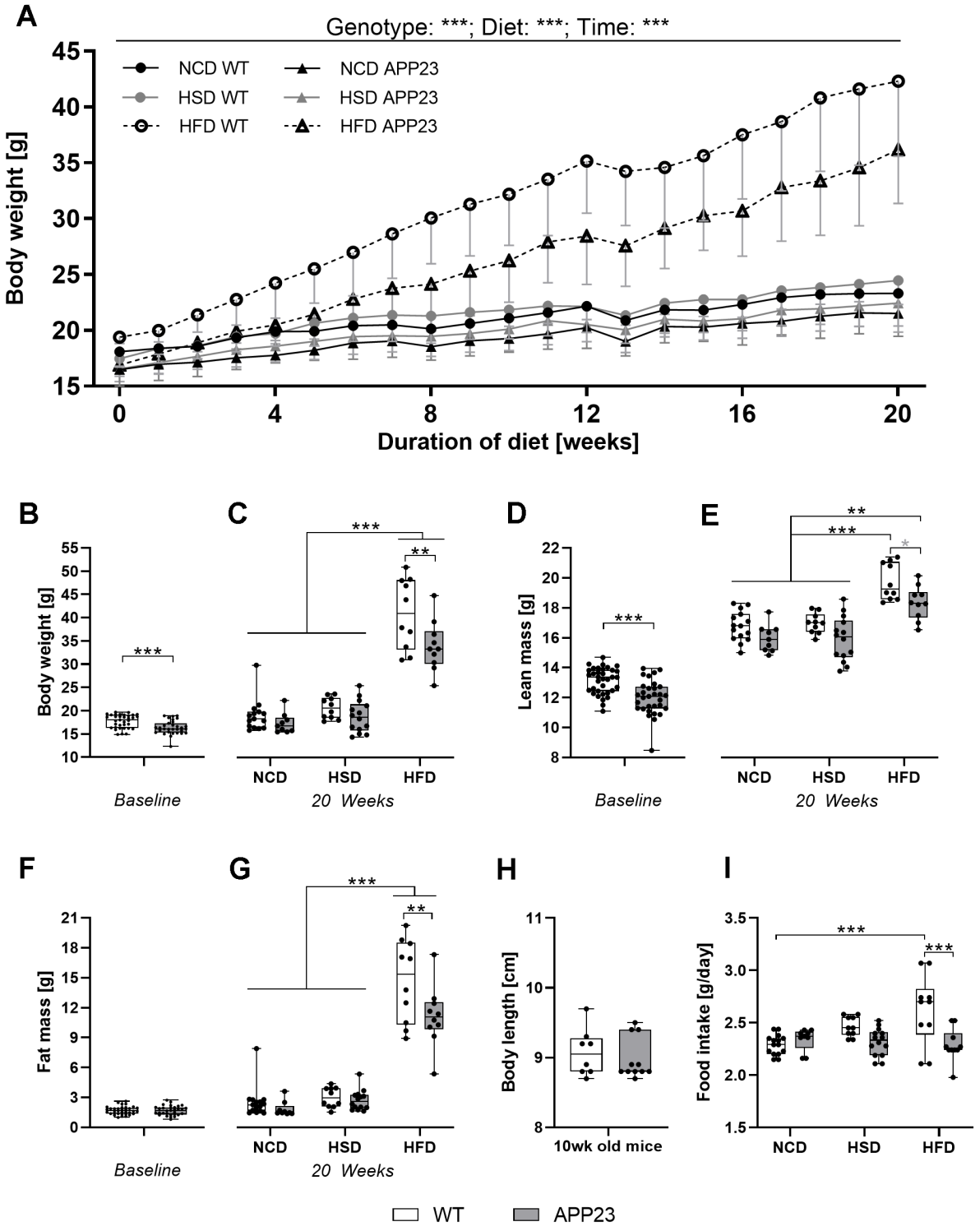

Figure 2. Body weight, body composition, body length, and food intake. (**A**) Development of body weight during 20 weeks of dietary intervention (NCD, HSD or HFD). (**B**) Body weight at baseline (week 0). (**C**) Body weight after 20 weeks of dietary intervention. (**D**) Lean mass at baseline (week 0). (**E**) Lean mass after 20 weeks of dietary intervention. (**F**) Fat mass at baseline (week 0). (**G**) Fat mass after 20 weeks of dietary intervention. (**H**) Exemplarily measured body length in male and female adult (mean age 10 weeks) APP23 and WT mice. (**I**) Mean daily food intake averaged over the entire intervention and across mice occupying the same cage. Data are represented as box (25^{th} to 75^{th} percentile) with median and whiskers from minimum to maximum. Black asterisks indicate significant differences between groups (*: $p<0.05$; **: $p<0.01$; ***: $p<0.001$), gray asterisk indicates a statistical trend towards significance ($p<0.1$) according to nonparametric ANOVA-type statistics (**A**), ordinary 2-way ANOVA with Tukey post-hoc test (**C**, **G**, **I**), multiple contrast Tukey-type test (**E**), or nonparametric t-test (**B**, **D**, **F**, **H**). $n_{Week\ 0\ WT}$=35, $n_{Week\ 0\ APP23}$=31, $n_{NCD\ WT}$=15, $n_{NCD\ APP23}$=9, $n_{HSD\ WT}$=10, $n_{HSD\ APP23}$=14, $n_{HFD\ WT}$=10, $n_{HFD\ APP23}$=10; for body length: n_{WT}=8, n_{APP23}=11.

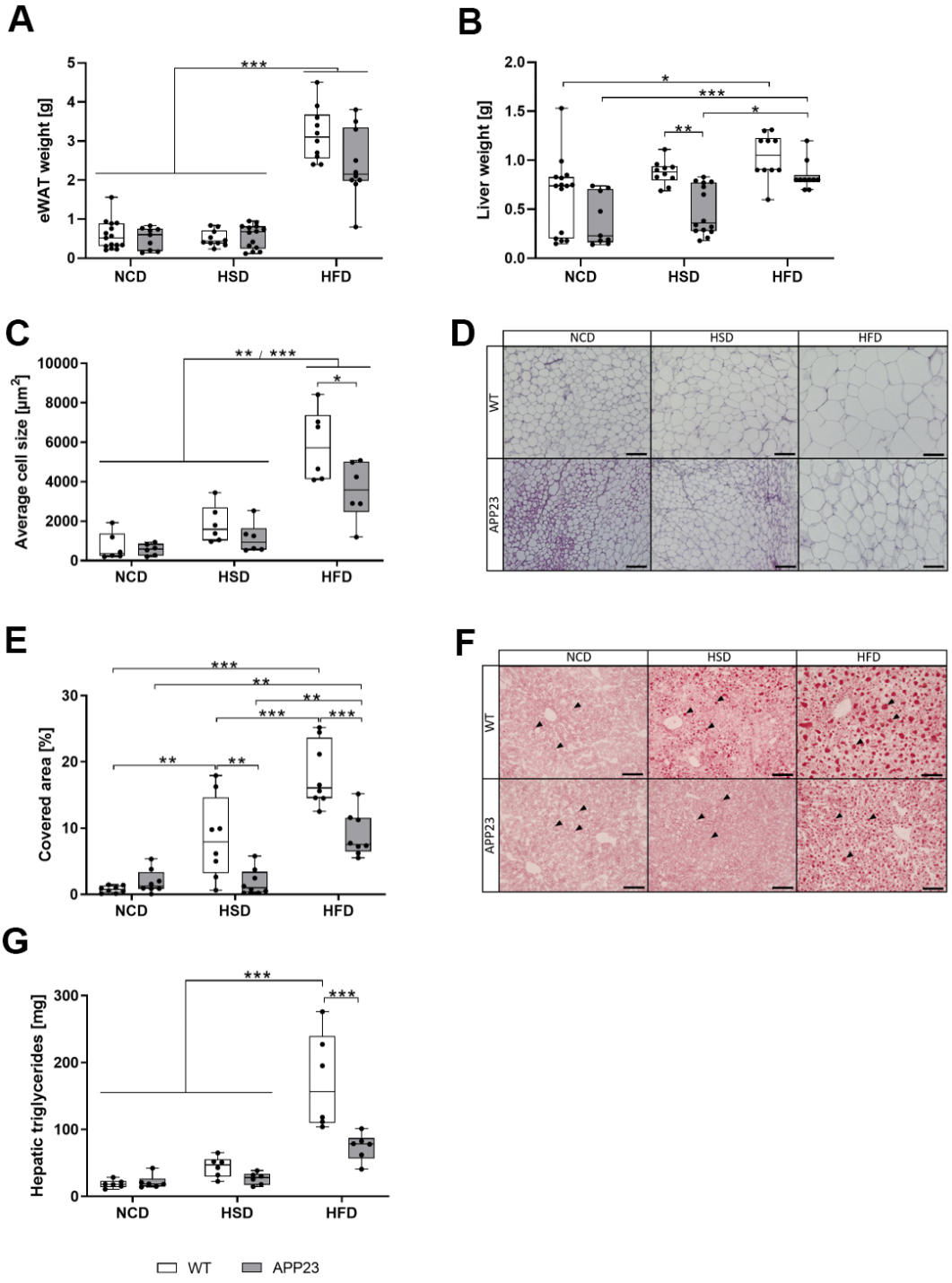

Figure 3. Weight of eWAT and liver, histological analysis of adipocyte size in eWAT and lipid droplets in liver tissue, and quantification of hepatic triglycerides. Weight of eWAT (**A**) and liver (**B**) upon sacrifice of mice after 20 weeks of dietary interventions (NCD, HSD or HFD). (**C**) Quantification of mean adipocyte size in eWAT sections analyzed with ImageJ (**D**) Representative hematoxylin/eosin stainings of eWAT tissue. Scale bar: 100 µm (**E**) Lipid quantification of Oil Red O-stained hepatic sections analyzed with ImageJ. (**F**) Representative Oil Red O stainings of liver tissue. Arrowheads point to individual Oil Red O-stained lipid droplets. Scale bar: 100 µm. (**G**) Quantification of hepatic triglycerides. Measured triglyceride concentrations were multiplied by liver weight to obtain absolute amounts of triglycerides. Data are represented as box (25^{th} to 75^{th} percentile) with median and whiskers from minimum to maximum. Black asterisks indicate significant differences between groups (*: p<0.05; **: p<0.01; ***: p<0.001), gray asterisk indicates a statistical trend towards significance (p<0.1) according to nonparametric multiple contrast Tukey-type test (**A**, **B**) and Tukey post-hoc test of an ordinary 2-way ANOVA (**C**, **E**, **G**). For (**A**, **B**) $n_{NCD\ WT}$=15, $n_{NCD\ APP23}$=9, $n_{HSD\ WT}$=10, $n_{HSD\ APP23}$=14, $n_{HFD\ WT}$=10, $n_{HFD\ APP23}$=10. For (**C**, **D**) n=6 each. For (**E**, **F**) n=8 each, For (**G**) n=6 each.

Altogether, APP23 mice resisted against HSD- and HFD-induced hepatic weight gain, lipid accumulation and adipocyte hypertrophy.

Insulin levels were unaltered in APP23 mice during NCD and HSD but lower during HFD

To investigate glucose homeostasis, we monthly analyzed plasma insulin levels in fed mice (Figure 4). NCD and HSD did not alter insulin levels, with APP23 mice showing no differences compared to WT mice (Figure 4A, 4B). In contrast, HFD elevated insulin levels over time ($F(2.75,49.50)=15.72$, $p<0.001$), starting around week 8 of dietary intervention (Figure 4C). Interestingly, genotypes were differentially affected by the HFD-induced elevation of insulin levels ($F(1,8)=6.915$, $p=0.017$). In week 16 ($p=0.019$) and 20 (n.s., $p=0.182$), insulin levels of WT mice were almost twice as high as those of APP23 mice. In all, only HFD elevated insulin levels, whereas APP23 mice were less affected. Additionally, corticosterone and non-esterified free fatty acid (NEFA) levels were measured in final plasma. Corticosterone levels were similar between genotypes and increased by trend from NCD to HFD (NCD WT vs. HFD WT, $p=0.098$) (Figure 4D). In contrast, NEFA levels slightly decreased during HFD but similarly between genotypes (NCD APP23 vs. HFD APP23, $p=0.062$; HSD APP23 vs. HFD APP23, $p=0.023$; Figure 4E).

HFD deteriorated glucose tolerance earlier and stronger than HSD but less in APP23 mice

To further analyze glucose homeostasis upon glucose challenge, an ipGTT was performed after 12 and 20 weeks (Figure 5, statistics see Supplementary Table 2). After 12 weeks, glucose handling was affected by diet ($F(1.941,49.542)=50.159$, $p<0.001$), such as HSD and HFD both delayed the glucose peak (Figure 5A). Additionally, the glucose peak of HFD-fed mice was 30% higher compared to NCD/HSD. Whereas NCD- and HSD-fed mice approximately returned to basal levels after 120 min, glucose levels remained 31% (APP23) and 82% (WT) elevated in HFD-fed mice. APP23 mice showed by trend 9% lower glucose levels than WT mice ($F(1.000,49.541)=3.764$, $p=0.052$). This was especially prominent in HFD-fed APP23 mice, which returned to 32% lower final glucose levels than WT mice. After 20 weeks, diet still affected glucose handling ($F(1.943,41.614)=82.409$, $p<0.001$) with HSD and HFD delaying the glucose peak, the effect of HFD having even grown (Figure 5B). Furthermore, HFD-fed mice remained far above basal glucose levels after 120 min (WT: 2.7-fold; APP23: 1.8-fold). Still, NCD- and HSD-fed mice nearly returned to fasting glucose levels. Again, APP23 mice showed 9% lower glucose levels compared to WT mice ($F(1.000,41.614)=4.183$, $p=0.041$), which was once more especially evident in HFD-fed APP23 mice. Evaluating the area under the curve (AUC) in week 12, HFD-fed mice displayed a significantly larger AUC compared to NCD- and HSD-fed mice (Figure 5C). However, AUC of HFD-fed APP23 mice was 20% smaller compared to HFD-fed WT mice. After 20 weeks, AUC of HFD-fed mice was even more increased compared to NCD- and HSD-fed mice (Figure 5D). Still, HFD-fed APP23 mice displayed a significantly smaller AUC than HFD-fed WT mice, although the difference decreased to 15%.

Fasting glucose levels gradually increased from NCD to HSD to HFD at both time-points (Figure 5E, 5F). HSD elevated fasting glucose levels up to 25% in APP23 but not in WT mice, while HFD increased fasting glucose levels up to 35% in both genotypes. Contrary, fasting insulin levels were only increased in HFD-fed mice (week 12: 3-fold; week 20: 6-fold) in both genotypes (Figure 5G, 5H**)**. Fasting insulin was similar between genotypes. In summary, glucose tolerance was deteriorated by HSD and HFD, with HFD exerting an earlier and stronger effect and APP23 mice being less affected. Moreover, HSD and HFD increased fasting glucose levels, but only HFD elevated fasting insulin levels, both parameters being similar across genotypes.

APP23 mice showed increased O_2 consumption, CO_2 production, energy expenditure, and locomotor activity at night

To further investigate whole-body metabolism of APP23 mice, indirect calorimetry was performed at baseline, week 12 and 20. Figure 6 (statistics see Supplementary Table 3) depicts results measured during active phase. Light phase data are displayed in Supplementary Figure 1. O_2 consumption and CO_2 production adjusted for lean mass were increased in APP23 mice at any time-point. Measurements adjusted for body weight were similar (Supplementary Figure 2). On closer examination, APP23 mice consumed 12% more O_2 at baseline (Figure 6A) and up to 22% in week 12 and 20 (Figure 6B, 6C). Diet alone did not affect O_2 consumption at any time-point. Correspondingly, CO_2 production was 10% elevated in APP23 mice at baseline (Figure 6D) and up to 14% in week 12 and 20 (Figure 6E, 6F). Contrary to O_2 consumption, CO_2 production was affected by diet, such as HFD-fed mice produced up to 22% less CO_2 compared to NCD/HSD at both time-points. The respiratory exchange ratio was similar between genotypes at baseline (Figure 6G). During HSD, it decreased up to 10% in APP23 mice at both time-points (Figure 6H, 6I**)**, while no genotype differences were observed during NCD and HFD. HSD increased the respiratory exchange ratio, however only

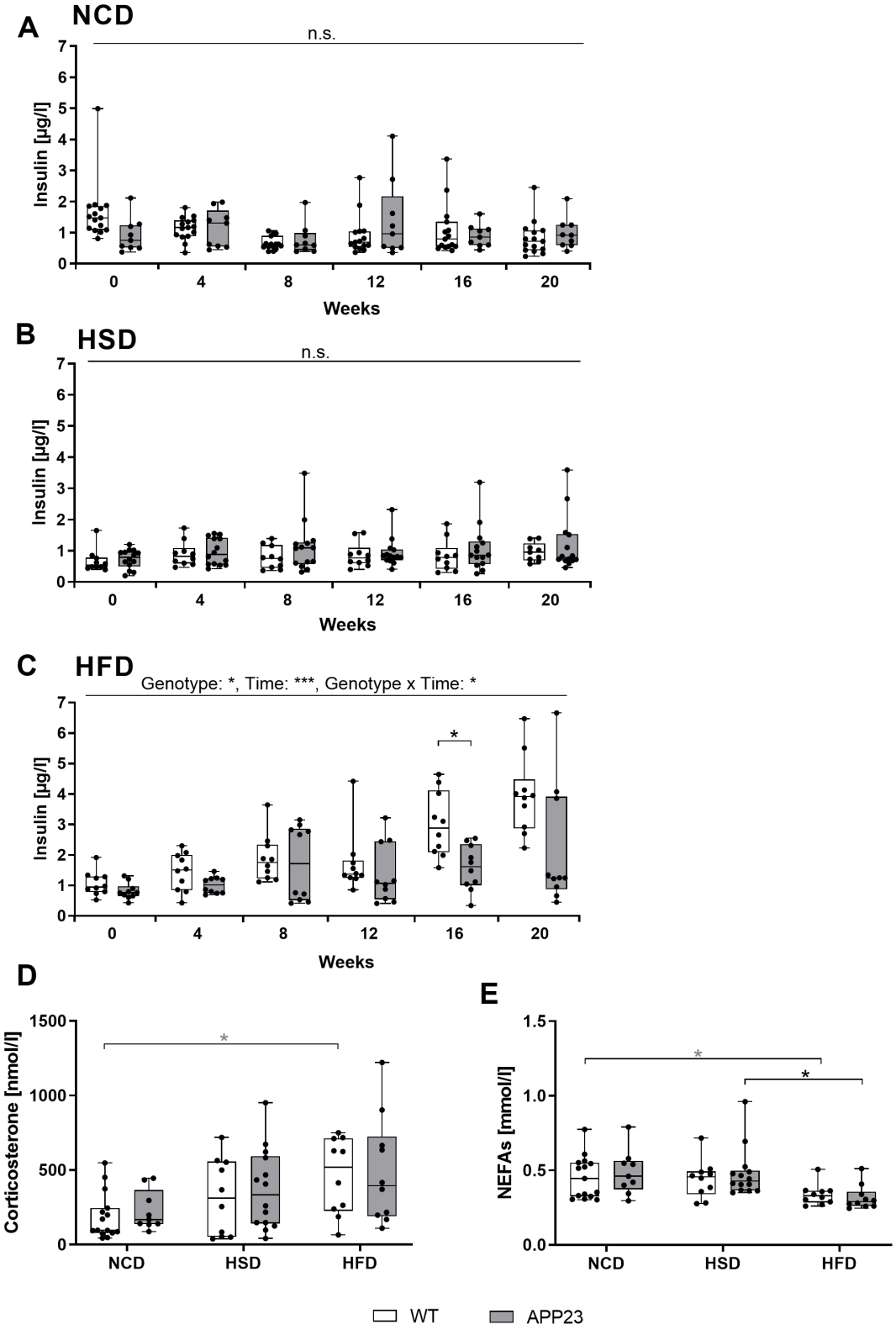

Figure 4. Analysis of basic metabolic parameters in blood of fed mice. (**A**–**C**) Plasma insulin measured in NCD-fed (**A**), HSD-fed (**B**) and HFD-fed (**C**) mice at baseline (week 0) and after 4, 8, 12, 16, and 20 weeks of diet. Corticosterone levels (**D**) and NEFA levels (**E**) measured in blood plasma obtained upon sacrifice after 20 weeks of diet. Data are represented as box (25^{th} to 75^{th} percentile) with median and whiskers from minimum to maximum. Black asterisks indicate significant differences between groups (*: p<0.05; **: p<0.01; ***: p<0.001), gray asterisk indicates a statistical trend towards significance (p<0.1) according to Tukey post-hoc test of repeated measures ANOVA (**A**–**C**) and nonparametric multiple contrast Tukey-type test (**D**, **E**). $n_{NCD\ WT}$=15, $n_{NCD\ APP23}$=9, $n_{HSD\ WT}$=10, $n_{HSD\ APP23}$=14, $n_{HFD\ WT}$=10, $n_{HFD\ APP23}$=10.

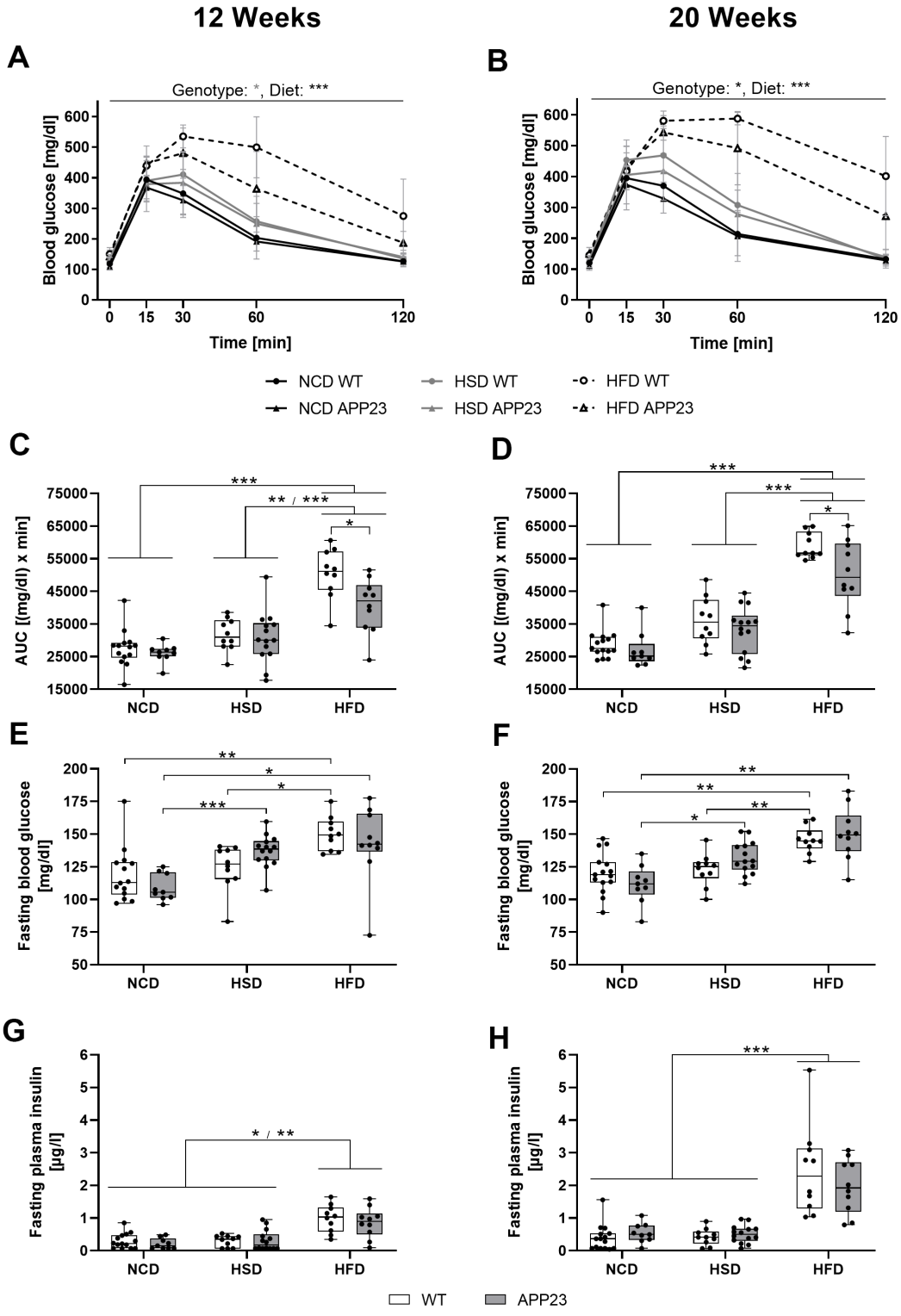

Figure 5. Acute glucose handling and fasting glucose homeostasis after 12 (left column) and 20 weeks (right column) of dietary interventions in APP23 and WT mice. (**A**, **B**) Course of blood glucose in an intraperitoneal glucose tolerance test (ipGTT) after 12 (**A**) and 20 weeks (**B**) and the corresponding area under the curve (AUC) (**C**, **D**). The corresponding basal blood glucose (**E**, **F**) and insulin levels (**G**, **H**) of WT and APP23 mice were analyzed after 6 h of fasting in the morning. Data are represented as box (25^{th} to 75^{th} percentile) with median and whiskers from minimum to maximum. Black asterisks indicate significant differences between groups (*: p<0.05; **: p<0.01; ***: p<0.001), gray asterisk indicates a statistical trend towards significance (p<0.1) according to nonparametric ANOVA-type statistics (**A**, **B**) ordinary 2-way ANOVA with Tukey post-hoc test (**C**, **D**) or nonparametric multiple contrast Tukey-type test (**E**–**H**). $n_{NCD\ WT}$=15, $n_{NCD\ APP23}$=9, $n_{HSD\ WT}$=10, $n_{HSD\ APP23}$=14, $n_{HFD\ WT}$=10, $n_{HFD\ APP23}$=10.

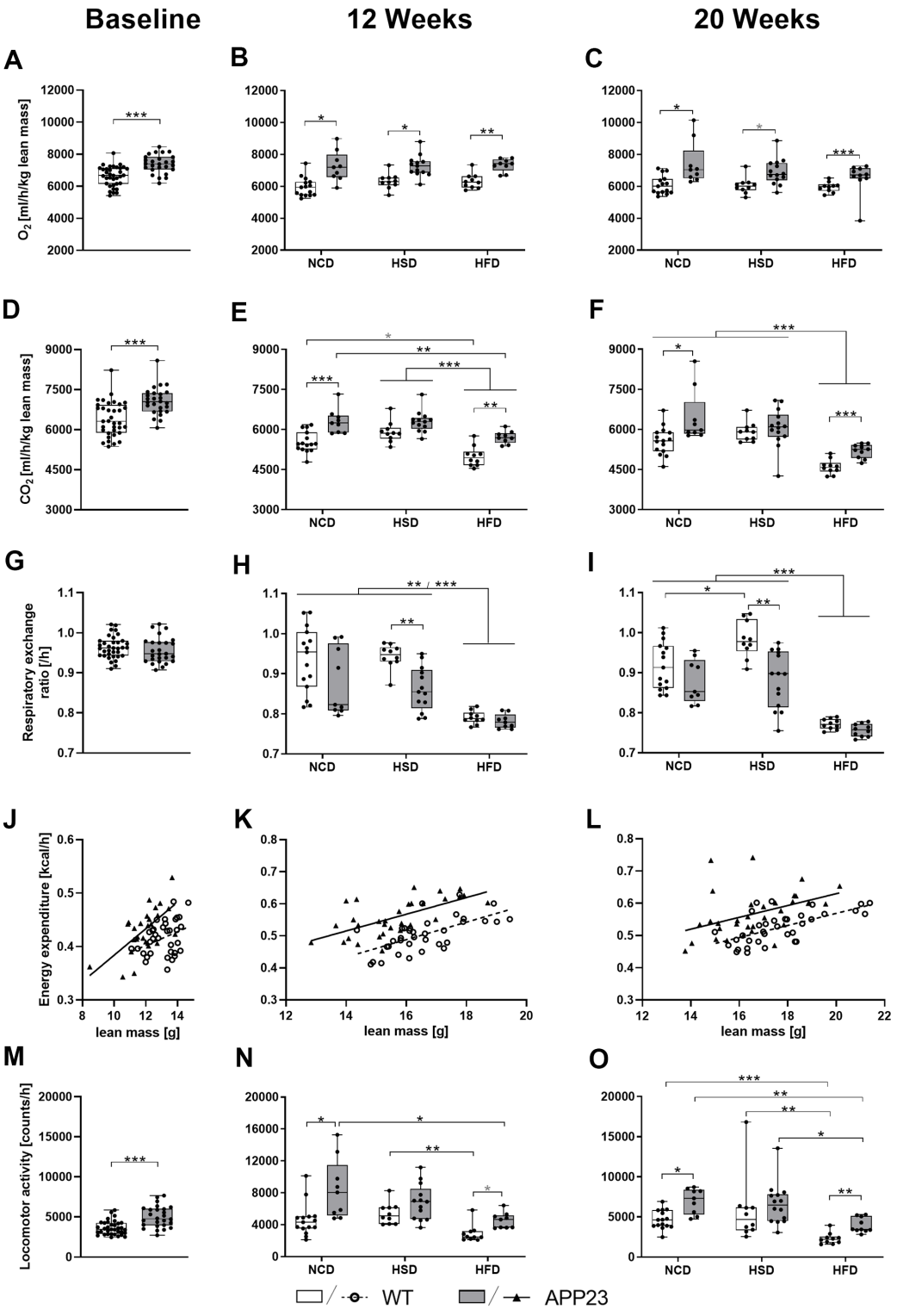

Figure 6. O_2 consumption, CO_2 production, respiratory exchange ratio, energy expenditure, and activity during active phase at baseline (left column), after 12 (middle column) and 20 weeks of diet (right column). (**A**–**C**) Averaged O_2 consumption per hour and (**D**–**F**) averaged CO_2 production per hour (both adjusted for lean mass) as well as (**G**–**I**) corresponding mean respiratory exchange ratio. (**J**–**L**) Averaged energy expenditure per hour correlated with lean mass and (**M**–**O**) averaged locomotor activity per hour. Data are represented as box (25^{th} to 75^{th} percentile) with median and whiskers from minimum to maximum. Black asterisks indicate significant differences between groups (*: p<0.05; **: p<0.01; ***: p<0.001), gray asterisk indicates a statistical trend towards significance (p<0.1) according to nonparametric t-tests (**A**, **D**, **G**, **M**), nonparametric multiple contrast Tukey-type test (**B**, **C**, **E**, **F**, **H**, **I**, **N**, **O**), and Spearman correlation followed by ANCOVA (**J**–**L**). $n_{NCD\ WT}$=15, $n_{NCD\ APP23}$=9, $n_{HSD\ WT}$=10, $n_{HSD\ APP23}$=14, $n_{HFD\ WT}$=10, $n_{HFD\ APP23}$=10.

in WT mice and week 20, whereas HFD decreased it up to 16% in both genotypes at both time-points.

Next, we evaluated energy expenditure and activity. To account for the major contribution of body weight, energy expenditure was correlated with lean mass (Figure 6J–6L and Supplementary Figure 1J–1L) or body weight (Supplementary Figure 2G–2I, 2P–2R; correlation statistics see Supplementary Table 4). Since diet alone did not affect energy expenditure, different dietary groups were pooled. APP23 mice showed 11% elevated energy expenditure compared to WT mice at baseline ($F(1,58)=15.488$, $p<0.001$ lean mass-corrected; Figure 6J), 9% in week 12 ($F(1,63)=51.102$, $p<0.001$ lean mass-corrected; Figure 6K) and 10% in week 20 ($F(1,65)=21.948$, $p<0.001$ lean mass-corrected; Figure 6L). Supplementary Figure 3 shows energy expenditure over the course of 24 h revealing a constantly increased energy expenditure of APP23 mice, especially pronounced during dark phase. Correspondingly, APP23 mice were 38% more active than WT mice at baseline (Figure 6M) and up to 84% and 71% in week 12 and 20 **(**Figure 6N, 6O). HFD feeding decreased locomotor activity up to 60% compared to NCD/HSD in both genotypes at both time-points.

Altogether, APP23 mice showed notably higher O_2 consumption, CO_2 production, and energy expenditure as well as increased activity. The effects of diet were mild and mainly represented by an HFD-induced reduction of activity and – as expected – of the respiratory exchange ratio.

Proteome analyses indicated potential mitochondrial dysfunction of APP23 mice

To investigate metabolic alterations in APP23 mice on protein level, we performed proteome analyses in liver (Figure 7) and brain (Supplementary Figure 4). Liver proteome profiles showed a genotype-clustering within NCD- and HSD-fed mice but a genotype-overlapping clustering within HFD-fed mice. (Figure 7A). Volcano plots displayed several differentially regulated proteins in APP23 mice, especially involved in lipid metabolism (CYP39A1, SDR39U1, AAMDC, FTO, ACOT8, VASP), oxidative phosphorylation, β-oxidation and general mitochondrial function (TBRG4, SCO2, MPV17, MRPL12, NDUFV2, NUBBPL, GLRX5, TIMM13, NFU1, COX5A, SCO1, CYP3A16, PDK4) or related to inflammation and metabolic stress (PRKAA2, SERPINB1A, TMEM258, LGALS3; Figure 7B–7D). Some mitochondria-related proteins were also differentially regulated in brain proteome of APP23 mice (MCEE, ADCK1) but the majority is involved in signal transduction, vesicle trafficking, synaptic function and neuronal plasticity (SYT17, DIP2A, BLOC1S1, SNCB, BAIAP3, WDR11, KCNIP3, TRAPPC13; Supplementary Figure 4). Simulation of metabolic capacities showed only minor differences in hepatic glucose tolerance. NCD-fed APP23 mice had slightly better glucose tolerance at low external glucose, while their glucose tolerance was slightly inferior at high external glucose ($F(9,90)=2.710$, $p=0.008$), contrary during HSD ($F(9,90)=5.750$, $p<0.001$) and without difference during HFD (Figure 7E–7G). NEFA tolerance seemed to be slightly decreased in NCD- and HSD-fed APP23 mice (n.s.; Figure 7H–7J). Gene Set Enrichment Analysis (GSEA) revealed downregulation of protein sets affecting lipid metabolism, oxidative phosphorylation, and mitochondrial function in NCD-fed APP23 mice (Figure 7K). Interestingly, the same protein sets were upregulated in HSD-fed APP23 mice but unchanged in HFD-fed APP23 mice. Instead, protein sets contributing to translation and amino acid metabolism were downregulated.

DISCUSSION

Involuntary weight loss advances with AD progression resulting in poorer health, reduced quality of life, and increased mortality [14]. Thus, identifying the role of (reduced) body weight in AD might contribute to the understanding of metabolic implications in AD pathogenesis. Therefore, we investigated APP23 mice during diet-induced metabolic challenge. To our knowledge, this is the first longitudinal study assessing metabolic features of APP23 females, revealing lower body weight, less adipocyte hypertrophy as well as steatosis, elevated energy expenditure as well as activity and evidence for potential mitochondrial damage.

A lower body weight already emerges in 4-week old APP23 mice due to lower lean mass, whereas plaque development starts around 6 months of age [20]. However, lower body weight of APP23 mice did not result from smaller body length, which was also reported for 24-months old APP23 females [21]. Although APP23 mice do not model AD-related weight loss, their lower body weight at a pre-plaque stage corresponds to lower body weight of AD patients, which arises from early weight loss prior to the onset of clinical AD symptoms [16, 22]. Consistent with literature, HSD induced a mild, but HFD a substantial body weight gain [19, 23–25], in which APP23 mice gained less fat mass. Analysis of food intake as a potential mechanism for lower body weight revealed lower HFD consumption, contradicting a study in APP23 males reporting increased food intake [26]. However, estrogen might have influenced food intake via its interaction with leptin [27], counterbalancing food intake in APP23 females. HFD contains less carbohydrates than NCD and HSD but similar amounts

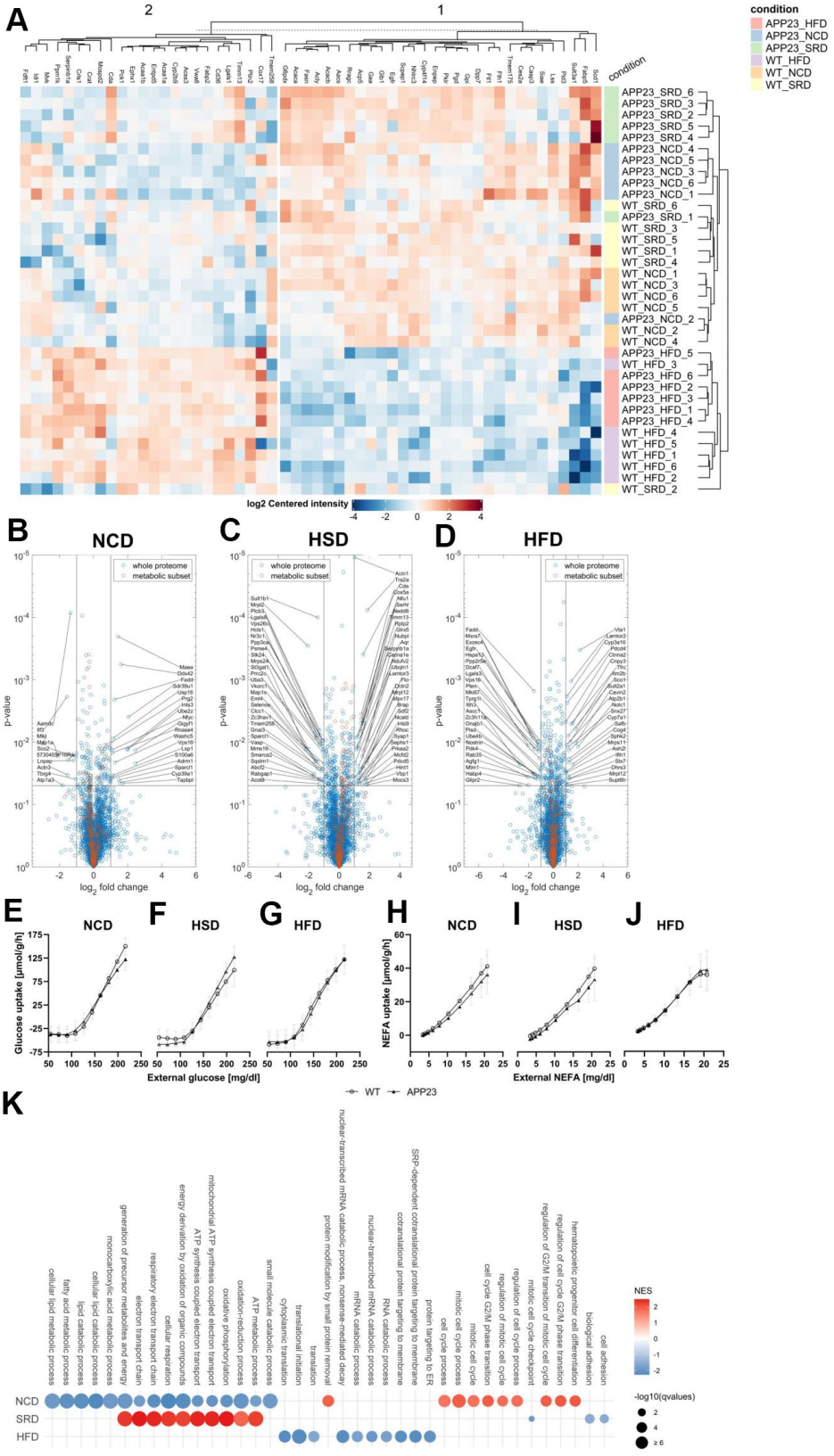

Figure 7. Proteome analyses of liver tissue. (**A**) Heatmap of differentially regulated proteins (**B**–**D**) Volcano plots of APP23 versus WT mice within each diet. (**E**–**G**) Simulated hepatic glucose tolerance of APP23 versus WT mice within each diet. (**H**–**J**) Simulated hepatic NEFA tolerance of APP23 versus WT mice within each diet. (**K**) GSEA of APP23 versus WT mice within each diet. (**B**, **E**, **H**) NCD; (**C**, **F**, **I**) HSD; (**D**, **G**, **J**) HFD. n=6 each.

of protein, which may explain the increased HFD-intake of WT mice, as mice adapt their food intake to a favored low protein/high carbohydrate ratio even by overeating [28]. In contrast, food intake of APP23 mice remained constant regardless of diet suggesting potential alterations of nutrient-specific feedback mechanisms. This is corroborated by a study in Tg2576 mice (same *App* mutation/different promoter) revealing dysfunctional hypothalamic leptin signaling depicted by decreased leptin levels [29]. The fact that hyperactivity and increased energy expenditure of APP23 mice were not compensated by higher food intake, as one could have expected [30], also suggests a dysregulation of energy balance. Since the hypothalamus plays a crucial role in regulating food intake and energy balance [31], altered nutrient-specific feedback and lacking compensatory hyperphagia in APP23 mice might be caused by altered hypothalamic leptin signaling [32]. Altogether, although APP23 mice displayed only reduced food intake during HFD, compensatory hyperphagia to account for increased energy expenditure was not observed during any diet and, thus, potentially contributing to lower body weight of APP23 mice. As a potential underlying mechanism, hypothalamic leptin signaling in APP23 mice deserves further investigations.

Necropsy showed that while HSD induced mild liver weight gain only in WT mice, HFD induced substantial liver weight gain in both genotypes. Histology and triglyceride quantification revealed progressive steatosis, however diminished in APP23 mice, especially during HFD. The lower degree of steatosis in APP23 mice corresponds to their lower body weight. Indeed, it has been shown in weight loss experiments that body weight strongly influences the extent of hepatic steatosis [33]. Furthermore, steatosis considerably contributes to insulin resistance via hepatic inflammation [34]. Actually, the degree of steatosis was to some extent reflected in insulin levels: HFD-fed WT mice showed the most prominent steatosis accompanied by the most prominent elevation of insulin levels, while the lower extent of steatosis in HFD-fed APP23 mice might contribute to a less prominent insulin resistance. HSD related body weight gain and the corresponding degree of steatosis might not be sufficient to induce insulin resistance. Consistently, only HFD but not HSD elevated eWAT weight. Adipocyte size gradually increased from NCD to HFD, APP23 mice exhibiting less hypertrophy. Hypertrophic instead of hyperplastic adipose tissue expansion indicates metabolic disease [35]. Thus, HSD-induced hypertrophy without increased fat mass suggests an incipient metabolic dysfunction.

We longitudinally monitored glycemic control via fed insulin concentrations. Gradually increasing insulin levels during HFD indicate a compensation of beginning insulin resistance via higher insulin secretion to maintain physiological glucose levels. As insulin sensitivity is strongly correlated with body weight [36], lower body weight of APP23 mice together with the lesser degree of steatosis potentially accounts for lower insulin levels in HFD-fed APP23 mice suggesting superior insulin sensitivity. Furthermore, we examined corticosterone as a functional antagonist of insulin and NEFA as a correlate for lipolysis. Corticosterone levels were similar between genotypes as already described [19], possibly due to young age and low Aβ load of APP23 mice [37]. NEFA levels were unaltered by genotype but reduced by HFD, potentially due to the lipolysis-inhibiting effect of elevated insulin levels [38]. This observation rather points to a still physiological insulin sensitivity, as obesity and insulin resistance lead to increased lipolysis [39]. Additionally, fasting glucose and insulin levels were unaltered in APP23 mice.

Although reduced brain glucose metabolism occurs early in AD progression [40], peripheral glycemic dysfunction is under debate and was not observed in APP23 mice. Evidence suggests that glycemic dysregulation in AD might be mediated by peripheral Aβ [41], which is low in APP23 mice [42]. Together with lower body weight and less steatosis this might account for an even slightly superior peripheral metabolism supporting current literature [43]. HFD considerably deteriorated glucose tolerance already after 12 weeks potentially via a combination of elevated hepatic and adipose tissue inflammation, lipid overload and hypothalamic alterations [44]. HSD aggravated glucose tolerance only moderately after 20 weeks, possibly due to the scarce effect on body weight considering obesity a major contributor to glucose intolerance.

To further investigate mechanisms underlying lower body weight of APP23 mice, indirect calorimetry was evaluated. We showed for the first time that APP23 mice consumed notably more O_2 and produced notably more CO_2, indicating an increased metabolic rate even before Aβ plaque development. This finding confirms a study in pre-plaque Tg2576 mice with increased O_2 consumption also at rest [29]. Interestingly, the respiratory exchange ratio of NCD- and HSD-fed APP23 mice was decreased, suggesting a tendency towards fat instead of carbohydrates burning, potentially contributing to lower body weight and adiposity in APP23 mice. Furthermore, energy expenditure was elevated in APP23 mice, accompanied by hyperactivity. Hyperactivity has previously been observed in APP23 males, especially towards the end of the active phase, potentially reflecting so-called sundowning behavior of AD patients [45]. Whereas

energy expenditure was unaffected by diet, activity was reduced during HFD as described [46]. The finding that HFD reduced activity but not energy expenditure and O_2 consumption, suggests that elevated energy expenditure of APP23 mice might not solely depend on increased activity. Altogether, this indicates that increased O_2 consumption, CO_2 production, and energy expenditure of APP23 mice are probably not only caused by hyperactivity but additionally by an increased resting metabolic rate.

Interestingly, our proteome analyses imply a mitochondrial dysfunction of APP23 mice. Studies indicate that dysfunctions of cerebral mitochondria, potentially induced by Aβ, might play a central role in AD pathogenesis [47]. Earlier proteome studies in APP23 brains revealed altered expression of proteins associated with glycolysis and oxidative phosphorylation as well as increased oxidative stress represented by a higher proportion of carbonylated proteins [48]. We also report alterations in mitochondria-related proteins in brain tissue. Even more interesting, we observed very similar modifications in liver tissue, revealing differential expression of proteins involved in oxidative phosphorylation, β-oxidation, and metabolic stress. Hence, our data might indicate a general mitochondrial dysfunction in APP23 mice not only limited to neurons. Notably, this dysfunction seems to be counterbalanced by HSD, potentially due to massive substrate provision (i.e. sucrose) possibly stimulating mitochondrial pathways. It has been shown previously that HSD induces overexpression of specific mitochondrial proteins in hepatocytes and increases the mitochondrial production of reactive oxygen species [49]. This reaction – normally a sign of oxidative stress – might be beneficial in HSD-fed APP23 mice to compensate for mitochondrial dysfunction represented by downregulated mitochondrial proteins in NCD-fed APP23 mice. This is in line with slightly inferior hepatic glucose tolerance in NCD-fed APP23 mice compared to slightly superior hepatic glucose tolerance in HSD-fed APP23 mice. As HFD and hepatic steatosis have been shown to induce oxidative stress and mitochondrial damage [50], we assumed a differential regulation of mitochondrial pathways in HFD-fed mice, however, found no such evidence. Moreover, a transcriptome analysis of HFD-fed APP23 brains has shown higher expression of genes involved in immune response and inflammation due to HFD [25], which was not obvious in our brain tissue on protein level. However, mice in the mentioned study were 12-months old, thus potentially being more prone to inflammation due to their advanced plaque pathology.

In summary, this study is the first to systematically analyze lower body weight of pre-plaque APP23 mice, extensively characterizing metabolic features of this murine AD model. Although our data is descriptive, we conclude that lower body weight of APP23 mice is most likely caused by a combination of hyperactivity, increased metabolism, and dysregulated energy balance reflected by the absence of compensatory feeding mechanisms. Furthermore, we found evidence of dysfunctional mitochondrial pathways not only in the brain but for the first time also in the liver. These findings are highly interesting with regard to emerging hypotheses about the implication of mitochondrial dysfunction in AD pathogenesis. Both, mitochondrial dysfunction as well as altered hypothalamic leptin signaling deserve further research as they might underlie the described metabolic changes in APP23 females. Interestingly, lower body weight of APP23 mice may partially protect from diet-induced metabolic stress depicted by extenuated steatosis and adipocyte hypertrophy, which seem to contribute to improved insulin sensitivity. As the translation of basic animal research into the clinic is challenging, we strongly encourage thorough metabolic investigation of AD patients to contribute to the understanding of metabolic implications in AD pathogenesis.

MATERIALS AND METHODS

Ethics statement

This study was approved by the local animal ethics committee (LAGeSo Berlin; G0074/16) and carried out in accordance with EU Directive 10/63/EU as well as in line with the ARRIVE guidelines.

Animal experiments

The study was conducted in 33 female transgenic APP23 mice (APP23) and 35 female healthy littermates (WT) on a C57BL/6J background. APP23 mice overexpress human APP_{751} cDNA with the Swedish double mutation under the murine Thy-1 promotor [20]. Aβ plaque deposition starts at 6 months of age [20]. Mice were group-housed (2-3/cage) in environmentally controlled, individually ventilated cages (21.5° C±1.5) with a 12-hour light/dark cycle and ad libitum access to food and water. 4-6-week old mice were randomly allocated to normal-control (NCD), high-sucrose (HSD) or high-fat diet (HFD; all Research Diets) for 20 weeks (Figure 1B and Supplementary Table 1). Body weight and food intake were recorded weekly (Figure 1A). Body length was exemplarily measured from tip of the nose to tail root in a separate set of young adult mice (8-11-week old female and male APP23 (n=11, thereof 4 females) and WT mice (n=8, thereof 2 females)). Monthly, body composition was measured by ^{1}H-magnetic-resonance-

spectroscopy (NMR) using a Minispec LF50 (Bruker) and blood was collected from *Vena facialis* in the morning. Serum was stored at -80° C for analysis of insulin levels. Indirect calorimetry and activity were analyzed in single-caged mice (LabMaster-System, TSE) for 48 h (12 h adaption/36 h evaluation: 1 light and mean of 2 dark phases) in week 0, 12, and 20. Intraperitoneal (i.p.) glucose tolerance tests (ipGTT) were performed in week 12 and 20 after a 6 h morning-fast and local analgesia of tail tip (lidocaine/prilocain, AstraZeneca). Glucose levels were measured in duplicates (Contour Next, Bayer) before (0 min), 15, 30, 60, and 120 min after injection of 2 g/kg body weight glucose. At 0 min, plasma was additionally collected and stored at -80° C for analysis of fasting insulin levels. Terminally, mice were sacrificed as described [19]. Plasma was stored at -80° C. Tissues were stored partially snap-frozen (-80° C) and partially in 4% PFA/PBS (4° C).

Histology and immunohistochemistry

PFA-fixed livers were transferred in O.C.T. Compound (Sakura) and 5 µm sections were cryocut using a Jung Frigocut 2800E (Leica). eWAT was dehydrated, infiltrated and embedded with paraffin and 5 µm sections were cut using a Microm Cool-Cut HM 325 (ThermoFisher).

eWAT and liver sections were stained with hematoxylin/eosin and Oil Red O, respectively, as described [51]. Hematoxylin/eosin-stained eWAT (4 sections of 6 random mice/genotype/diet) and Oil Red O-stained liver (4 sections of 8 random mice/genotype/diet) were recorded with 20x on a BZ-9000 microscope (Keyence). Average adipocyte size and mean percentage Oil Red O-covered area were analyzed with ImageJ (V1.52a).

Biochemical analyses

Triglycerides were quantified in liver tissue (6 random mice/genotype/diet). Frozen liver (~60 mg) was suspended in 600 µl alcoholic KOH and incubated at 60° C for 6 h. 540 µl 1M $MgCl_2$ were added to 500 µl of the saponificated sample, followed by 10 min incubation on ice and 30 min centrifugation at full speed. Supernatant was collected and analyzed according to manufacturer instructions using the Triglycerides FS 10' kit (Diagnostic Systems). Triglyceride concentrations were multiplied by actual liver weight measured upon sacrifice to obtain absolute values.

Fed insulin was quantified in serum and fasting insulin in plasma using the Mouse Insulin ELISA kit (Mercodia). Corticosterone and NEFAs were measured in final plasma using the Corticosterone ELISA kit (IBL International) and the NEFA-HR(2) kit (Wako).

Proteomics

Frozen whole-brain (350-450 mg, 4 random mice/genotype/diet) was prepared and homogenized. 18-55 mg were used for lysates, 30 µg digested and 1 µg was analyzed using nano-LC-MS/MS as described [52, 53]. Data were processed with MaxQuant (V1.6.0.1) [54] and searched against mouse UniProtKB with 21,074 entries, released 12/2018.

Frozen liver (~5mg, 6 random mice/genotype/diet) was suspended in 75 µl lysis buffer (1% SDS/100 mM ABC+1.25x PIC), sonicated twice (Covaris ML230: PIP 375 W, DF 25%, CPB 50, 20 repeats, 10 s pulse, 10 s delay, 12 C, dither 3 mm Y-axis) and insoluble particles were removed by centrifugation. 15 µl lysate was adjusted to 50 µl with water and processed on a Biomek i7 workstation using protocol SP3 [55]. On a two-column-system 1.25 µg tryptic peptides were analyzed by LC-MS/MS [53]. Separation was done by applying a gradient from 7.5% to 55% B in 120 min at a flow rate of 300 nL/min (solvent A: 0.1% formic acid in water; solvent B: 80% acetonitrile and 0.1% formic acid). The Orbitrap was configured to acquire 25 × 24 m/z (covering 400-1000 m/z), precursor isolation window data independent acquisition (DIA) spectra (17,500 resolution, AGC target 1e6, maximum inject time 60ms, normalized HCD collision energy 27%) using overlapping windows. A full scan MS spectra (m/z 400-1000) was recorded at 35,000 resolution after 60 ms accumulation of ions to a 1e6 target value in profile mode. Raw data were processed using DIA-NN 1.7.12 [56], scan window size set to 14 and MS2 and MS1 mass accuracies to 20 and 10 ppm, respectively. A project-independent public spectral library [57] and mouse UniProt (UP000000589) were used for annotation. The library was automatically refined based on the dataset, global q=0.01 (using the "Generate spectral library" option in DIA-NN) [58].

Modeling of metabolic capacities

Metabolic capabilities of individual mice were evaluated using an established kinetic model of the energy metabolism of hepatic and neuronal cells encompassing glycolysis, citric acid cycle, the respiratory chain and oxidative phosphorylation [59, 60]. This model describes the dynamic of metabolites and fluxes via ordinary differential equations taking into account the regulatory properties of the underlying metabolic enzymes, such as substrate affinities (K_m-values), allosteric properties (K_i-values and K_a-values) and alterations in these parameters due to

phosphorylation (interconversion). It distinguished between different cellular compartments (cytosol, mitochondria, endoplasmatic reticulum). As maximal enzyme activity is proportional to protein abundance, individualized models were generated scaling the maximal enzyme activities (V_{max}) of each metabolic enzyme and transporter by the relation $V_{max}^{animal} = V_{max}^{control} . \frac{E^{animal}}{E^{control}}$, where $E^{control}$ is the average enzyme intensity in all controls and E^{animal} is the enzyme concentration in the individual animal. Metabolic capacities were simulated by systemic variation of the external conditions (plasma nutrient and hormone composition). Hepatic glucose exchange flux was simulated by simultaneous variation of plasma glucose concentration, plasma free fatty acid concentration and plasma insulin and glucagon concentrations as in [59, 61, 62]. MATLAB (Release2012a; optimization toolbox) was used for simulations and respective graphs.

Statistics

Data are represented as boxes (25^{th} to 75^{th} percentile) with median and min/max-whiskers or as mean with standard deviation. SPSS Statistics (V25), GraphPad Prism (V8), and R (V3.6.3; packages nparcomp, nparLD, car, DEP, clusterProfiler) were used for statistics and graphs.

MS output was filtered (FDR=0.01) at peptide level and for completeness in at least one experimental group, missing values were imputed and all contrasts between experimental groups were analyzed for differentially expressed proteins ($\alpha \leq 0.05$, absolute log2 fold-change≥ 1). Volcano plots and heatmaps were automatically generated. For GSEA, data were mapped to the human annotation and biological processes from the gene ontology database were selected. Results were filtered (20-500 gene set size, $q \leq 0.01$) and the top-10 enriched terms per contrast and direction were plotted.

Shapiro-Wilk test for normal distribution and Levene's test for equality of variances were applied. If passed, 2-way ANOVA (ordinary/repeated measures) with Tukey post-hoc test was performed. Otherwise, nonparametric t-test, nonparametric multiple contrast test type Tukey, or nonparametric (repeated measures) ANOVA-type statistics were chosen. According to [63], ANCOVA was performed for analysis of pooled energy expenditure data to correct for lean mass-/body weight-effects. Therefore, equality of slopes was checked by simple linear regression before pooling dietary groups in a first step, energy expenditure was correlated with lean mass/body weight using Spearman correlation in a second step and finally ANCOVA was performed. Significance was considered *$p \leq 0.05$, **$p \leq 0.01$, ***$p \leq 0.001$, trends towards significance ($p < 0.1$) are displayed in gray. No data were excluded from any analysis.

Data availability

The datasets generated and/or analyzed during the current study are available from the corresponding author on reasonable request.

Abbreviations

APP23: transgenic mouse model; AD: Alzheimer's disease; AUC: area under the curve; BL: blood withdrawal; BW: body weight; EE: energy expenditure; eWAT: epigonadal white adipose tissue; GSEA: gene set enrichment analysis; GTT: glucose tolerance test; HFD: high-fat diet; HSD: high-sucrose diet; i.p.: intraperitoneal; LM: LabMaster; MS: mass spectrometry; NCD: normal-control diet; NEFA: non-esterified free fatty acids; n.s.: non-significant; RER: respiratory exchange ratio; WT: wild type control littermates.

AUTHOR CONTRIBUTIONS

S. S.: Conceptualization, Methodology, Investigation, Formal analysis, Visualization, Writing - original draft, Funding acquisition. N. B.: Software, Formal analysis. J. E.: Software, Formal analysis. M. M.: Methodology, Investigation Software, Formal analysis, Visualization. S. H.-S.: Writing - review and editing. C. K.: Conceptualization, Writing - review and editing. B. A.: Investigation. A. P.: Investigation, Writing - review and editing. D. M.: Investigation, Resources. J. S.: Resources, Funding acquisition, Writing - review and editing. B. S.: Resources, Funding acquisition, Project administration, Writing - review and editing. S. B.: Conceptualization, Methodology, Investigation, Formal analysis, Resources, Funding acquisition, Supervision, Writing - review and editing.

ACKNOWLEDGMENTS

The authors thank Diana Woellner, Marie-Christin Gaerz, Nadine Huckauf, and Candy Kalischke (Charité – Universitätsmedizin Berlin) for excellent assistance with mouse and biochemical experiments, as well as Beata Lukaszewska-McGreal (Max Planck Institute for Molecular Genetics) and Dr. Kathrin Textoris-Taube (High Throughput Mass Spectrometry Core Facility of Charité – Universitätsmedizin Berlin) for brain and liver proteome sample preparation and measurements. Proteome analyses for brain were conducted at Max Planck Institute for Molecular

Genetics and for liver at the High Throughput Mass Spectrometry Core Facility of Charité – Universitätsmedizin Berlin.

Sebastian Brachs and Joachim Spranger are further associated with the Center for Cardiovascular Research (CCR) at the Charité – Universitätsmedizin Berlin, Hessische Straße 3-4, 10115 Berlin, Germany.

CONFLICTS OF INTEREST

The authors declare that they have no conflicts of interest.

FUNDING

This work was supported by the Department of Endocrinology and Metabolism, Charité – Universitätsmedizin Berlin, Deutsches Zentrum für Herz-Kreislauf-Forschung (DZHK/BMBF), the Deutsche Diabetes Gesellschaft (DDG), and the Berlin Institute of Health (BIH). Stefanie Schreyer was granted the Elsa-Neumann-Scholarship of the state Berlin and the graduation scholarship of Charité – Universitätsmedizin Berlin. Johannes Eckstein was funded by "LiSyM" 31L0057 (BMBF). Furthermore, brain proteome analyses were funded by the Max Planck Society.

REFERENCES

1. Korczyn AD. Why have we failed to cure Alzheimer's disease? J Alzheimers Dis. 2012; 29:275–82. https://doi.org/10.3233/JAD-2011-110359 PMID:22258512

2. Atri A. The Alzheimer's Disease Clinical Spectrum: Diagnosis and Management. Med Clin North Am. 2019; 103:263–93. https://doi.org/10.1016/j.mcna.2018.10.009 PMID:30704681

3. Patterson C. World Alzheimer Report 2018. Alzheimer's Dis Int. 2018. https://doi.org/10.1111/j.0033-0124.1950.24_14.x

4. Glenner GG, Wong CW. Alzheimer's disease: initial report of the purification and characterization of a novel cerebrovascular amyloid protein. Biochem Biophys Res Commun. 1984; 120:885–90. https://doi.org/10.1016/S0006-291X(84)80190-4 PMID:6375662

5. Grundke-Iqbal I, Iqbal K, Tung YC, Quinlan M, Wisniewski HM, Binder LI. Abnormal phosphorylation of the microtubule-associated protein tau (tau) in Alzheimer cytoskeletal pathology. Proc Natl Acad Sci USA. 1986; 83:4913–17. https://doi.org/10.1073/pnas.83.13.4913 PMID:3088567

6. Larson EB, Kukull WA, Katzman RL. Cognitive impairment: dementia and Alzheimer's disease. Annu Rev Public Health. 1992; 13:431–49. https://doi.org/10.1146/annurev.pu.13.050192.002243 PMID:1599598

7. Hardy JA, Higgins GA. Alzheimer's disease: the amyloid cascade hypothesis. Science. 1992; 256:184–85. https://doi.org/10.1126/science.1566067 PMID:1566067

8. Foroutan N, Hopkins RB, Tarride JE, Florez ID, Levine M. Safety and efficacy of active and passive immunotherapy in mild-to-moderate Alzheimer's disease: a systematic review and network meta-analysis. Clin Invest Med. 2019; 42:E53–65. https://doi.org/10.25011/cim.v42i1.32393 PMID:30904037

9. Li X, Song D, Leng SX. Link between type 2 diabetes and Alzheimer's disease: from epidemiology to mechanism and treatment. Clin Interv Aging. 2015; 10:549–60. https://doi.org/10.2147/CIA.S74042 PMID:25792818

10. Correia SC, Santos RX, Carvalho C, Cardoso S, Candeias E, Santos MS, Oliveira CR, Moreira PI. Insulin signaling, glucose metabolism and mitochondria: major players in Alzheimer's disease and diabetes interrelation. Brain Res. 2012; 1441:64–78. https://doi.org/10.1016/j.brainres.2011.12.063 PMID:22290178

11. de la Monte SM. Type 3 diabetes is sporadic Alzheimer's disease: mini-review. Eur Neuropsychopharmacol. 2014; 24:1954–60. https://doi.org/10.1016/j.euroneuro.2014.06.008 PMID:25088942

12. Emmerzaal TL, Kiliaan AJ, Gustafson DR. 2003-2013: a decade of body mass index, Alzheimer's disease, and dementia. J Alzheimers Dis. 2015; 43:739–55. https://doi.org/10.3233/JAD-141086 PMID:25147111

13. Power BD, Alfonso H, Flicker L, Hankey GJ, Yeap BB, Almeida OP. Changes in body mass in later life and incident dementia. Int Psychogeriatr. 2013; 25:467–78. https://doi.org/10.1017/S1041610212001834 PMID:23151427

14. Gillette Guyonnet S, Abellan Van Kan G, Alix E, Andrieu S, Belmin J, Berrut G, Bonnefoy M, Brocker P, Constans T, Ferry M, Ghisolfi-Marque A, Girard L, Gonthier R, et al, and International Academy on Nutrition and Aging Expert Group. IANA (International Academy on Nutrition and Aging)

Expert Group: weight loss and Alzheimer's disease. J Nutr Health Aging. 2007; 11:38–48. PMID:17315079

15. Cova I, Clerici F, Rossi A, Cucumo V, Ghiretti R, Maggiore L, Pomati S, Galimberti D, Scarpini E, Mariani C, Caracciolo B. Weight Loss Predicts Progression of Mild Cognitive Impairment to Alzheimer's Disease. PLoS One. 2016; 11:e0151710. https://doi.org/10.1371/journal.pone.0151710 PMID:26990757

16. Johnson DK, Wilkins CH, Morris JC. Accelerated weight loss may precede diagnosis in Alzheimer disease. Arch Neurol. 2006; 63:1312–17. https://doi.org/10.1001/archneur.63.9.1312 PMID:16966511

17. Ross R, Soni S, Houle SA. Negative Energy Balance Induced by Exercise or Diet: Effects on Visceral Adipose Tissue and Liver Fat. Nutrients. 2020; 12:891. https://doi.org/10.3390/nu12040891 PMID:32218121

18. Knight EM, Verkhratsky A, Luckman SM, Allan SM, Lawrence CB. Hypermetabolism in a triple-transgenic mouse model of Alzheimer's disease. Neurobiol Aging. 2012; 33:187–93. https://doi.org/10.1016/j.neurobiolaging.2010.02.003 PMID:20359775

19. Schreyer S, Klein C, Pfeffer A, Rasińska J, Stahn L, Knuth K, Abuelnor B, Panzel AE, Rex A, Koch S, Hemmati-Sadeghi S, Steiner B. Chia seeds as a potential cognitive booster in the APP23 Alzheimer's disease model. Sci Rep. 2020; 10:18215. https://doi.org/10.1038/s41598-020-75209-z PMID:33106576

20. Sturchler-Pierrat C, Abramowski D, Duke M, Wiederhold KH, Mistl C, Rothacher S, Ledermann B, Bürki K, Frey P, Paganetti PA, Waridel C, Calhoun ME, Jucker M, et al. Two amyloid precursor protein transgenic mouse models with Alzheimer disease-like pathology. Proc Natl Acad Sci USA. 1997; 94:13287–92. https://doi.org/10.1073/pnas.94.24.13287 PMID:9371838

21. Lalonde R, Dumont M, Staufenbiel M, Strazielle C. Neurobehavioral characterization of APP23 transgenic mice with the SHIRPA primary screen. Behav Brain Res. 2005; 157:91–98. https://doi.org/10.1016/j.bbr.2004.06.020 PMID:15617775

22. Stewart R, Masaki K, Xue QL, Peila R, Petrovitch H, White LR, Launer LJ. A 32-year prospective study of change in body weight and incident dementia: the Honolulu-Asia Aging Study. Arch Neurol. 2005; 62:55–60. https://doi.org/10.1001/archneur.62.1.55 PMID:15642850

23. Yeh SH, Shie FS, Liu HK, Yao HH, Kao PC, Lee YH, Chen LM, Hsu SM, Chao LJ, Wu KW, Shiao YJ, Tsay HJ. A high-sucrose diet aggravates Alzheimer's disease pathology, attenuates hypothalamic leptin signaling, and impairs food-anticipatory activity in APPswe/PS1dE9 mice. Neurobiol Aging. 2020; 90:60–74. https://doi.org/10.1016/j.neurobiolaging.2019.11.018 PMID:31879131

24. Oliveira LS, Santos DA, Barbosa-da-Silva S, Mandarim-de-Lacerda CA, Aguila MB. The inflammatory profile and liver damage of a sucrose-rich diet in mice. J Nutr Biochem. 2014; 25:193–200. https://doi.org/10.1016/j.jnutbio.2013.10.006 PMID:24445044

25. Nam KN, Mounier A, Wolfe CM, Fitz NF, Carter AY, Castranio EL, Kamboh HI, Reeves VL, Wang J, Han X, Schug J, Lefterov I, Koldamova R. Effect of high fat diet on phenotype, brain transcriptome and lipidome in Alzheimer's model mice. Sci Rep. 2017; 7:4307. https://doi.org/10.1038/s41598-017-04412-2 PMID:28655926

26. Vloeberghs E, Van Dam D, Franck F, Serroyen J, Geert M, Staufenbiel M, De Deyn PP. Altered ingestive behavior, weight changes, and intact olfactory sense in an APP overexpression model. Behav Neurosci. 2008; 122:491–97. https://doi.org/10.1037/0735-7044.122.3.491 PMID:18513119

27. Fungfuang W, Terada M, Komatsu N, Moon C, Saito TR. Effects of estrogen on food intake, serum leptin levels and leptin mRNA expression in adipose tissue of female rats. Lab Anim Res. 2013; 29:168–73. https://doi.org/10.5625/lar.2013.29.3.168 PMID:24106512

28. Solon-Biet SM, McMahon AC, Ballard JW, Ruohonen K, Wu LE, Cogger VC, Warren A, Huang X, Pichaud N, Melvin RG, Gokarn R, Khalil M, Turner N, et al. The ratio of macronutrients, not caloric intake, dictates cardiometabolic health, aging, and longevity in ad libitum-fed mice. Cell Metab. 2014; 19:418–30. https://doi.org/10.1016/j.cmet.2014.02.009 PMID:24606899

29. Ishii M, Wang G, Racchumi G, Dyke JP, Iadecola C. Transgenic mice overexpressing amyloid precursor protein exhibit early metabolic deficits and a pathologically low leptin state associated with hypothalamic dysfunction in arcuate neuropeptide Y neurons. J Neurosci. 2014; 34:9096–106. https://doi.org/10.1523/JNEUROSCI.0872-14.2014 PMID:24990930

30. Drenowatz C. Reciprocal Compensation to Changes in Dietary Intake and Energy Expenditure within the Concept of Energy Balance. Adv Nutr. 2015; 6:592–99. https://doi.org/10.3945/an.115.008615 PMID:26374181

31. Abdalla MM. Central and peripheral control of food intake. Endocr Regul. 2017; 51:52–70. https://doi.org/10.1515/enr-2017-0006 PMID:28222022

32. Xu AW, Kaelin CB, Morton GJ, Ogimoto K, Stanhope K, Graham J, Baskin DG, Havel P, Schwartz MW, Barsh GS. Effects of hypothalamic neurodegeneration on energy balance. PLoS Biol. 2005; 3:e415. https://doi.org/10.1371/journal.pbio.0030415 PMID:16296893

33. Vilar-Gomez E, Martinez-Perez Y, Calzadilla-Bertot L, Torres-Gonzalez A, Gra-Oramas B, Gonzalez-Fabian L, Friedman SL, Diago M, Romero-Gomez M. Weight Loss Through Lifestyle Modification Significantly Reduces Features of Nonalcoholic Steatohepatitis. Gastroenterology. 2015; 149:367–78.e5. https://doi.org/10.1053/j.gastro.2015.04.005 PMID:25865049

34. Cai D, Yuan M, Frantz DF, Melendez PA, Hansen L, Lee J, Shoelson SE. Local and systemic insulin resistance resulting from hepatic activation of IKK-beta and NF-kappaB. Nat Med. 2005; 11:183–90. https://doi.org/10.1038/nm1166 PMID:15685173

35. Laforest S, Labrecque J, Michaud A, Cianflone K, Tchernof A. Adipocyte size as a determinant of metabolic disease and adipose tissue dysfunction. Crit Rev Clin Lab Sci. 2015; 52:301–13. https://doi.org/10.3109/10408363.2015.1041582 PMID:26292076

36. Clamp LD, Hume DJ, Lambert EV, Kroff J. Enhanced insulin sensitivity in successful, long-term weight loss maintainers compared with matched controls with no weight loss history. Nutr Diabetes. 2017; 7:e282. https://doi.org/10.1038/nutd.2017.31 PMID:28628125

37. Dong H, Yuede CM, Yoo HS, Martin MV, Deal C, Mace AG, Csernansky JG. Corticosterone and related receptor expression are associated with increased beta-amyloid plaques in isolated Tg2576 mice. Neuroscience. 2008; 155:154–63. https://doi.org/10.1016/j.neuroscience.2008.05.017 PMID:18571864

38. Stich V, Berlan M. Physiological regulation of NEFA availability: lipolysis pathway. Proc Nutr Soc. 2004; 63:369–74. https://doi.org/10.1079/PNS2004350 PMID:15294057

39. Arner P, Langin D. Lipolysis in lipid turnover, cancer cachexia, and obesity-induced insulin resistance. Trends Endocrinol Metab. 2014; 25:255–62. https://doi.org/10.1016/j.tem.2014.03.002 PMID:24731595

40. Mosconi L. Brain glucose metabolism in the early and specific diagnosis of Alzheimer's disease. FDG-PET studies in MCI and AD. Eur J Nucl Med Mol Imaging. 2005; 32:486–510. https://doi.org/10.1007/s00259-005-1762-7 PMID:15747152

41. Wijesekara N, Gonçalves RA, De Felice FG, Fraser PE. Impaired peripheral glucose homeostasis and Alzheimer's disease. Neuropharmacology. 2018; 136:172–81. https://doi.org/10.1016/j.neuropharm.2017.11.027 PMID:29169962

42. Kuo YM, Beach TG, Sue LI, Scott S, Layne KJ, Kokjohn TA, Kalback WM, Luehrs DC, Vishnivetskaya TA, Abramowski D, Sturchler-Pierrat C, Staufenbiel M, Weller RO, Roher AE. The evolution of A beta peptide burden in the APP23 transgenic mice: implications for A beta deposition in Alzheimer disease. Mol Med. 2001; 7:609–18. PMID:11778650

43. Lin B, Hasegawa Y, Takane K, Koibuchi N, Cao C, Kim-Mitsuyama S. High-Fat-Diet Intake Enhances Cerebral Amyloid Angiopathy and Cognitive Impairment in a Mouse Model of Alzheimer's Disease, Independently of Metabolic Disorders. J Am Heart Assoc. 2016; 5:e003154. https://doi.org/10.1161/JAHA.115.003154 PMID:27412896

44. Williams LM, Campbell FM, Drew JE, Koch C, Hoggard N, Rees WD, Kamolrat T, Thi Ngo H, Steffensen IL, Gray SR, Tups A. The development of diet-induced obesity and glucose intolerance in C57BL/6 mice on a high-fat diet consists of distinct phases. PLoS One. 2014; 9:e106159. https://doi.org/10.1371/journal.pone.0106159 PMID:25170916

45. Van Dam D, D'Hooge R, Staufenbiel M, Van Ginneken C, Van Meir F, De Deyn PP. Age-dependent cognitive decline in the APP23 model precedes amyloid deposition. Eur J Neurosci. 2003; 17:388–96. https://doi.org/10.1046/j.1460-9568.2003.02444.x PMID:12542676

46. Bjursell M, Gerdin AK, Lelliott CJ, Egecioglu E, Elmgren A, Törnell J, Oscarsson J, Bohlooly-Y M. Acutely reduced locomotor activity is a major contributor to

Western diet-induced obesity in mice. Am J Physiol Endocrinol Metab. 2008; 294:E251–60. https://doi.org/10.1152/ajpendo.00401.2007 PMID:18029443

47. Albensi BC. Dysfunction of mitochondria: Implications for Alzheimer's disease. Int Rev Neurobiol. 2019; 145:13–27. https://doi.org/10.1016/bs.irn.2019.03.001 PMID:31208523

48. Hartl D, Schuldt V, Forler S, Zabel C, Klose J, Rohe M. Presymptomatic alterations in energy metabolism and oxidative stress in the APP23 mouse model of Alzheimer disease. J Proteome Res. 2012; 11:3295–304. https://doi.org/10.1021/pr300021e PMID:22568827

49. Ruiz-Ramírez A, Chávez-Salgado M, Peñeda-Flores JA, Zapata E, Masso F, El-Hafidi M. High-sucrose diet increases ROS generation, FFA accumulation, UCP2 level, and proton leak in liver mitochondria. Am J Physiol Endocrinol Metab. 2011; 301:E1198–207. https://doi.org/10.1152/ajpendo.00631.2010 PMID:21917631

50. Ajith TA. Role of mitochondria and mitochondria-targeted agents in non-alcoholic fatty liver disease. Clin Exp Pharmacol Physiol. 2018; 45:413–21. https://doi.org/10.1111/1440-1681.12886 PMID:29112771

51. Brachs S, Winkel AF, Tang H, Birkenfeld AL, Brunner B, Jahn-Hofmann K, Margerie D, Ruetten H, Schmoll D, Spranger J. Inhibition of citrate cotransporter Slc13a5/mINDY by RNAi improves hepatic insulin sensitivity and prevents diet-induced non-alcoholic fatty liver disease in mice. Mol Metab. 2016; 5:1072–82. https://doi.org/10.1016/j.molmet.2016.08.004 PMID:27818933

52. Guo J, Bertalan G, Meierhofer D, Klein C, Schreyer S, Steiner B, Wang S, Vieira da Silva R, Infante-Duarte C, Koch S, Boehm-Sturm P, Braun J, Sack I. Brain maturation is associated with increasing tissue stiffness and decreasing tissue fluidity. Acta Biomater. 2019; 99:433–42. https://doi.org/10.1016/j.actbio.2019.08.036 PMID:31449927

53. Gielisch I, Meierhofer D. Metabolome and proteome profiling of complex I deficiency induced by rotenone. J Proteome Res. 2015; 14:224–35. https://doi.org/10.1021/pr500894v PMID:25361611

54. Cox J, Mann M. MaxQuant enables high peptide identification rates, individualized p.p.b.-range mass accuracies and proteome-wide protein quantification. Nat Biotechnol. 2008; 26:1367–72. https://doi.org/10.1038/nbt.1511 PMID:19029910

55. Müller T, Kalxdorf M, Longuespée R, Kazdal DN, Stenzinger A, Krijgsveld J. Automated sample preparation with SP3 for low-input clinical proteomics. Mol Syst Biol. 2020; 16:e9111. https://doi.org/10.15252/msb.20199111 PMID:32129943

56. Demichev V, Messner CB, Vernardis SI, Lilley KS, Ralser M. DIA-NN: neural networks and interference correction enable deep proteome coverage in high throughput. Nat Methods. 2020; 17:41–44. https://doi.org/10.1038/s41592-019-0638-x PMID:31768060

57. Krasny L, Bland P, Burns J, Lima NC, Harrison PT, Pacini L, Elms ML, Ning J, Martinez VG, Yu YR, Acton SE, Ho PC, Calvo F, et al. A mouse SWATH-mass spectrometry reference spectral library enables deconvolution of species-specific proteomic alterations in human tumour xenografts. Dis Model Mech. 2020; 13:dmm044586. https://doi.org/10.1242/dmm.044586 PMID:32493768

58. Messner CB, Demichev V, Wendisch D, Michalick L, White M, Freiwald A, Textoris-Taube K, Vernardis SI, Egger AS, Kreidl M, Ludwig D, Kilian C, Agostini F, et al. Ultra-High-Throughput Clinical Proteomics Reveals Classifiers of COVID-19 Infection. Cell Syst. 2020; 11:11–24.e4. https://doi.org/10.1016/j.cels.2020.05.012 PMID:32619549

59. Berndt N, Bulik S, Wallach I, Wünsch T, König M, Stockmann M, Meierhofer D, Holzhütter HG. HEPATOKIN1 is a biochemistry-based model of liver metabolism for applications in medicine and pharmacology. Nat Commun. 2018; 9:2386. https://doi.org/10.1038/s41467-018-04720-9 PMID:29921957

60. Berndt N, Kann O, Holzhütter HG. Physiology-based kinetic modeling of neuronal energy metabolism unravels the molecular basis of NAD(P)H fluorescence transients. J Cereb Blood Flow Metab. 2015; 35:1494–506. https://doi.org/10.1038/jcbfm.2015.70 PMID:25899300

61. Berndt N, Kolbe E, Gajowski R, Eckstein J, Ott F, Meierhofer D, Holzhütter HG, Matz-Soja M. Functional Consequences of Metabolic Zonation in Murine Livers: Insights for an Old Story. Hepatology. 2021; 73:795–810. https://doi.org/10.1002/hep.31274 PMID:32286709

62. Bulik S, Holzhütter HG, Berndt N. The relative importance of kinetic mechanisms and variable enzyme abundances for the regulation of hepatic glucose metabolism--insights from mathematical modeling. BMC Biol. 2016; 14:15. https://doi.org/10.1186/s12915-016-0237-6 PMID:26935066

63. Tschöp MH, Speakman JR, Arch JR, Auwerx J, Brüning JC, Chan L, Eckel RH, Farese RV Jr, Galgani JE, Hambly C, Herman MA, Horvath TL, Kahn BB, et al. A guide to analysis of mouse energy metabolism. Nat Methods. 2011; 9:57–63. https://doi.org/10.1038/nmeth.1806 PMID:22205519

SUPPLEMENTARY MATERIALS

Supplementary Figures

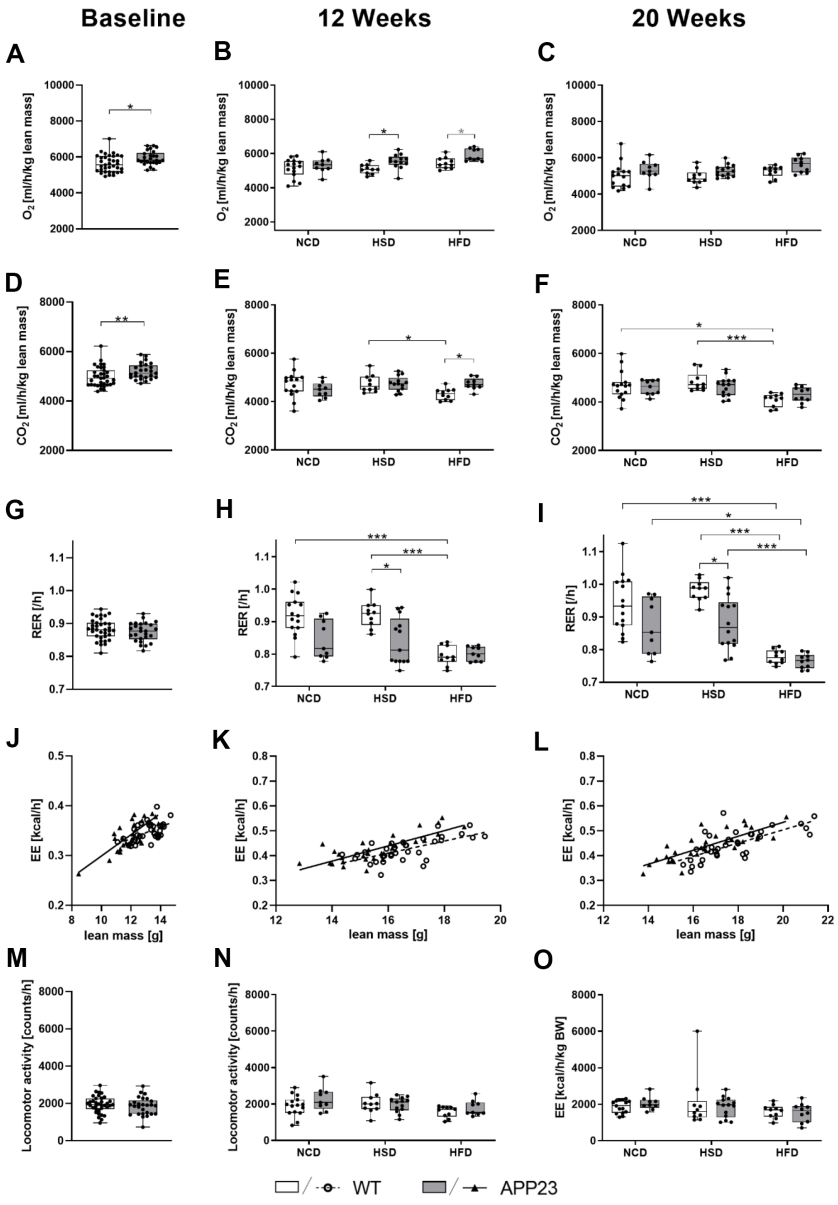

Supplementary Figure 1. Oxygen (O_2) consumption, carbon dioxide (CO_2) production, respiratory exchange ratio (RER), energy expenditure (EE), and locomotor activity of mice measured in metabolic cages during the light (inactive) phase at baseline (left column) and after 12 (middle column) and 20 weeks of diet (right column). (**A**–**C**) Averaged O_2 consumption per hour and (**D**–**F**) averaged CO_2 production per hour (both adjusted for lean mass) as well as (**G**–**I**) corresponding mean RER at baseline (**A**, **D**, **G**), after 12 (**B**, **E**, **H**) and 20 weeks of intervention (**C**, **F**, **I**). (**J**–**L**) Averaged EE per hour correlated with lean mass and (**M**–**O**) averaged locomotor activity per hour at baseline (**J**, **M**) and after 12 (**K**, **N**) and 20 weeks of diet (**L**, **O**). Metabolic cage data was collected after 12 h adaption time during 36 h analysis (1 light and mean of 2 dark phases) with 2 cycles per hour. Date of light and dark phase were analyzed separately. Data are shown averaged per hour and except for RER and locomotor activity adjusted for lean mass. Data are represented as box (25^{th} to 75^{th} percentile) with median and whiskers from minimum to maximum. Black asterisks indicate significant differences between groups (*: $p < 0.05$; **: $p < 0.01$; ***: $p < 0.001$), gray asterisk indicates a statistical trend towards significance ($p<0.1$) according to nonparametric t-tests (**A**, **D**, **G**, **J**, **M**) or nonparametric multiple contrast Tukey-type test (**B**, **C**, **E**, **F**, **H**, **I**, **K**, **L**, **N**, **O**). Abbreviations: WT: wild type control; APP23: transgenic mouse model; NCD: normal-control diet; HSD: high-sucrose diet; HFD: high-fat diet; RER: respiratory exchange ratio; EE: energy expenditure.

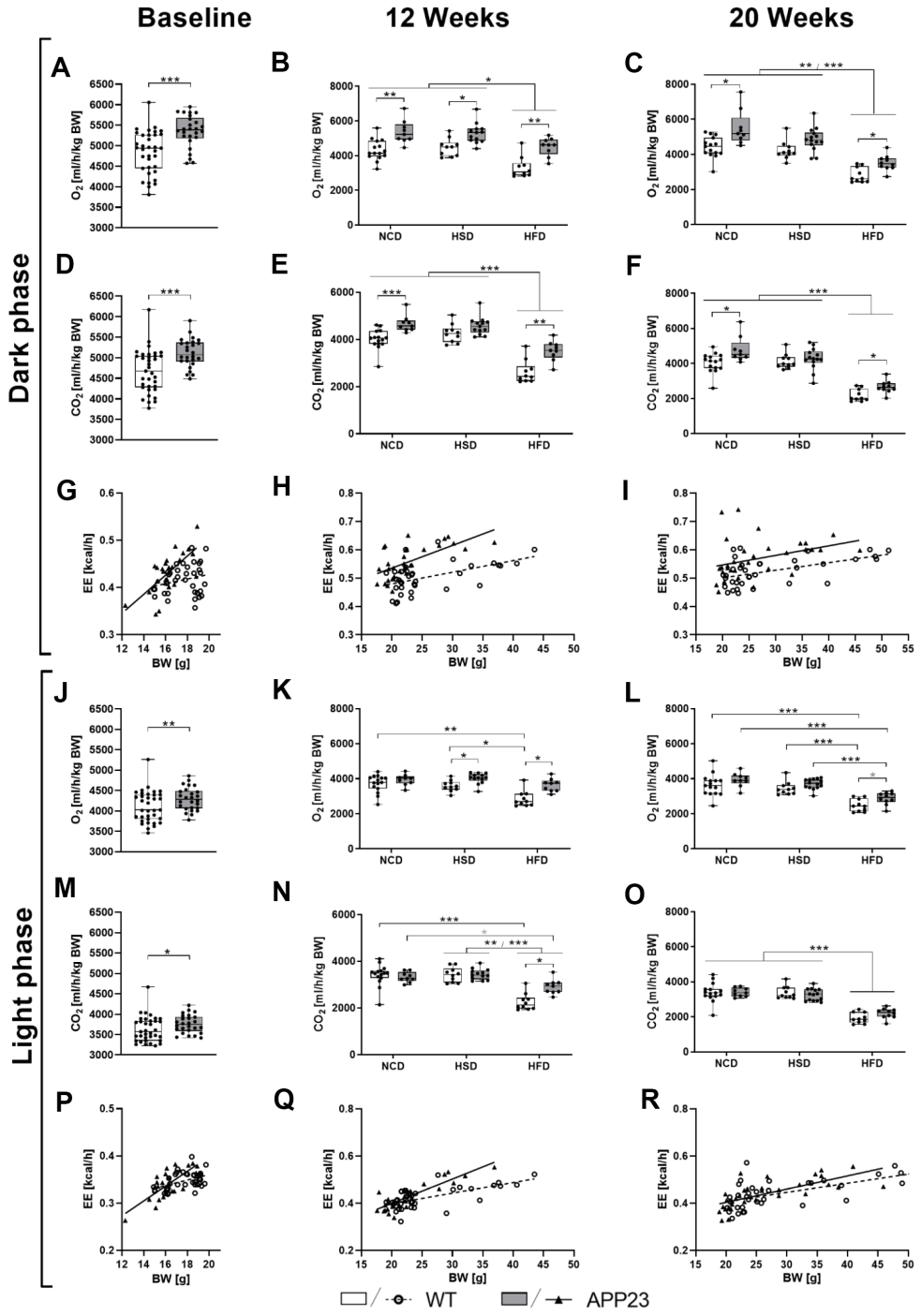

Supplementary Figure 2. Oxygen (O_2) consumption, carbon dioxide (CO_2) production, and, energy expenditure (EE) of mice measured in metabolic cages during the light (inactive) and dark (active) phase at baseline (left column) and after 12 (middle column) and 20 weeks of diet (right column). (**A**–**C**) and (**J**–**L**) Averaged O_2 consumption per hour adjusted for total BW during dark (active) phase (**A**–**C**) and during light (inactive) phase (**J**–**L**). (**D**–**F**) and (**M**–**O**) Averaged CO_2 production per hour adjusted for total BW during dark (active) phase (**D**–**F**) and during light (inactive) phase (**M**–**O**). (**G**–**I**) and (**P**–**R**) Averaged EE per hour correlated with total BW during dark (active) phase (**G**–**I**) and during light (inactive) phase (**P**–**R**). Metabolic cage data was collected after 12 h adaption time during 36 h analysis (1 light and mean of 2 dark phases) with 2 cycles per hour. Date of light and dark phase were analyzed separately. Data are shown averaged per hour and except for RER and locomotor activity adjusted for lean mass. Data are represented as box (25^{th} to 75^{th} percentile) with median and whiskers from minimum to maximum. Black asterisks indicate significant differences between groups (*: $p < 0.05$; **: $p < 0.01$; ***: $p < 0.001$), gray asterisk indicates a statistical trend towards significance ($p<0.1$) according to nonparametric t-tests (**A**, **D**, **G**, **J**, **M**) or nonparametric multiple contrast Tukey-type test (**B**, **C**, **E**, **F**, **H**, **I**, **K**, **L**, **N**, **O**). Abbreviations: WT: wild type control; APP23: transgenic mouse model; NCD: normal-control diet; HSD: high-sucrose diet; HFD: high-fat diet; EE: energy expenditure.

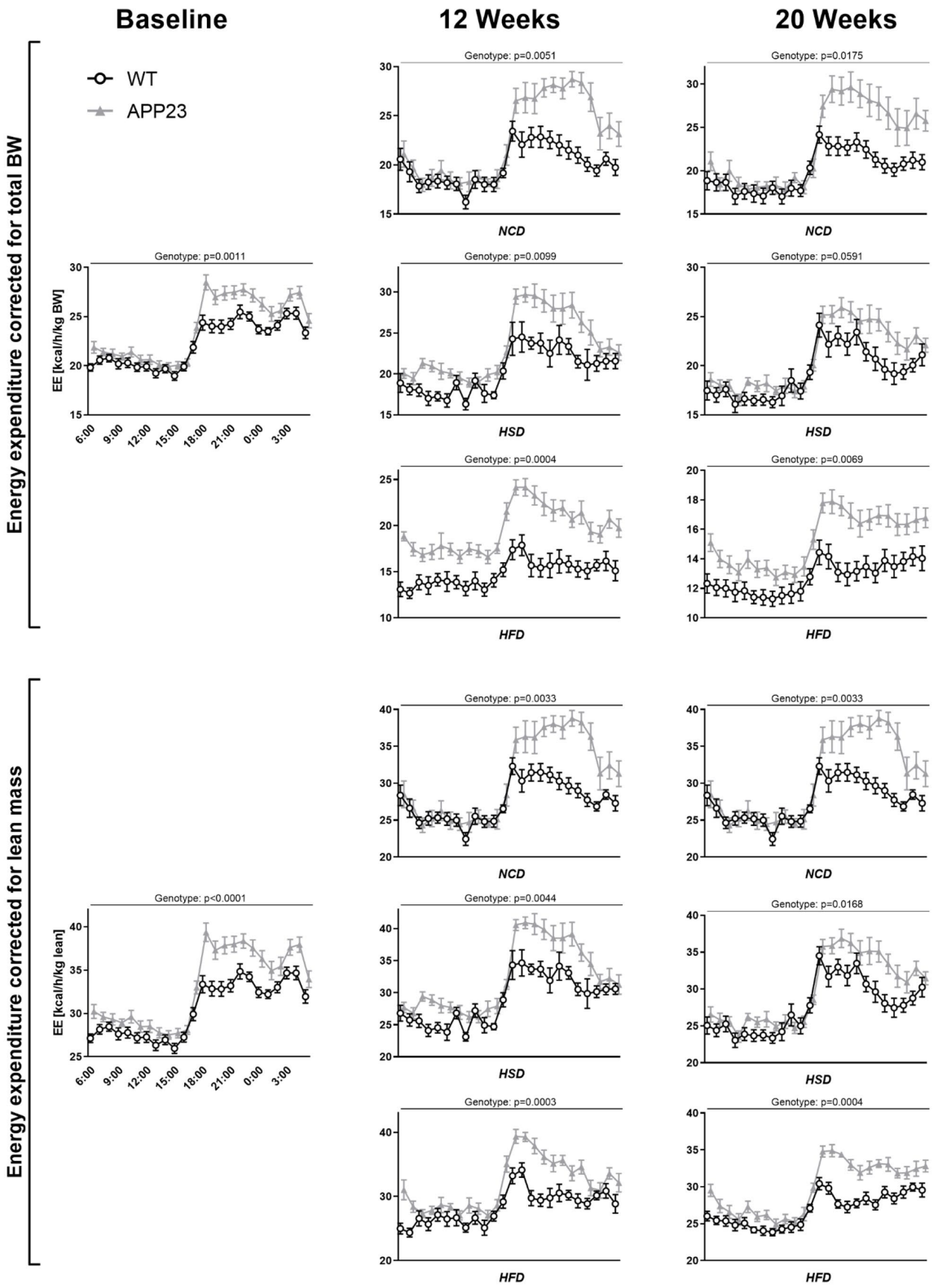

Supplementary Figure 3. Energy expenditure (EE) over the course of 24 hours (one light, one dark phase) at baseline (left column) and after 12 (middle column) and 20 weeks of diet (right column). Upper panel: Energy expenditure corrected for total body weight (BW). Lower panel: Energy expenditure corrected for lean mass. APP23 mice showed increased EE compared to WT regardless of time-point and diet. Data are represented as mean with standard deviation. Repeated measures 2-way ANOVA was performed. Abbreviations: WT: wild type control; APP23: transgenic mouse model; NCD: normal-control diet; HSD: high-sucrose diet; HFD: high-fat diet; BW: body weight; EE: energy expenditure.

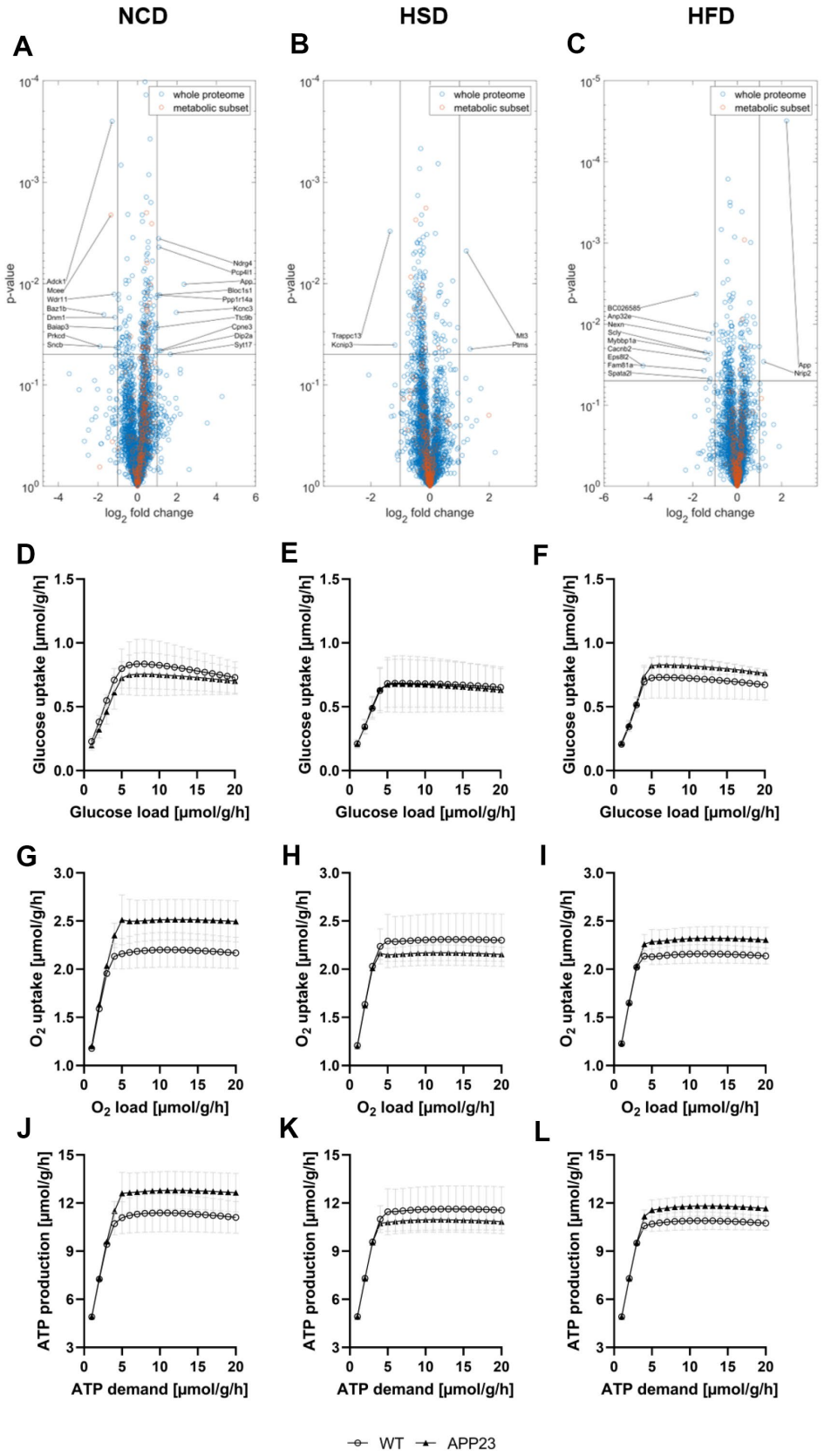

Supplementary Figure 4. Proteome analysis of brain tissue. (**A**–**C**) Volcano plots of APP23 mice versus WT mice within each diet. Such as seen in liver proteome profiles, some mitochondria-related genes were differentially regulated in brain proteome profiles of APP23 mice (MCEE, ADCK1). However, the majority of differentially regulated proteins is involved in signal transduction, vesicle trafficking, synaptic

function and neuronal plasticity (Syt17, DIP2a, BLOC1s1, SNCB, BAIAP3, WDR11, KCNIP3, TRAPPC13). (**D**–**F**) Simulated neuronal glucose tolerance of APP23 mice versus WT mice within each diet. Simulated neuronal glucose tolerance did not differ between genotypes and dietary groups. (**G**–**I**) Simulated neuronal oxygen consumption of APP23 mice versus WT mice within each diet. (**J**–**L**) Simulated neuronal ATP production of APP23 mice versus WT mice within each diet. Simulated neuronal oxygen consumption and ATP production were slightly elevated in NCD-fed APP23 mice, which might be an overcompensation of beginning mitochondrial dysfunction, resulting in yet unaltered glucose tolerance. Thus, similar analyses in aged APP23 mice with advanced AD pathology would be of interest. Differences in HSD- and HFD-fed APP23 mice were too small to be interpreted. (**A**, **D**, **G**, **J**) NCD; (**B**, **E**, **H**, **K**) HSD; (**C**, **F**, **I**, **L**) HFD. Abbreviations: WT: wild type control; APP23: transgenic mouse model; NCD: normal-control diet; HSD: high-sucrose diet; HFD: high-fat diet.

Supplementary Tables

Supplementary Table 1. Detailed ingredients of NCD, HSD, and HFD.

	NCD	HSD	HFD
Product No.	D16022602	D16022604	D12492
Ingredient (g)			
Casein	160.5	160.5	200
DL-Methionine	3.0	3.0	0
L-Cystine	0	0	3.0
Corn starch	442.5	0	0
Maltodextrin 10	125.0	25.0	125.0
Sucrose	0	542.5	68.8
Cellulose, BW200	50.0	50.0	50.0
Corn oil	98.4	98.4	0
Soybean oil	0	0	25.0
Lard	0	0	245.0
t-Butylhydroquinone	0.02	0.02	0
Mineral mix S10022M	35.0	35.0	0
Mineral mix S10026	0	0	10.0
Vitamin mix V10037	10.0	10.0	0
Vitamin mix V10001	0	0	10.0
Choline bitartate	2.5	2.5	2.0
Dicalcium phosphate	0	0	13.0
Calcium carbonate	0	0	5.5
Potassium citrate	0	0	16.5

Abbreviations: NCD: normal-control diet; HSD: high-sucrose diet; HFD: high-fat diet.

Supplementary Table 2. Corresponding p-values to significant comparisons shown in Figure 5.

Parameter	Time-point	Comparison *(A vs. B)*	Difference *(B in relation to A)*	p
AUC	Week 12	NCD WT vs. HFD WT	+ 83%	<0.001
		NCD APP23 vs. HFD APP23	+ 56%	<0.001
		HSD WT vs. HFD WT	+ 59%	<0.001
		HSD APP23 vs. HFD APP23	+ 76%	0.009
		HFD WT vs. HFD APP23	- 20%	0.017
	Week 20	NCD WT vs. HFD WT	+ 104%	<0.001
		NCD APP23 vs. HFD APP23	+ 85%	<0.001
		HSD WT vs. HFD WT	+ 63%	<0.001
		HSD APP23 vs. HFD APP23	+ 51%	<0.001
		HFD WT vs. HFD APP23	- 15%	0.049
Fasting glucose	Week 12	NCD APP23 vs. HSD APP23	+ 25%	<0.001
		NCD WT vs. HFD WT	+ 26%	0.004
		NCD APP23 vs. HFD APP23	+ 30%	0.011
		HSD WT vs. HFD WT	+ 21%	0.014
	Week 20	NCD APP23 vs. HSD APP23	+ 18%	0.027
		NCD WT vs. HFD WT	+ 21%	0.002
		HSD WT vs. HFD WT	+ 19%	0.004
		NCD APP23 vs. HFD APP23	+ 35%	0.003
Fasting insulin	Week 12	NCD WT vs. HFD WT	+ 231%	0.001
		NCD APP23 vs. HFD APP23	+ 305%	0.009
		HSD WT vs. HFD WT	+ 231%	0.003
		HSD APP23 vs. HFD APP23	+ 174%	0.039
	Week 20	NCD WT vs. HFD WT	+ 522%	<0.001
		NCD APP23 vs. HFD APP23	+ 267%	<0.001
		HSD WT vs. HFD WT	+ 479%	<0.001
		HSD APP23 vs. HFD APP23	+ 288%	<0.001

Statistical tests are described in the respective figure legend. Differences are displayed as percentage in relation to the first group of the comparison (e.g. NCD WT vs HFD WT +83% means that HFD WT shows 83% more than NCD WT). Abbreviations: AUC: area under the curve.

Supplementary Table 3. Corresponding p-values to significant comparisons shown in Figure 6.

Parameter	Time-point	Comparison *(A vs. B)*	Difference *(B in relation to A)*	p
O_2 consumption	Baseline	WT vs. APP23	+ 12%	<0.001
	Week 12	NCD WT vs. NCD APP23	+ 22%	0.030
		HSD WT vs. HSD APP23	+ 15%	0.013
		HFD WT vs. HFD APP23	+ 16%	0.002
	Week 20	NCD WT vs. NCD APP23	+ 22%	0.013
		HSD WT vs. HSD APP23	+ 14%	0.057
		HFD WT vs. HFD APP23	+ 10%	<0.001
CO_2 production	Baseline	WT vs. APP23	+ 11%	<0.001
	Week 12	NCD WT vs. NCD APP23	+ 14%	<0.001
		HFD WT vs. HFD APP23	+ 14%	0.003
		NCD WT vs. HFD WT	- 10%	0.051
		NCD APP23 vs. HFD APP23	- 10%	0.003
		HSD WT vs. HFD WT	- 15%	<0.001
		HSD APP23 vs. HFD APP23	- 9%	<0.001
	Week 20	NCD WT vs. NCD APP23	+ 16%	0.018
		HFD WT vs. HFD APP23	+ 13%	<0.001
		NCD WT vs. HFD WT	- 18%	<0.001
		NCD APP23 vs. HFD APP23	- 20%	<0.001
		HSD WT vs. HFD WT	- 22%	<0.001
		HSD APP23 vs. HFD APP23	- 15%	<0.001
Respiratory exchange ratio	Week 12	HSD WT vs. HSD APP23	- 9%	0.010
		NCD WT vs. HFD WT	- 16%	<0.001
		NCD APP23 vs. HFD APP23	- 11%	0.009
		HSD WT vs. HFD WT	- 16%	<0.001
		HSD APP23 vs. HFD APP23	- 9%	0.003
	Week 20	HSD WT vs. HSD APP23	- 10%	0.020
		NCD WT vs. HSD WT	+ 7%	0.049
		NCD WT vs. HFD WT	- 16%	<0.001
		NCD APP23 vs. HFD APP23	- 14%	<0.001
		HSD WT vs. HFD WT	- 22%	<0.001
		HSD APP23 vs. HFD APP23	- 14%	<0.001
Activity	Baseline	WT vs. APP23	+ 38%	0.009
	Week 12	NCD WT vs. NCD APP23	+ 84%	0.016
		HFD WT vs. HFD APP23	+ 57%	0.061
		NCD APP23 vs. HFD APP23	- 46%	0.016
		HSD WT vs. HFD WT	- 46%	0.004
	Week 20	NCD WT vs. NCD APP23	+ 50%	0.010
		HFD WT vs. HFD APP23	+ 71%	0.007
		NCD APP23 vs. HFD APP23	- 44%	0.001
		NCD WT vs. HFD WT	- 50%	<0.001
		HSD WT vs. HFD WT	- 60%	0.007
		HSD APP23 vs. HFD APP23	- 40%	0.002

Statistical tests are described in the respective Figure legend. Differences are displayed as percentage in relation to the first group of the comparison (e.g. NCD WT vs HFD WT +83% means that HFD WT shows 83% more than NCD WT).

Supplementary Table 4. Results of spearman correlation of energy expenditure with lean mass, corresponding to Figure 6J–6L and Supplementary Figure 1J–1L, and to Supplementary Figure 2G–2I, 2P–2R.

Figure	Time-point	r_{WT}	p_{WT}	r_{APP23}	p_{APP23}
Figure 6J-L	Baseline	0.348	0.041	0.607	0.001
	Week 12	0.662	<0.001	0.673	<0.001
	Week 20	0.615	<0.001	0.550	0.003
Supplementary Figure 1J–1L	Baseline	0.511	0.002	0.696	<0.001
	Week 12	0.662	<0.001	0.769	<0.001
	Week 20	0.734	<0.001	0.816	<0.001
Supplementary Figure 2G–2I	Baseline	0.179	0.305	0.642	<0.001
	Week 12	0.503	0.002	0.653	<0.001
	Week 20	0.488	0.003	0.489	0,004
Supplementary Figure 2P–2R	Baseline	0.417	0.013	0.629	<0.001
	Week 12	0.624	<0.001	0.793	<0.001
	Week 20	0.638	<0.001	0.826	<0.001

Version of Record – Study II

scientific reports

Check for updates

OPEN

Chia seeds as a potential cognitive booster in the APP23 Alzheimer's disease model

Stefanie Schreyer[1]✉, Charlotte Klein[1], Anna Pfeffer[1], Justyna Rasińska[1], Laura Stahn[1], Karlotta Knuth[1], Basim Abuelnor[1], Alina Elisabeth Catharina Panzel[1], André Rex[2], Stefan Koch[2,3], Shabnam Hemmati-Sadeghi[1,4] & Barbara Steiner[1,4]

Glucose hypometabolism potentially contributes to Alzheimer's disease (AD) and might even represent an underlying mechanism. Here, we investigate the relationship of diet-induced metabolic stress and AD as well as the therapeutic potential of chia seeds as a modulator of glucose metabolism in the APP23 mouse model. 4–6 (pre-plaque stage, PRE) and 28–32 (advanced-plaque stage, ADV) weeks old APP23 and wild type mice received pretreatment for 12 weeks with either sucrose-rich (SRD) or control diet, followed by 8 weeks of chia seed supplementation. Although ADV APP23 mice generally showed functioning glucose homeostasis, they were more prone to SRD-induced glucose intolerance. This was accompanied by elevated corticosterone levels and mild insulin insensitivity. Chia seeds improved spatial learning deficits but not impaired cognitive flexibility, potentially mediated by amelioration of glucose tolerance, attenuation of corticosterone levels and reversal of SRD-induced elevation of pro-inflammatory cytokine levels. Since cognitive symptoms and plaque load were not aggravated by SRD-induced metabolic stress, despite enhanced neuroinflammation in the PRE group, we conclude that impairments of glucose metabolism do not represent an underlying mechanism of AD in this mouse model. Nevertheless, chia seeds might provide therapeutic potential in AD as shown by the amelioration of cognitive symptoms.

Alzheimer's disease (AD), affecting about 50 million people worldwide, is the most common form of dementia[1]. Pathological hallmarks of AD are extracellular amyloid beta (Aβ) plaques, neurofibrillary tangles of hyperphosphorylated tau protein and chronic neuroinflammation mediated by activated microglia, potentially further promoting disease progression[2]. Cognitive decline, induced by neurodegeneration, is the most apparent symptom of AD[2]. The hippocampus is very early affected during AD pathogenesis[3]. Alterations of adult hippocampal neurogenesis (AHN) have been shown in animal models and AD patients and might contribute to cognitive symptoms due to a loss of neuroplasticity[4]. Owing to the unknown underlying mechanisms of AD, currently no curative therapies are available.

So far, AD research focused on the amyloid cascade hypothesis, stating that the accumulation of Aβ, cleaved from the amyloid precursor protein (APP), and its formation into Aβ plaques is the underlying mechanism of cognitive decline[5]. However, the majority of clinical trials reducing Aβ burden with antibodies have shown no clinically significant improvements of cognitive performance[6]. Therefore, alternative potential causes, such as cerebral glucose metabolism, have been focused on recently. Cerebral glucose metabolism is reduced in AD patients, resulting in glucose intolerance and insulin resistance[7]. Glucose hypometabolism already occurs years before the onset of clinical symptoms of AD[7], thus representing a potential underlying mechanism. Nevertheless, the implication of glucose hypometabolism in AD raises the question of causality. On the one hand, Aβ alters glucose metabolism, e.g. by reducing glucose uptake into cells[8]. On the other hand, glucose hypometabolism leads to energy deficiency and oxidative stress, which in turn induce Aβ overproduction[9]. Glucose hypometabolism

[1]Department of Neurology, Charité-Universitätsmedizin Berlin, Freie Universität Berlin, Humboldt-Universität Zu Berlin, and Berlin Institute of Health, Charitéplatz 1, 10117 Berlin, Germany. [2]Department of Experimental Neurology and Center for Stroke Research Berlin, Charité-Universitätsmedizin Berlin, Freie Universität Berlin, Humboldt-Universität Zu Berlin, and Berlin Institute of Health, Charitéplatz 1, 10117 Berlin, Germany. [3]NeuroCure Cluster of Excellence and Charité Core Facility 7T Experimental MRIs, Charité-Universitätsmedizin Berlin, Freie Universität Berlin, Humboldt-Universität Zu Berlin, and Berlin Institute of Health, Charitéplatz 1, 10117 Berlin, Germany. [4]These authors contributed equally: Shabnam Hemmati-Sadeghi and Barbara Steiner. ✉email: stefanie.schreyer@charite.de

a

Disease stage (age at start)	Pre-plaque stage (4 to 6 weeks)								Advanced-plaque stage (28 to 32 weeks)							
Genotype	APP23				WT				APP23				WT			
Pretreatment	CD		SRD		CD		SRD		CD		SRD		CD		SRD	
Therapy	CD	Chia	SRD	Chia	CD	Chia	SRD	Chia	CD	Chia	SRD	Chia	CD	Chia	SRD	Chia
n per group	10	11	11	12	14	12	14	13	12	11	15	13	12	13	15	11
n histology	5	6	5	6	7	6	8	7	6	6	5	7	6	6	7	7

b

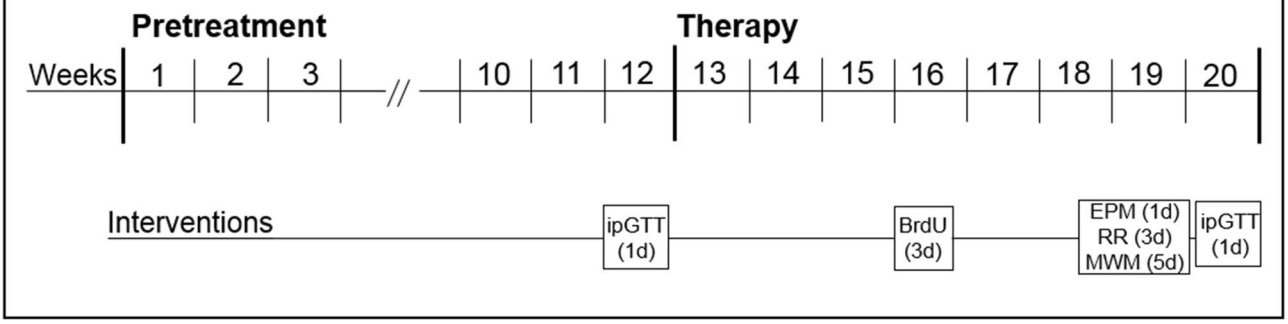

c **d**

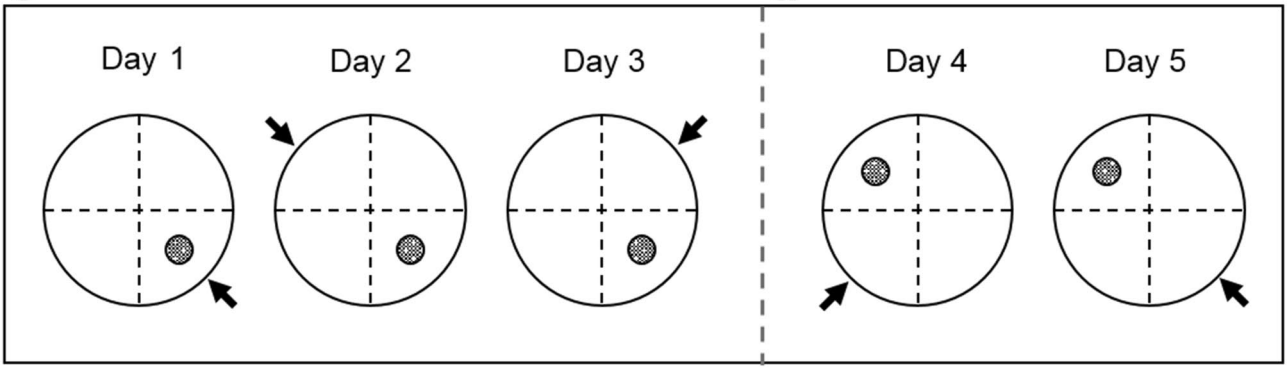

Figure 1. Study design (**a**,**b**) and reversal learning paradigm of the MWM (**c**,**d**). (**a**) The study was conducted in pre-plaque stage transgenic mice (PRE APP23 mice; 4–6 weeks old at start) and advanced-plaque stage transgenic mice (ADV APP23 mice; 28–32 weeks old at start) and age-matched healthy littermates (WT) as controls. Mice received either sucrose-rich diet (SRD) or control diet (CD) as a pretreatment. After pretreatment, mice underwent a therapy of either chia seed supplementation (CD + Chia or SRD + Chia) or of their respective diet from pretreatment (CD + CD or SRD + SRD) as a control. The last two rows display the group sizes for all measurements performed on the living animal and with the animals' blood or for histological analyses of brain tissue, respectively. (**b**) Mice received pretreatment for 12 weeks, followed by 8 weeks of therapy. Glucose tolerance was assessed with an intraperitoneal glucose tolerance test (ipGTT) on the last day of pretreatment (week 12) and of therapy (week 20). In week 16, mice received injections of 5-bromo-2′-deoxyuridine (BrdU) on 3 consecutive days. At the end of therapy, mice underwent behavioral testing, using the Elevated Plus Maze (EPM) on 1 day, the Rotarod Performance Test (RR) on 3 consecutive days, and the Morris Water Maze (MWM) on 5 consecutive days. Mice were given a break of 2 days after the last day of MWM, before the second ipGTT was conducted. After 20 weeks of experiment, mice were sacrificed the day after the second ipGTT at the age of 24–26 weeks (PRE group) and 48–52 weeks (ADV group), respectively. (**c**) Position of the hidden escape platform (filled circle) and release position of mice for all trials of the respective day (arrow) during 3 days of acquisition phase in the MWM. (**d**) Position of the hidden escape platform (filled circle) and release position of mice for all trials of the respective day (arrow) during 2 days of reversal learning phase in the MWM.

in AD brains is similar to pathogenic changes occurring during type 2 diabetes mellitus (T2DM)[10]. Additionally, T2DM is a major risk factor for developing AD and T2DM patients often show symptoms of cognitive decline, which might be partially mediated by peripheral and central inflammation[11]. Another aspect linking AD to glucose metabolism is the dysregulation of the hypothalamic–pituitary–adrenal (HPA) axis, leading to alterations in glucocorticoid (GC) levels[12]. GCs act as functional antagonists of insulin, whereupon chronically elevated levels of GCs cause insulin resistance and glucose intolerance[13]. Elevated GC levels observed in AD patients correlate with hippocampal degeneration and cognitive decline[14]. Similarly, GC secretion is elevated in T2DM patients[15].

Chia seeds (*Salvia hispanica* L.) are a low glycemic index food due to their low amount of carbohydrates compared to traditional grains, which is useful for glycemic control in diabetes[16,17]. The fat content of chia seeds contains a great proportion of essential omega-3 and omega-6 polyunsaturated fatty acids (PUFAs), such as the omega-3 PUFA α-linolenic acid (ALA)[18,19]. ALA is the precursor of eicosapentaenoic acid (EPA) and docosahexaenoic acid (DHA)[20]. Both, EPA and DHA are crucial for numerous brain functions such as signal transduction and exert neuroprotective effects like the reduction of neuroinflammation[21]. Furthermore, alterations in PUFA metabolism occur in AD patients[22]. Studies in diabetic rats have shown that chia seeds normalize insulin resistance and reduce visceral adiposity as well as cardiac and hepatic inflammation[23,24]. Likewise, human studies have shown the potential of chia seeds to reduce blood pressure, to promote weight loss, to stabilize blood glucose in diabetes and to increase serum omega-3 PUFAs[25]. However, to our knowledge no study has examined the effect of chia seeds on cognitive functions in healthy or diseased humans. Only two studies have investigated the effect of chia seeds in AD animal models so far, finding either no or detrimental effects on cognitive performance and on Aβ levels[26,27]. However, these studies were based on models that might not ideally mimic alterations of glucose metabolism occurring in AD, as present in genetically induced AD models.

This study further investigates the role of glucose metabolism in AD by the induction of metabolic stress in an AD mouse model. Based on the assumption that impairments in cerebral glucose metabolism represent an underlying mechanism of AD pathology, we hypothesize that (1) the AD mouse model displays disturbed glucose homeostasis and that (2) metabolic stress further aggravates cognitive symptoms and AD histopathology. Additionally, this study examines the therapeutic potential of chia seeds as a dietary supplement in AD. Assuming that chia seeds are able to improve glucose homeostasis, we hypothesize that (3) chia seed supplementation reverses or attenuates the effects of metabolic stress, thus ameliorating AD pathology and that (4) chia seed supplementation also leads to an improvement of AD pathology in mice that are not metabolically stressed due to their amelioration of underlying metabolic impairments.

Materials and methods

Animals. Animal experiments were approved by the local animal ethics committee (Landesamt für Gesundheit und Soziales, Berlin, Germany; G0074/16) and carried out in accordance with the European Communities Council Directive of 22 September 2010 (10/63/EU). APP23 mice overexpress human APP_{751} cDNA with the Swedish double mutation under the murine Thy-1 promotor with Aβ plaque deposition starting at 6 months of age[28]. Breeding pairs were obtained from Novartis Pharma, the colony was maintained on a C57BL/6J background, and genotype was confirmed by PCR (Primers: APP ct forward: 5′ GAA TTC CGA CAT GAC TCA GG 3′, APP ct reverse: 5′ GTT CTG CTG CTG CAT CTT CGA CA 3′). Two age groups of female mice were observed: 44 APP23 mice and 53 healthy littermates (WT) entered the experiment aged 4–6 weeks old, (pre-plaque stage, PRE), 51 APP23 and 51 WT mice entered the experiment aged 28–32 weeks old (advanced-plaque stage, ADV). Animals were group-housed in a temperature- and humidity-controlled room (21.5 ± 1.5 °C, 40–60%) on a 12-h light/dark cycle with unrestricted access to food and water. Animals were randomly assigned to the different dietary conditions as described below (Fig. 1a). The experimenter was blinded to age, genotype and group allocation. The body weight (BW) of mice was measured weekly. 50 mg/kg BW 5-bromo-2′-deoxyuridine (BrdU) dissolved in sodium chloride were injected intraperitoneally (i.p.) every 24 h on 3 consecutive days in week 16 for examination of AHN (Fig. 1b).

Diets. Mice received a 12 weeks long pretreatment of either a sucrose-rich diet (SRD) to induce metabolic stress or a control diet (CD) (Fig. 1a,b). SRD provided 4.28 kcal/g, CD provided 4.15 kcal/g, and both diets were composed of 17% protein, 23% fat and 60% carbohydrates. After 12 weeks, each group was randomly further subdivided into two groups for additional 8 weeks (Fig. 1a,b); the therapy group receiving their respective diet supplemented with 286 g/kg diet milled chia seeds (Onset Worldwide LC, Frenchtown, NJ, USA) (SRD + Chia or CD + Chia), the control group continuing with their original diet (SRD or CD). The amount of chia seeds added to the diets was based on a study of Chicco et al.[23] and modified according to their content of nutrients and energy of the CD and SRD. SRD + Chia and CD + Chia had the same nutritional composition and value as SRD and CD, respectively. The exact composition of all diets and the nutritional facts of chia seeds can be found in Supplemental Tables S1 and S2.

Intraperitoneal glucose tolerance test. Glucose tolerance was measured on the last day of pretreatment and on the last day of therapy (Fig. 1b) with an intraperitoneal glucose tolerance test (ipGTT) after a 6 h morning fast. Blood was obtained from a small incision of the distal tail vein after applying lidocaine/prilocaine ointment. Blood glucose was measured before (0 min) and 15, 30, 60, and 120 min after i.p. injection of 2 mg/g BW glucose solution. Glucose tolerance is expressed as area under the curve (AUC) in (mg/dl) × min. Higher blood glucose levels over a prolonged period of time result in a higher AUC, indicating a lower glucose tolerance.

Behavioral testing of anxiety, motor coordination, and cognition. All behavioral tests were conducted during the last 2 weeks of therapy (Fig. 1b). The Elevated Plus Maze (EPM) measures anxiety-related behavior. Each mouse was placed in the center region facing a closed arm and had a single trial of 5 min. The software TSE VideoMot 3D Classic Version 8.02 automatically recorded the percentaged time mice spent in the open arms, the number of entries into the open arms and the latency of the first entry into an open arm.

The Rotarod Performance Test measures motor coordination and fatigue resistance and was conducted as reported previously[29] to preclude limitations in motility that might negatively affect the Morris Water Maze (MWM) performance. Briefly, mice had a maximum running time of 5 min per trial with gradually accelerating rotation speeds from 4 to 40 rpm. The time mice balanced on the rod was measured by the software TSE-ROD Version 4.0. 2 days prior to the test day, mice were habituated to the procedure, performing 4 trials per day with an inter-trial-interval of 15–30 min. On the test day, the animals went through 3 equally conducted test trials. The mean of 3 trials was calculated.

In the MWM, spatial learning is assessed during the acquisition phase and cognitive flexibility is examined during a reversal learning phase. The MWM task was performed as previously described[29]. Briefly, the circular pool was filled with opaque water (22 ± 2 °C) and virtually divided into four quadrants with a circular escape platform submerged 1 cm below the water surface in the center of one quadrant (Fig. 1c,d). A different visual cue was placed at the wall above each quadrant. During the acquisition phase (day 1–3), the platform location remained the same (Fig. 1c), whereas it was shifted to the opposite quadrant during the reversal learning phase (day 4–5) (Fig. 1d). Each day consisted of 6 trials with an inter-trial-interval of 30–45 min. The starting position remained the same over these 6 trials, but was alternated each day (Fig. 1c,d, arrow). A trial was finished either with reaching the platform or after 2 min. If the mouse was unable to detect the platform, it was guided to its position after 2 min had elapsed. Each mouse was given 10 s to memorize the platform position. The software TSE VideoMot 2 Version 5.68 was used to automatically track the swim paths of mice, measuring a.o. the total distance covered to the escape platform. Swim trajectories were used to generate spatial presence probability maps using Matlab R2011b as described in the legend of Fig. 3.

Perfusion and tissue preparation. Animals were deeply anesthetized after a 6 h morning fast via i.p. injection of 300 mg/kg BW ketamine hydrochloride and 30 mg/kg BW xylazine hydrochloride. Laparotomy and a final blood withdrawal from the *Inferior Vena Cava* were performed. Blood was mixed with 10 µl heparin per 500 µl and immediately centrifuged at 4 °C and 13,000 rpm for 3 min. Plasma was collected and instantly deep-frozen. Thoracotomy and transcardial perfusion using 40 ml of 0.1 M phosphate buffered saline (PBS) were performed. In half of each experimental group, the hippocampus was directly dissected from the fresh brain and deep-frozen in liquid nitrogen for analysis of inflammatory cytokine levels. In the other half, a second perfusion with 40 ml of 4% paraformaldehyde (PFA) in PBS was performed, before brains were removed, post-fixated overnight in 4% PFA in PBS at 4 °C, dehydrated for 48 h in 30% aqueous sucrose solution at 4 °C, and subsequently deep-frozen. Frozen coronal sections of 40 µm thickness were prepared for histological analyses with a cryostat.

Histological analysis of plaque load, microglia, and adult hippocampal neurogenesis. Aβ plaque load was determined using the fluorescent pentameric oligothiophene (pFTAA) and only assessed in APP23 mice. A one-in-twelve series of brain slices containing the hippocampus was incubated for 30 min with 20 µg/ml pFTAA and counterstained with 4′,6-diamidino-2-phenylindole (DAPI). The percentaged area covered with Aβ plaques in both hippocampi and cortices was calculated automatically via the "Analyze Particles" tool of ImageJ in 6 sections per animal.

Brain slices containing the hippocampus were used for quantification of microglia and macrophages by staining against the ionized calcium-binding adapter molecule 1 (Iba1) in a one-in-twelve series. Sections of a one-in-six series were stained to assess AHN by quantification of survival of newborn cells, marked by the incorporation of BrdU, and by quantification of immature neurons, marked by the expression of doublecortin (DCX), as previously described[30]. Brain slices were pretreated with 0.6% H_2O_2. For BrdU, additional pretreatment with 2 M HCl was conducted. Subsequently, slices were incubated overnight at 4 °C with the primary antibody:

polyclonal rabbit anti-Iba1 (Fujifilm Wako Chemicals Europe, 1:500), monoclonal rat anti-BrdU (Biozol, 1:500), or polyclonal guinea pig anti-DCX (Merck Millipore, 1:1000). The next day, the tissue was incubated with the secondary antibody for 2 h at room temperature: Biotin-SP-conjugated goat anti-rabbit, donkey anti-rat, or goat anti-guinea pig (each dianova, 1:250). This was followed by incubation with streptavidin peroxidase complex and the reaction was visualized by applying diaminobenzidine-nickel staining. The labeled microglia and macrophages in both hippocampi of 6 sections per animal were stereologically extrapolated using the "Optical Fractionator Probe" of MBF Bioscience Stereo Investigator with a grid size of 500 × 500 µm and a counting frame of 75 × 75 µm. The labeled $BrdU^+$ and DCX^+ cells in the granule cell layer and subgranular zone of both dentate gyri (DG) of 6 sections per animal were counted manually.

Analysis of inflammatory cytokine levels in hippocampal tissue. A single hippocampus of 5 animals per group was suspended in radioimmunoprecipitation assay (RIPA) buffer mixed with protease inhibitor (100 µl buffer mix per 10 mg tissue) and mechanically minced. After 30 min of incubation on ice, samples were centrifuged at 13,000 rpm for 15 min at 4 °C and the supernatant was collected. Total protein concentration of samples was measured using the Pierce™ BCA Protein Assay Kit (Thermo Scientific) as described in the handbook. Samples were diluted 1:10 with PBS and a final volume of 10 µl was analyzed in duplicates. Concentrations of interferon-γ (IFN-γ), keratinocyte chemoattractant/human growth-regulated oncogene (KC/GRO), tumor necrosis factor-α (TNF-α) and interleukins (IL) IL-1β, IL-2, IL-4, IL-5, IL-6, IL-10, IL-12p70 were measured using the V-PLEX Plus Proinflammatory Panel1 Mouse Kit (Meso Scale Discovery) as described in the handbook. Duplicates of 50 µl undiluted samples were analyzed. Cytokine concentrations were normalized for total protein concentration. Measured levels of IL-10 were under detection range of the kit and thus excluded from the analysis.

Quantification of fasting insulin and corticosterone levels in blood plasma. Blood plasma was analyzed using enzyme-linked immunosorbent assay (ELISA). Mouse Insulin ELISA kit (Mercodia) was used as described in the handbook to quantify fasting insulin levels. Duplicates of 5 µl undiluted plasma samples per animal were analyzed. Corticosterone ELISA kit (for human, rat and mouse, IBL International) was used as described in the handbook to analyze fasting corticosterone levels. For each animal, plasma samples were diluted 1:5 with the included "Standard 0" to a final volume of 20 µl and analyzed in duplicates.

Statistical analysis. All data sets were analyzed with IBM SPSS Statistics 25 to verify, whether the data meet the assumptions for parametric testing. The Shapiro–Wilk test was performed to check for normal distribution and the Levene's test was conducted to check for equal variances. In all data sets, one or more assumptions for parametric testing were violated, therefore nonparametric tests were chosen. Data sets were analyzed with R Version 3.6.3 using the packages nparcomp and nparLD as described elsewhere[31,32]. The function mctp from the package nparcomp was used to perform nonparametric multiple contrast test (type Tukey) between groups. The function f2.ld.f1 from the package nparLD was used to perform nonparametric ANOVA-type statistics of data sets that include repeated measures. The effects of the two independent factors (f2) genotype (g) and diet (d) and the longitudinal factor (f1) time (t) on the respective outcome parameters were analyzed. For further analyses, nparcomp was used to examine differences between groups at crucial time points within longitudinal data. The Rotarod performance was correlated with BW using Spearman's rank correlation. A p-value ≤ 0.05 was considered significant. Results were plotted using GraphPad Prism 8.4.2.

Results

Chia seeds and SRD positively affect spatial learning impairments in APP23 mice. The daily MWM performance of mice is expressed as the mean distance covered to the escape platform of all trials (Fig. 2). Figure 3 shows exemplary heatmaps of presence probabilities. Complete heatmaps can be found in Supplemental Figure S3. Mice of both the PRE and the ADV group successfully learned the platform position during the acquisition phase, represented by a significant time-dependent reduction of the distance covered to the platform (PRE: $F(1.682,78.596) = 38.286$, $p < 0.001$; ADV: $F(1.684,84.952) = 32.354$, $p < 0.001$) (Fig. 2a,b). However, PRE and ADV APP23 mice performed inferior to age-matched WT mice during the acquisition phase (PRE: $F(1,78.596) = 21.148$, $p < 0.001$; ADV: $F(1,84.952) = 25.685$, $p < 0.001$), as shown by up to 46% longer distances (Fig. 2a,b). Only in the ADV group, diet significantly improved the performance of mice ($F(2.838,84.952) = 3.275$, $p = 0.022$), as seen by a 16% distance reduction each due to CD + Chia and SRD + Chia and unexpectedly also a 25% distance reduction due to SRD + SRD (Fig. 2b). In summary, PRE and ADV mice successfully learned the platform position during acquisition phase, but APP23 mice covered longer distances and thus showed weaker spatial learning capabilities than WT mice.

At the last day of acquisition (day 3), no statistically significant differences between groups were detectable, indicating that all mice learned the platform position equally well. Nevertheless, we want to point out some notable differences. Both PRE and ADV APP23 mice had more difficulties in detecting the escape platform than age-matched WT mice, reflected by up to 54% longer distances (Fig. 2c,d). Interestingly, CD + Chia improved the performance of both PRE and ADV APP23 mice, as represented by an almost equal distance covered to the platform compared to age-matched WT mice (Fig. 2c,d). In ADV APP23 mice, CD + Chia even reduced the covered distance by 36% compared to CD + CD ($p = 0.078$) (Fig. 2d). Unexpectedly, also SRD + SRD improved the performance of ADV APP23 mice by reducing the covered distance by 14% compared to CD + CD ($p = 0.068$) (Fig. 2d). Both, the effect of chia supplementation and SRD, were also apparent as more targeted swim patterns in the heatmaps (Fig. 3, Supplemental Figure S3). In summary, both chia supplementation as well as SRD positively affected spatial learning in APP23 mice, especially with age.

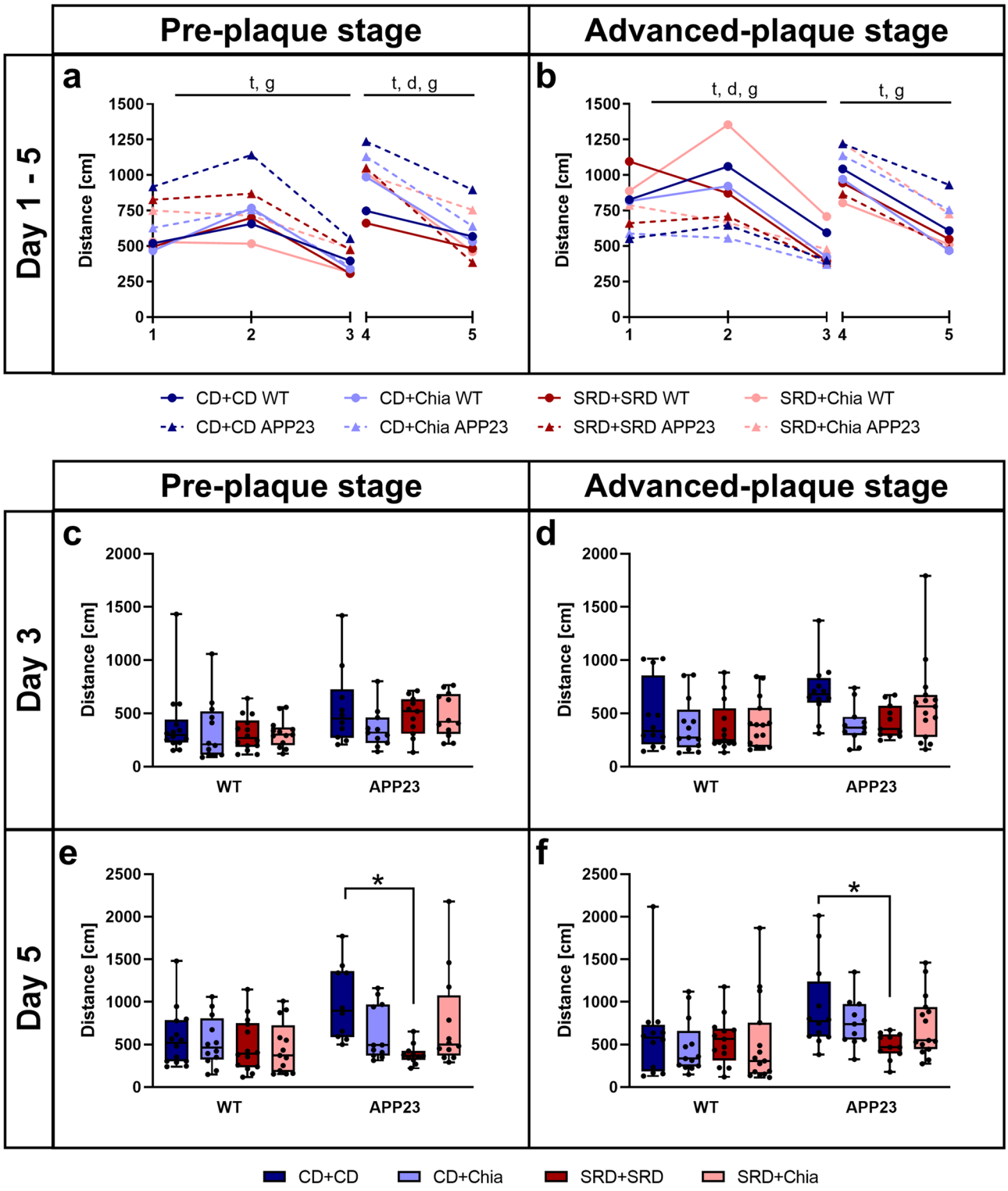

Figure 2. APP23 mice show impaired spatial learning, which is moderately improved by chia seeds, especially with age. APP23 mice show deteriorated reversal learning, which is improved by SRD. (**a**,**b**) Mean distance per day covered by PRE (**a**) and ADV mice (**b**) during acquisition phase (day 1–3) and reversal learning phase (day 4–5) in the MWM. Letters indicate significant factors (t = time, d = diet, g = genotype, combination of letters = interaction of two or three factors) regardless of significance level ($p < 0.05$), according to nonparametric repeated measures ANOVA-type test statistic. (**c**–**f**) Mean distance covered in the MWM by PRE (**c**, **e**) and ADV mice (**d**, **f**) on day 3, the last day of the acquisition phase, and day 5, the last day of the reversal learning phase, respectively. Each box represents the 25th to 75th percentile, the line represents the median, whiskers reach from minimum to maximum. An asterisk indicates significant differences between groups regardless of significance level ($p < 0.05$), according to nonparametric multiple contrast Tukey-type test. *WT* wild type control, *APP23* transgenic mouse model, *PRE* pre-plaque stage, *ADV* advanced-plaque stage, *CD* control, *SRD* sucrose-rich, *Chia* chia seed supplementation.

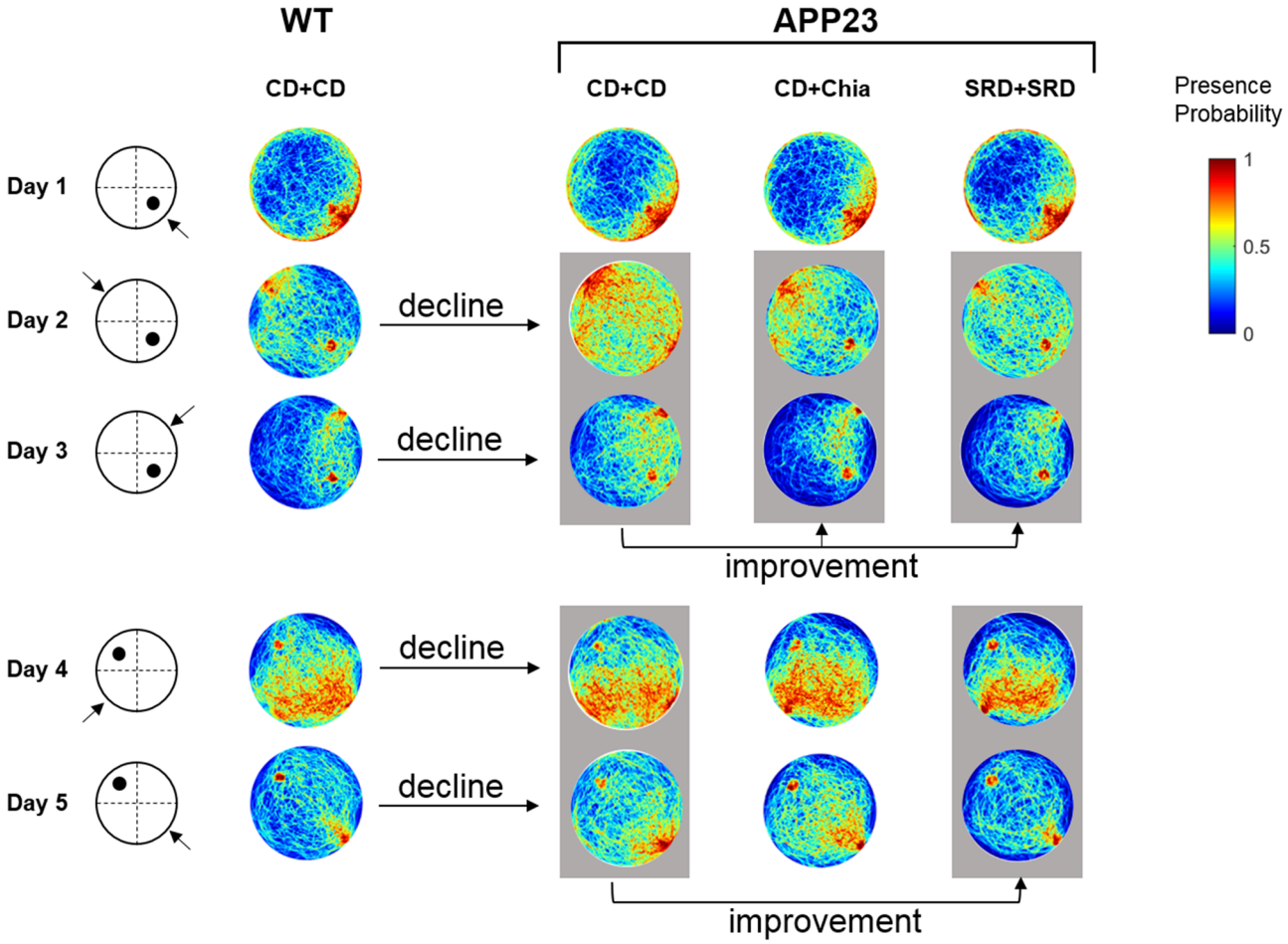

Figure 3. Visual representation of the effect of chia seeds and SRD during acquisition and reversal learning phase by exemplary pseudocolor coded heatmaps showing presence probabilities of ADV mice in the MWM. Reddish tones denote high presence probabilities and bluish tones denote low presence probabilities. The left panel indicates the day, the platform position (black dot) and the starting position of mice (arrow). The first row of heatmaps shows the presence probabilities of WT mice receiving CD + CD. The second row of heatmaps represents the presence probabilities of ADV APP23 mice receiving CD + CD, showing notably less directed swimming trajectories. The third row of heatmaps represents the presence probabilities of ADV APP23 mice receiving CD + Chia. Day 2 and 3 (marked by gray box) show more targeted swimming trajectories, compared to APP23 mice on CD + CD. The last row of heatmaps represents the presence probabilities of ADV APP23 mice receiving SRD + SRD. Day 2 and 3, as well as day 4 and 5 (marked by gray boxes), show more targeted swimming trajectories compared to APP23 mice receiving CD + CD. Heatmaps were generated with Matlab R2011b as follows. First, for each mouse swim paths of all 6 trials per day were projected to planar space as binary images (swim trajectory was set to value 1, non-swim path was set to value 0). Second, a single swim path per mouse and day was obtained using the mathematical union operation with values set to 1, if the animal traversed this position in at least 1 out of 6 trials. Third, probabilistic maps were created based on the binary images of all mice in one group on one day, such that the probability of 1 was assigned to a pixel that was crossed by every mouse in the respective group on the respective day. Conversely, a probability of 0 was allocated to a pixel that was never traversed by any mouse in the respective group on the respective day. *WT* wild type control, *APP23* transgenic mouse model, *PRE* pre-plaque stage, *ADV* advanced-plaque stage, *CD* control, *SRD* sucrose-rich, *Chia* chia seed supplementation.

SRD improves impaired cognitive flexibility in APP23 mice. During the reversal learning phase, mice of both the PRE and the ADV group successfully learned the new platform position, reflected by a significant time-dependent reduction of the distance covered to the platform (PRE: $F(1,82.512) = 55.473$, $p < 0.001$; ADV: $F(1,89.701) = 106.916$, $p < 0.001$) (Fig. 2a, b). Consistently, PRE and ADV APP23 mice performed inferior to age-matched WT mice also during the reversal learning phase (PRE: $F(1,82.512) = 12.035$, $p < 0.001$; ADV: $F(1,89.701) = 10.169$, $p < 0.001$), as shown by up to 30% longer distances (Fig. 2a,b). In both the PRE and ADV group, diet improved the performance of mice (PRE: $F(2.924,82.512) = 3.760$, $p = 0.010$; ADV: $F(2.968,89.701) = 2.558$, $p = 0.053$), although this missed statistical significance in the ADV group. The effect of diet was represented by a distance reduction of up to 25% due to SRD + SRD (Fig. 2a,b). In summary, all mice

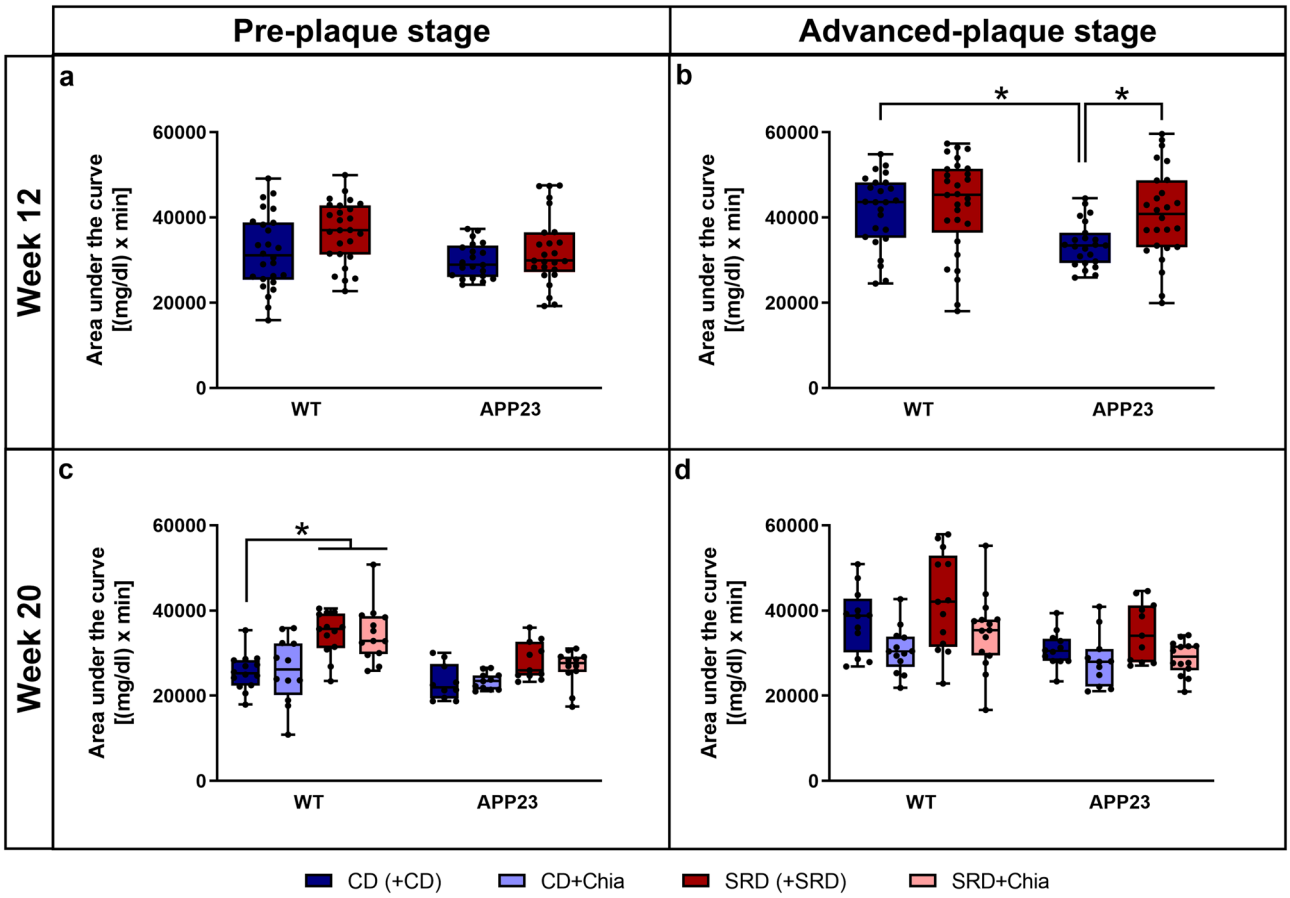

Figure 4. APP23 mice show a better glucose tolerance than WT mice, but ADV APP23 mice are more vulnerable to SRD-induced glucose intolerance. Glucose tolerance can be moderately improved by chia seeds in ADV APP23 and age-matched WT mice. (**a**,**b**) Glucose tolerance of PRE (**a**) and ADV mice (**b**) represented by area under the curve in (mg/dl) × min in week 12 at the end of pretreatment. (**c**,**d**) Glucose tolerance of PRE (**c**) and ADV mice (**d**) represented by area under the curve in (mg/dl) × min in week 20 at the end of therapy. Each box represents the 25th to 75th percentile, the line represents the median, whiskers reach from minimum to maximum. An asterisk indicates significant differences between groups regardless of significance level ($p < 0.05$), according to nonparametric multiple contrast Tukey-type test. *WT* wild type control, *APP23* transgenic mouse model, *PRE* pre-plaque stage, *ADV* advanced-plaque stage, *CD* control, *SRD* sucrose-rich, *Chia* chia seed supplementation.

successfully re-learned the platform position during the reversal learning phase, with APP23 mice again covering longer distances and thus showing less cognitive flexibility.

At the last day of reversal learning (day 5), SRD + SRD significantly improved the performance of both PRE and ADV APP23 mice compared to CD + CD, represented by a distance reduction of 57% ($p < 0.001$) and 48% ($p = 0.048$), respectively (Fig. 2e,f). The same effect was visible as more targeted swim patterns in the heatmaps (Fig. 3, Supplemental Figure S3). In summary, SRD improved cognitive flexibility in both PRE and ADV APP23 mice, whereas chia seeds had no effect on reversal learning.

Chia seeds positively influence glucose tolerance with age. In the PRE group, no significant differences in the AUC of the ipGTT were detectable after 12 weeks of pretreatment, indicating that SRD did not induce glucose intolerance in any genotype (Fig. 4a). However, after additional 8 weeks of therapy, glucose tolerance of WT mice of the PRE group was impaired due to SRD, as shown by an up to 35% increased AUC (SRD + SRD: $p = 0.027$; SRD + Chia: $p = 0.008$) (Fig. 4c).

In the ADV group, 12 weeks of pretreatment resulted in impaired glucose tolerance in APP23 mice, indicated by a 21% increase in the AUC of APP23 mice due to SRD ($p = 0.015$) (Fig. 4b). In contrast, glucose tolerance of WT mice was not impaired after 12 weeks of SRD (Fig. 4b). Interestingly, not metabolically stressed APP23 mice showed significantly superior glucose tolerance compared to WT mice, as shown by a 19% smaller AUC ($p = 0.001$) (Fig. 4b). In the ADV group, we could not detect significant differences in the AUC after 8 weeks of therapy. However, we want to point out that both CD + Chia and SRD + Chia ameliorated glucose tolerance, indicated by a 13% reduction of AUC in APP23 mice and a 18% reduction of AUC in WT mice (Fig. 4d). To sum up, although ADV APP23 mice showed an overall better glucose tolerance than age-matched WT mice,

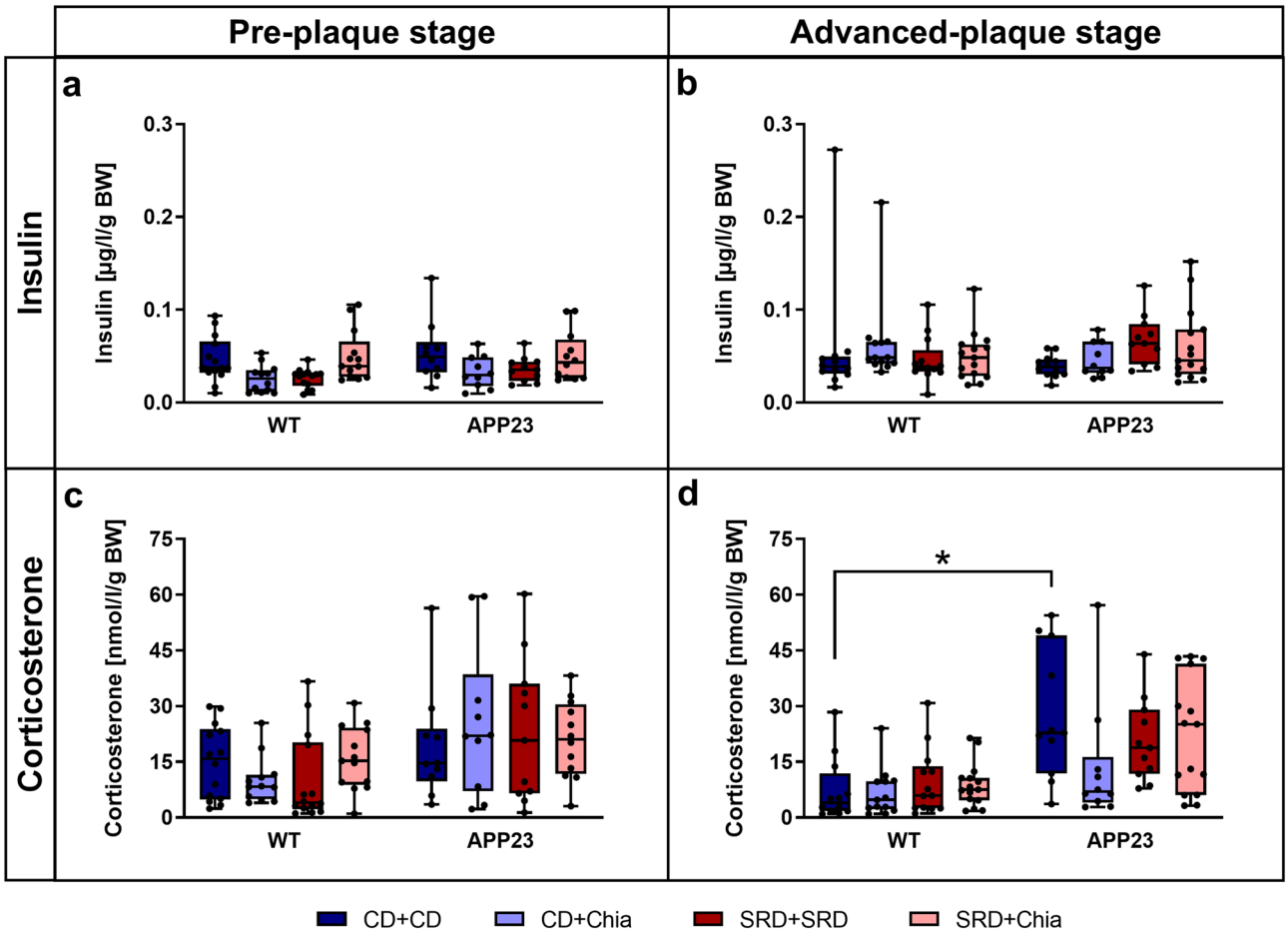

Figure 5. ADV APP23 mice show slight SRD-induced insulin insensitivity and generally increased corticosterone levels compared to age-matched WT mice, the latter being moderately improved by chia seeds. (**a**,**b**) Fasting plasma insulin levels adjusted for BW [µg/l/g] of PRE (**a**) and ADV mice (**b**). (**c**,**d**) Fasting plasma corticosterone levels adjusted for BW [nmol/l/g] of PRE (**c**) and ADV mice (**d**). Each box represents the 25th to 75th percentile, the line represents the median, whiskers reach from minimum to maximum. An asterisk indicates significant differences between groups regardless of significance level ($p < 0.05$), according to nonparametric multiple contrast Tukey-type test. *WT* wild type control, *APP23* transgenic mouse model, *PRE* pre-plaque stage, *ADV* advanced-plaque stage, *CD* control, *SRD* sucrose-rich, *Chia* chia seed supplementation, *BW* body weight.

they were more prone to SRD-induced glucose intolerance. Chia seeds mildly ameliorated glucose tolerance in mice of both genotypes in the ADV group.

Old APP23 mice show mild SRD-induced insulin insensitivity and generally elevated corticosterone levels, which are positively affected by chia seeds. Fasting insulin and corticosterone levels are displayed adjusted for BW (Fig. 5), since both hormones are linked to the regulation of BW. Insulin levels did not significantly differ between mice of the PRE group (Fig. 5a). Although insulin levels did not significantly differ in the ADV group either, we want to point out that SRD + SRD increased insulin levels by on average 74% in ADV APP23 mice compared to CD + CD ($p = 0.079$) (Fig. 5b). In summary, we observed that ADV APP23 mice might show slight insulin insensitivity induced by SRD. Insulin levels were not affected by chia seeds.

Corticosterone levels did not significantly differ between mice of the PRE group (Fig. 5c). Generally, ADV APP23 mice displayed on average 2.5 times higher corticosterone levels than age-matched WT mice (Fig. 5d). Interestingly, chia seeds reduced corticosterone levels by 51% in ADV APP23 mice compared to CD + CD. However, this difference was not statistically significant ($p = 0.349$) (Fig. 5d). In summary, ADV APP23 mice showed elevated corticosterone levels compared to age-matched WT mice. Nevertheless, chia seeds exerted a mild positive effect on corticosterone levels in ADV APP23 mice.

Chia seeds reverse SRD-induced elevation of pro-inflammatory cytokine levels, whereas Aβ plaque load and microglia abundance are not affected by diet. PRE APP23 mice only showed very few and very small plaques in hippocampus and cortex and there were no differences in Aβ plaque load between the dietary groups (Fig. 6a). Aβ plaque load in ADV APP23 mice was more than 250 times higher compared to

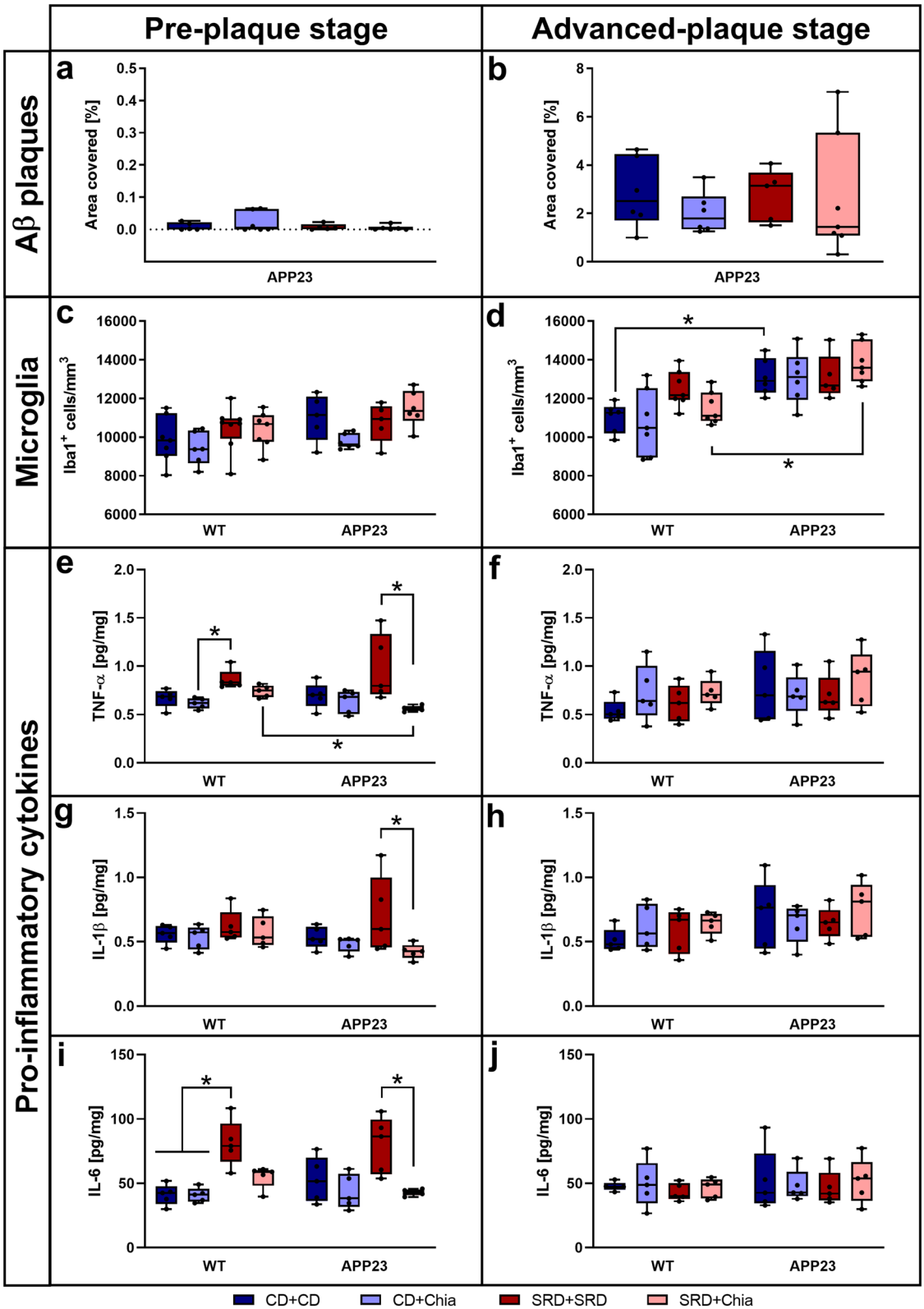

Figure 6. ADV APP23 mice show increased Aβ plaque load and elevated numbers of microglia in the hippocampus. Pro-inflammatory cytokine levels are increased by SRD but only in the PRE group. (**a**,**b**) Aβ plaque load represented by the percentage of area covered with pFTAA-positive plaques in the hippocampus and cortex of PRE (**a**) and ADV mice (**b**). (**c**,**d**) Number of microglia/macrophages expressing Iba1$^+$ per mm^3 in the hippocampus of PRE (**c**) and ADV mice (**d**). (**e**,**f**) TNF-α levels [pg/mg] in the hippocampus of PRE (**e**) and ADV (**f**) mice. (**g**,**h**) IL-1β levels [pg/mg] in the hippocampus of PRE (**g**) and ADV (**h**) mice. (**i**,**j**) IL-6 levels [pg/mg] in the hippocampus of PRE (**i**) and ADV (**j**) mice. Each box represents the 25th to 75th percentile, the line represents the median, whiskers reach from minimum to maximum. An asterisk indicates significant differences between groups regardless of significance level ($p < 0.05$), according to nonparametric multiple contrast Tukey-type test. *WT* wild type control, *APP23* transgenic mouse model, *PRE* pre-plaque stage, *ADV* advanced-plaque stage, *CD* control, *SRD* sucrose-rich, *Chia* chia seed supplementation, *Iba1* allograft inflammatory factor 1, *TNF-α* tumor necrosis factor-α, *IL* interleukin.

PRE APP23 mice (on average 2.57% of hippocampus and cortex covered with plaques) but also showed no differences between dietary groups (Fig. 6b). No statistically significant differences in the number of hippocampal microglia were detectable in mice of the PRE group (Fig. 6c). Generally, ADV APP23 mice showed about 20% increased amounts of hippocampal microglia compared to age-matched WT mice (within CD + CD: $p = 0.025$; within SRD + Chia: $p = 0.020$) (Fig. 6d). Nevertheless, diet did not affect the number of hippocampal microglia. Representative images of pFTAA- and Iba1-stainings are presented in Supplemental Figure S4.

The analysis of pro-inflammatory cytokines was focused on TNF-α, IL-1β, and IL-6 as early players in the switch of microglia from an anti-inflammatory to a pro-inflammatory phenotype. However, results of the remaining measured pro-inflammatory cytokines were very similar and are presented in Supplemental Figure S5. In the PRE group, hippocampal levels of pro-inflammatory cytokines were similar between APP23 and WT mice (Fig. 6e,g,i). TNF-α levels were significantly increased due to SRD by 40% in WT mice (CD + Chia vs. SRD + SRD, $p = 0.008$) and by 73% in APP23 mice (SRD + SRD vs. SRD + Chia, $p = 0.049$) (Fig. 6e). Similarly, hippocampal IL-1β levels were significantly increased due to SRD by 65% in APP23 mice (SRD + SRD vs. SRD + Chia, $p = 0.040$) (Fig. 6g). Consistently, IL-6 levels were significantly elevated due to SRD by 98% in WT mice (CD + CD/CD + Chia vs. SRD + SRD, $p = 0.048$ and $p = 0.027$) and by 86% in APP23 mice (SRD + SRD vs. SRD + Chia, $p = 0.047$) (Fig. 6i). Interestingly, all pro-inflammatory cytokine levels were normalized due to chia supplementation of SRD in the PRE group (Fig. 6e,g,i). In contrast, there were no significant differences detectable in the ADV group (Fig. 6f,h,j). In summary, both Aβ plaque load and microglia abundance were increased in ADV APP23 mice but unaffected by diet. In contrast, pro-inflammatory cytokine levels were similar between genotypes but elevated by SRD in the PRE group but not in the ADV group. This effect was reversed by chia seeds.

Cell survival of newborn cells and the number of immature neurons together with representative images are shown in Supplemental Figure S6. In summary, AHN was not altered in APP23 mice and unaffected by diet.

Reduced body weight in APP23 mice tends to be increased by chia seeds. The development of BW over time is shown in Supplemental Figure S7. In summary, APP23 mice weighed significantly less than WT mice with the difference becoming more pronounced with age (up to 15% difference in BW in the PRE group and up to 22% in the ADV group) (PRE: $F(1,71.940) = 71.498$, $p < 0.001$; ADV: $F(1,64.711) = 136.102$, $p < 0.001$). Chia seeds moderately increased BW by about 10% in the PRE group and about 9% in the ADV group (PRE: $F(2.823,71.940) = 8.763$, $p < 0.001$; ADV: $F(2.873,64.711) = 3.692$, $p = 0.012$).

Anxiety-related behavior is neither altered by genotype nor by diet. Supplemental Figure S8 shows the analysis of animals' behavior in the EPM. In summary, anxiety-related behavior did not differ between APP23 and WT mice, neither in the PRE nor in the ADV group. It was also not affected by any diet.

Motor coordination negatively correlates with body weight. Motor coordination is displayed as the time until mice fell off the accelerating rotating rod in Supplemental Figure S9. In summary, there were no relevant differences between any of the groups. Nevertheless, time on the rod negatively correlated with BW of mice (PRE: $r = -0.4212$, $p < 0.001$; ADV: $r = -0.4102$, $p < 0.001$), i.e. mice weighing more spent less time on the rod. Since APP23 mice weighed significantly less than WT mice and hence showed better motor coordination, we conclude that the observed inferior performance of APP23 mice in the MWM is truly related to cognitive impairment and not to motoric deficits.

Discussion

This study was conducted to examine the effects of diet-induced metabolic stress as well as the therapeutic potential of chia seeds in AD pathology.

PRE and ADV APP23 mice showed impaired spatial learning and cognitive flexibility. Cognitive deficits of APP23 mice have been demonstrated before by us and others, in some studies even preceding the onset of Aβ plaque deposition[29,33]. The fact that cognitive performance was already affected in PRE APP23 mice, which scarcely displayed Aβ plaques, further supports the idea that Aβ plaques might not represent the neuropathologic correlate and exclusive underlying mechanism of cognitive decline in AD.

Diet differentially influenced both spatial learning and cognitive flexibility. We showed for the first time that chia seed supplementation mildly improved spatial learning especially in ADV APP23 mice. Our data suggest that this effect might be due to an accumulation of several aspects, although some of them on their own did not reach statistical significance. Firstly, chia seeds seemed to slightly improve glucose tolerance in ADV APP23 mice. It has been shown that impaired glucose tolerance correlates with cognitive decline and that the amelioration of glucose homeostasis positively affects cognitive performance[34,35]. Secondly, chia seeds led to a slight reduction of elevated corticosterone levels in ADV APP23 mice. Studies have shown that long-term elevated corticosterone levels induce cognitive deficits and that a reduction of corticosterone levels ameliorates cognitive impairment[36,37]. Thirdly, chia seeds reversed SRD-induced elevation of pro-inflammatory cytokine levels in the PRE group. Recent studies suggest that enhanced neuroinflammation might directly correlate with inferior cognitive perfomance[38]. Lastly, chia seeds are rich in PUFAs, which are further metabolized into EPA and DHA[18,20]. EPA and DHA have been shown to stimulate synaptogenesis, to act neuroprotective, to improve long-term potentiation and to ameliorate Aβ-induced cognitive deficits[39,40]. Thus, these minor contributions might add up to an improvement of spatial learning. Nevertheless, chia seeds failed to ameliorate impaired cognitive flexibility in APP23 mice. This seems controversial, since supplementation with DHA has been shown to improve reversal learning in healthy mice and reduction of corticosterone levels has been shown to correlate with improved cognitive flexibility in healthy rats[41,42]. However, reversal learning requires the suppression of the previously learnt platform position, cognitive flexibility to imprint the new position, as well as attention and

motivation[43]. Therefore, a high degree of functional plasticity is needed, which is clearly impaired in AD[44,45]. Reduction of corticosterone levels or DHA supplementation might be adequate to improve cognitive flexibility in otherwise healthy animals. However, it appears to be insufficient in diseased animals used in the present study, potentially due to a lack of functional plasticity.

In contrast to our initial hypothesis, SRD improved both spatial learning and cognitive flexibility especially in ADV APP23 mice. Numerous studies have shown the detrimental effects of energy-rich diets on cognitive abilities, such as spatial and reversal learning[46,47]. However, most of these studies have compared energy-rich diets to normal lab chow, thus the observed effects might not primarily depend on sugar or fat itself but rather on increased calorie intake. The detrimental effect of high calorie intake on brain function and AHN has been shown before[48]. In the present study, we used isocaloric diets in order to ensure similar calorie intake in all groups. We hypothesize that the observed beneficial effect of SRD on cognition might be mediated by a fast access to energy supplied by short-chained carbohydrates. APP23 mice, which were—especially in the ADV group—substantially leaner compared to WT mice, potentially profited from this quickly accessible energy. In conclusion, rapidly accessible energy delivered by SRD might have provided mice with more capacities for cognitive tasks. A less physically challenging cognitive test, such as the Barnes Maze, might have been more suitable for this mouse model.

PRE and ADV APP23 mice treated with CD showed better glucose tolerance than WT mice. This contradicts our initial hypothesis of inferior glucose tolerance of APP23 mice. However, while cerebral glucose hypometabolism is reliably detectable very early in disease progression[49], alterations of peripheral glucose metabolism do not always occur in relation with AD. Both human and animal studies have revealed controversial outcomes, in which peripheral glucose tolerance and insulin sensitivity in AD were either inferior, not altered or even superior compared to controls[50–56]. For example, intact glucose tolerance has been shown in male APP23 mice of different ages[56] and in both male and female APP/PS1 mice[54]. On the one hand, these inconsistencies might result from different disease models, the influence of the estrous cycle in females and different protocols of the highly stress-sensitive glucose tolerance test. On the other hand, it has been shown that peripheral glycemic dysregulation in AD might be mediated by peripheral Aβ levels, which are very low in APP23 mice[10,56]. Thus, APP23 mice might not ideally mimic peripheral AD-induced metabolic alterations. Additionally, the significantly lower BW of APP23 mice might have accounted for better glucose tolerance compared to WT mice, since weight loss is a key intervention in the improvement of glucose tolerance[57]. Consistently with not being glucose intolerant per se, APP23 mice fed with CD did not show insulin resistance compared to WT mice.

We showed for the first time that ADV but not PRE APP23 mice displayed impaired glucose tolerance due to SRD. It has been shown that age drives an incline in glucose tolerance over time[58]. Our findings are in line with other studies showing that aged APP/PS1 mice are more prone to diet-induced glucose intolerance, when challenged with a high-fat diet[59]. These findings suggest that the presence of Aβ, potentially together with an age-related decrease of glucose tolerance per se, promotes diet-induced glucose intolerance. A possible mechanism might be interference of Aβ with hypothalamic insulin signaling. This has been shown to be crucial for the inhibition of further glucose production, thus leading to peripheral hyperglycemia[53,60]. In line with these findings, ADV APP23 mice showed a mildly enhanced vulnerability to SRD-induced insulin insensitivity.

Chia seeds improved glucose tolerance in both genotypes of the ADV group but not of the PRE group, although this difference was not statistically significant. This supports earlier findings, which have shown that chia seeds decrease diet-induced elevated plasma glucose level in rats[23,24] and improve glycemic control in humans[61,62]. Since ageing itself drives glucose intolerance, as described above, it is plausible that the positive effect of chia seeds is more prominent in ADV mice than in PRE mice.

ADV but not PRE APP23 mice showed notably increased levels of corticosterone compared to WT mice, indicating a dysregulation of the HPA axis. The hippocampus plays a crucial role in HPA axis regulation[63]. It has been shown that intracerebroventricular injection of Aβ in healthy rats results in disturbed feedback of the HPA axis[64]. Considering the early affection of the hippocampus in AD, elevated GCs observed in AD patients might reflect an HPA axis dysregulation as a reaction to Aβ toxicity[65]. This matches our observation that PRE APP23 mice barely exhibited Aβ deposits and showed normal corticosterone levels, whereas ADV APP23 mice exhibited significant amounts of Aβ plaques and displayed increased corticosterone levels. Additionally, elevated levels of GCs have been shown to deteriorate insulin sensitivity and glucose tolerance[66]. Therefore, we suggest that Aβ-induced HPA axis dysregulation in ADV APP23 mice led to increased corticosterone levels, which in turn resulted in glucose intolerance and moderate insulin insensitivity, when mice were challenged with SRD. Due to the absence of Aβ deposits in PRE APP23 mice, corticosterone levels, glucose tolerance and insulin sensitivity were unaffected.

Aβ plaque load and the number of microglia were considerably increased in ADV APP23 mice compared to PRE APP23 mice and age-matched WT mice, respectively. These findings are consistent with previous descriptions of plaque pathology slowly starting at 6 months of age and of Aβ plaques being surrounded by activated microglia in APP23 mice[28,67]. However, pro-inflammatory cytokine levels were similar between APP23 and WT mice of both age groups. Thus, although more abundant in ADV APP23 mice, microglia do not seem to release higher levels of pro-inflammatory cytokines. This is in line with a longitudinal study in APP23 mice showing that neuroinflammation in the hippocampus first occurs at 20 months of age[68]. Furthermore, estrogen directly influences microglial responses. For example, estrogen supplementation in ovariectomized APP23 mice has been shown to reduce the expression of pro-inflammatory cytokines[69]. Thus, the low levels of pro-inflammatory cytokines despite elevated numbers of microglia might be due to an estrogen-mediated delay in the inflammatory response of microglia to Aβ plaques[69]. Pro-inflammatory cytokine levels were increased by SRD but only in the PRE group. The inflammatory response to SRD is in line with earlier studies that have demonstrated increased neuroinflammation due to excessive sugar intake[70]. It has also been shown that this response is age-dependent. Though, normally aged individuals are more prone to diet-induced neuroinflammation than young individuals[71].

Here, younger mice show a more pronounced inflammatory response to SRD. This might be due to elevated corticosterone levels in the ADV group, since GCs counteract the pro-inflammatory action of cytokines[72]. Nevertheless, corticosterone levels were only elevated in ADV APP23 mice, hence giving no explanation for the absence of an inflammatory response to SRD in aged WT mice, the reasons for which we can only speculate about. A possible explanation might lie in the composition of gut microbiota, which have been shown to influence neuroinflammation via the gut-brain axis and to be superior in WT mice compared to AD mouse models[73]. SRD-induced elevation of pro-inflammatory cytokine levels in the PRE group was entirely reversed by chia seed supplementation. We suggest that this anti-inflammatory effect might be mediated by omega-3 PUFAs, since it has been shown that EPA and DHA decrease the expression of pro-inflammatory factors[21]. The number of microglia and Aβ plaque load were not affected by diet. In contrast to our results, it has been shown that DHA supplementation is able to reduce Aβ deposition in two different AD mouse models overexpressing APP[74,75]. ALA and EPA instead increase Aβ production *in vitro*[75]. Thus, ALA and EPA might counteract the beneficial effects of DHA, which leads to unaltered Aβ burden in our study.

APP23 mice weighed significantly less than WT mice, the difference becoming more prominent with age, as already observed by others[76,77]. Weight loss also occurs in AD patients, the causative reasons remaining elusive[78]. We addressed this question in a different study. First analyses suggest an increased energy expenditure, respiratory exchange rate, and hyperactivity of APP23 mice (data not yet published). Chia seeds showed an overall tendency of inducing weight gain. Others observed increased food intake and subsequent weight gain in rats due to chia seed supplementation[24]. We also observed enthusiastic feeding on food pellets including chia seeds, potentially leading to weight gain. A human study instead reported moderate weight loss in overweight and obese patients due to chia seed supplementation[79]. These different findings might result from ad libitum feeding in animal studies, whereas calorie intake was restricted in the human study.

The genetic induction of Aβ deposition in the APP23 mouse model might limit the insights into the relationship of glucose metabolism and AD, since Aβ pathology in this case obviously represents the underlying mechanism. However, animal models accurately modeling sporadic late-onset AD still have to be developed. Although we intentionally chose female mice considering that AD is more prevalent in women, the estrous cycle potentially interferes with other hormone systems such as the HPA-axis. Hence, future studies should carefully monitor the estrous cycle to assess its impact on study outcomes. Another aspect that might limit the significance of chia seed supplementation in AD is the high dose used in this and other animal studies as such a high dose might not be applicable to a person's diet. However, already lower doses of chia seeds successfully improved metabolic features in human studies, making a similar effect on cognition possible.

Conclusion

We initially hypothesized that APP23 mice would display a disturbed peripheral glucose metabolism. Contrary, we show here that the peripheral glucose metabolism of APP23 mice is generally functioning. Nevertheless, we show for the first time an age-dependent increase in vulnerability to metabolic stress in APP23 mice. But in contrast to our hypothesis that metabolic stress would aggravate AD pathology in APP23 mice, cognitive performance as well as Aβ plaque load are not negatively influenced by SRD, despite a SRD-induced elevation of pro-inflammatory cytokine levels. This suggests that glucose hypometabolism might not be the underlying mechanism driving AD pathology in this AD mouse model. Furthermore, we hypothesized that chia seeds would attenuate AD pathology by improving metabolic parameters. Our data reveal a moderate therapeutic potential of chia seeds in alleviating spatial learning impairments by a mild amelioration of glucose tolerance, a slight reduction of corticosterone levels, and a reversal of SRD-induced elevation of pro-inflammatory cytokine levels.

Data availability

The datasets generated during and/or analysed during the current study are available from the corresponding author on reasonable request.

Received: 19 June 2020; Accepted: 12 October 2020
Published online: 26 October 2020

References

1. Patterson, C. World Alzheimer Report 2018. *Alzheimer's Dis. Int.* https://doi.org/10.1111/j.0033-0124.1950.24_14.x (2018).
2. Lane, C. A., Hardy, J. & Schott, J. M. Alzheimer's disease. *Eur. J. Neurol.* **25**, 59–70 (2018).
3. Serrano-Pozo, A., Frosch, M. P., Masliah, E. & Hyman, B. T. Neuropathological alterations in Alzheimer disease. *Cold Spring Harb Perspect Med* 1–24 (2011).
4. Mu, Y. & Gage, F. H. Adult hippocampal neurogenesis and its role in Alzheimer's disease. *Mol. Neurodegener.* **6**, 1–9 (2011).
5. Hardy, J. A. & Higgins, G. A. Alzheimer's disease: The amyloid cascade hypothesis. *Science (80-.).* **256**, 184–185 (1992).
6. Foroutan, N., Hopkins, R. B., Tarride, J.-E., Florez, I. D. & Levine, M. Safety and efficacy of active and passive immunotherapy in mild-to-moderate Alzheimer's disease: a systematic review and network meta-analysis. *Clin. Invest. Med.* **42**, 53–65 (2019).
7. Calsolaro, V. & Edison, P. Alterations in glucose metabolism in Alzheimer's disease. *Recent Pat. Endocr. Metab. Immune Drug Discov.* **1**, 31–39 (2016).
8. Ivanov, A. I., Malkov, A., Buldakova, S., Zilberter, M. & Zilberter, Y. Seizures and amyloid-ß induce similar changes in neuronal network metabolic parameters in mouse hippocampal slices. *PeerJ Prepr.* **4**, 10–13 (2016).
9. Zilberter, Y. & Zilberter, M. The vicious circle of hypometabolism in neurodegenerative diseases: ways and mechanisms of metabolic correction. *J. Neurosci. Res.* **95**, 2217–2235 (2017).
10. Wijesekara, N., Gonçalves, R. A., De Felice, F. G. & Fraser, P. E. Impaired peripheral glucose homeostasis and Alzheimer's disease. *Neuropharmacology* **136**, 172–181 (2018).
11. Pugazhenthi, S., Qin, L. & Reddy, P. H. Common neurodegenerative pathways in obesity, diabetes, and Alzheimer's disease. *BBA Mol. Basis Dis.* **1863**, 1037–1045 (2017).

12. Ahmad, M. H., Fatima, M. & Mondal, A. C. Role of hypothalamic-pituitary-adrenal axis, hypothalamic-pituitary-gonadal axis and insulin signaling in the pathophysiology of Alzheimer's disease. *Neuropsychobiology* **77**, 197–205 (2019).
13. Martínez, B. B. *et al.* Experimental model of glucocorticoid-induced insulin resistance. *Acta Cir. Bras.* **31**, 645–649 (2016).
14. Huang, C.-W. *et al.* Elevated basal cortisol level predicts lower hippocampal volume and cognitive decline in Alzheimer's disease. *J. Clin. Neurosci.* **16**, 1283–1286 (2009).
15. Chiodini, I. *et al.* Cortisol secretion in patients with type 2 diabetes: relationship with chronic complications. *Diabetes Care* **30**, 83–88 (2007).
16. Rendón-villalobos, J. R., Ortíz-sánchez, A. & Flores-Huicochea, E. (2018) Nutritionally enhanced foods incorporating Chía seed. in *Therapeutic Foods* 257–281 (Elsevier Inc., 2018). doi:https://doi.org/10.1016/B978-0-12-811517-6/00009-X.
17. Brand-Miller, J., Hayne, S., Petocz, P. & Colagiuri, S. Low-glycemic index diets in the management of diabetes: a meta-analysis of randomized controlled trials. *Diabetes Care* **26**, 2261–2267 (2003).
18. Ayerza, R. Oil content and fatty acid composition of chia (*Salvia hispanica* L.) from five northwestern locations in Argentina. *J. Am. Oil Chem. Soc.* **72**, 1079–1081 (1995).
19. Bushway, A. A., Belyea, P. R. & Bushway, R. J. Chia seed as a source of oil, polysaccharide, and protein. *J. Food Sci.* **46**, 1349–1350 (1981).
20. Singh, M. Essential fatty acids, DHA and human brain. *Indian J. Pediatr.* **72**, 239–242 (2005).
21. Devassy, J. G., Leng, S., Gabbs, M., Monirujjaman, M. & Aukema, H. M. Omega-3 polyunsaturated fatty acids and oxylipins in neuroinflammation and management of Alzheimer disease. *Adv. Nutr.* **7**, 905–916 (2016).
22. Bazinet, R. P. & Layé, S. Polyunsaturated fatty acids and their metabolites in brain function and disease. *Nat. Rev. Neurosci.* **15**, 771–785 (2014).
23. Chicco, A. G., D'Alessandro, M. E., Hein, G. J., Oliva, M. E. & Lombardo, Y. B. Dietary chia seed (*Salvia hispanica* L.) rich in alpha-linolenic acid improves adiposity and normalises hypertriacylglycerolaemia and insulin resistance in dyslipaemic rats. *Br. J. Nutr.* **101**, 41–50 (2009).
24. Poudyal, H., Panchal, S. K., Waanders, J., Ward, L. & Brown, L. Lipid redistribution by α-linolenic acid-rich chia seed inhibits stearoyl-CoA desaturase-1 and induces cardiac and hepatic protection in diet-induced obese rats. *J. Nutr. Biochem.* **23**, 153–162 (2012).
25. Ullah, R. *et al.* Nutritional and therapeutic perspectives of chia (*Salvia hispanica* L.): a review. *J. Food Sci. Technol.* **53**, 1750–1758 (2016).
26. Bilgic, Y. *et al.* Detrimental effects of chia (*Salvia hispanica* L.) seeds on learning and memory in aluminium chloride-induced experimental Alzheimer's disease. *Acta Neurobiol. Exp.* **1**, 322–331. https://doi.org/10.21307/ane (2018).
27. Rui, Y. *et al.* Chia seed does not improve cognitive impairment in SAMP8 mice fed with high fat diet. *Nutrients* **10**, 1 (2018).
28. Sturchler-Pierrat, C. *et al.* Two amyloid precursor protein transgenic mouse models with Alzheimer disease-like pathology. *Proc. Natl. Acad. Sci. U. S. A.* **94**, 13287–13292 (1997).
29. Pfeffer, A. *et al.* Behavioral and psychological symptoms of dementia (BPSD) and impaired cognition reflect unsuccessful neuronal compensation in the pre-plaque stage and serve as early markers for Alzheimer's disease in the APP23 mouse model. *Behav. Brain Res.* **347**, 300–313 (2018).
30. Klein, C. *et al.* Stimulation of adult hippocampal neurogenesis by physical exercise and enriched environment is disturbed in a CADASIL mouse model. *Sci. Rep.* **7**, 1 (2017).
31. Konietschke, F., Placzek, M., Schaarschmidt, F. & Hothorn, L. A. nparcomp: an R software package for nonparametric multiple comparisons and simultaneous confidence intervals. *J. Stat. Softw.* **64**, 1–17 (2015).
32. Noguchi, K., Gel, Y. R., Brunner, E. & Konietschke, F. nparLD: an R software package for the nonparametric analysis of longitudinal data in factorial experiments. *J. Stat. Softw.* **50**, 1 (2012).
33. Van Dam, D. *et al.* Age-dependent cognitive decline in the APP23 model precedes amyloid deposition. *Eur. J. Neurosci.* **17**, 388–396 (2003).
34. Kerti, L. *et al.* Higher glucose levels associated with lower memory and reduced hippocampal microstructure. *Neurology* **83**, 102 (2014).
35. Reay, J. L., Kennedy, D. O. & Scholey, A. B. Single doses of panax ginseng (G115) reduce blood glucose levels and improve cognitive performance during sustained mental activity. *J. Psychopharmacol.* **19**, 357–365 (2005).
36. Dachir, S., Kadar, T., Robinzon, B. & Levy, A. Cognitive deficits induced in young rats by long-term corticosterone administration. *Behav. Neural Biol.* **60**, 103–109 (1993).
37. Hashim, S., Haider, A., Khan, S. & Abbas, G. B- Glucan, a polysaccharide found in avena sativa (oat), attenuated chronic unpredictable mild stress induced cognitive impairment in rodents via normalizing corticosterone levels. *Iran. J. Pharmacol. Ther.* **15**, 1 (2017).
38. Passamonti, X. L. *et al.* Neuroinflammation and functional connectivity in Alzheimer's disease: interactive influences on cognitive performance. *J. Neurosci.* **39**, 7218–7226 (2019).
39. Dyall, S. C. Long-chain omega-3 fatty acids and the brain: a review of the independent and shared effects of EPA, DPA and DHA. *Front. Aging Neurosci.* **7**, 1 (2015).
40. Wen, M. *et al.* Eicosapentaenoic acid-enriched phospholipids improve Aβ1-40-induced cognitive deficiency in a rat model of Alzheimer's disease. *J. Funct. Foods* **24**, 537–548 (2016).
41. Rusu, S. I. *et al.* Corticosterone impairs flexible adjustment of spatial navigation in an associative place–reward learning task. *Behav. Pharmacol.* **29**, 1 (2018).
42. Jašarević, E., Hecht, P. M., Fritsche, K. L., Beversdorf, D. Q. & Geary, D. C. Dissociable effects of dorsal and ventral hippocampal DHA content on spatial learning and anxiety-like behavior. *Neurobiol. Learn. Mem.* **116**, 59–68 (2014).
43. Izquierdo, A., Brigman, J. L., Radke, A. K., Rudebeck, P. H. & Holmes, A. The neural basis of reversal learning: an updated perspective. *Neuroscience* **345**, 12–26 (2017).
44. Garthe, A., Behr, J. & Kempermann, G. Adult-generated hippocampal neurons allow the flexible use of spatially precise learning strategies. *PLoS ONE* **4**, 1 (2009).
45. Styr, B. & Slutsky, I. Imbalance between firing homeostasis and synaptic plasticity drives early-phase Alzheimer's disease. *Nat. Neurosci.* **21**, 463–473 (2018).
46. Molteni, R., Barnard, R. J., Ying, Z., Roberts, C. K. & Gómez-Pinilla, F. A high-fat, refined sugar diet reduces hippocampal brain-derived neurotrophic factor, neuronal plasticity, and learning. *Neuroscience* **112**, 803–814 (2002).
47. Kanoski, S. E., Meisel, R. L., Mullins, A. J. & Davidson, T. L. The effects of energy-rich diets on discrimination reversal learning and on BDNF in the hippocampus and prefrontal cortex of the rat. *Behav. Brain Res.* **182**, 57–66 (2007).
48. Morgan, A. H., Andrews, Z. B. & Davies, J. S. Less is more: Caloric regulation of neurogenesis and adult brain function. *J. Neuroendocrinol.* **29**, 1–11 (2017).
49. Mosconi, L. Brain glucose metabolism in the early and specific diagnosis of Alzheimer's disease: FDG-PET studies in MCI and AD. *Eur. J. Nucl. Med. Mol. Imaging* **32**, 486–510 (2005).
50. Razay, G. & Wilcock, G. K. Hyperinsulinaemia and Alzheimer's disease. *Age Ageing* **23**, 396–399 (1994).
51. Matsuzaki, T. *et al.* Insulin resistance is associated with the pathology of Alzheimer disease: the Hisayama study. *Neurology* **75**, 764–770 (2010).

52. Landin-Wilhelmsen, K., Blennow, K., Wallin, A. & Gottfries, C.-G. Low blood pressure and blood glucose levels in Alzheimer's disease: evidence for a hypometabolic disorder?. *J. Intern. Med.* **233**, 357–363 (1993).
53. Jiménez-Palomares, M. *et al.* Increased Aβ production prompts the onset of glucose intolerance and insulin resistance. *Am. J. Physiol. Endocrinol. Metab.* **302**, 1373–1380 (2012).
54. Walker, J. M., Dixit, S., Saulsberry, A. C., May, J. M. & Harrison, F. E. Reversal of high fat diet-induced obesity improves glucose tolerance, inflammatory response, β-amyloid accumulation and cognitive decline in the APP/PSEN1 mouse model of Alzheimer's disease. *Neurobiol. Dis.* **100**, 87–98 (2017).
55. Macklin, L. *et al.* Glucose tolerance and insulin sensitivity are impaired in APP/PS1 transgenic mice prior to amyloid plaque pathogenesis and cognitive decline. *Exp. Gerontol.* **88**, 9–18 (2017).
56. Takeda, S. *et al.* Elevation of plasma β-amyloid level by glucose loading in Alzheimer mouse models. *Biochem. Biophys. Res. Commun.* **385**, 193–197 (2009).
57. Long, S. D. *et al.* Weight loss in severely obese subjects prevents the progression of impaired glucose tolerance to type II diabetes: a longitudinal interventional study. *Diabetes Care* **17**, 372–375 (1994).
58. Shimokata, H. *et al.* Age as independent determinant of glucose tolerance. *Diabetes* **40**, 44–51 (1991).
59. Mody, N., Agouni, A., Mcilroy, G. D., Platt, B. & Delibegovic, M. Susceptibility to diet-induced obesity and glucose intolerance in the APP/PSEN1 mouse model of Alzheimer's disease is associated with increased brain levels of PTP1B and RBP4, and basal phosphorylation of S6 ribosomal protein. *Diabetologia* **54**, 2143–2151 (2011).
60. Obici, S., Zhang, B. B., Karkanias, G. & Rossetti, L. Hypothalamic insulin signaling is required for inhibition of glucose production. *Nat. Med.* **8**, 1 (2002).
61. Ho, H. *et al.* Effect of whole and ground Salba seeds (*Salvia Hispanica* L.) on postprandial glycemia in healthy volunteers: a randomized controlled, dose-response trial. *Eur. J. Clin. Nutr.* **67**, 786–788 (2013).
62. Vuksan, V. *et al.* (2016) Comparison of fl ax (*Linum usitatissimum*) and Salba-chia (*Salvia hispanica* L.) seeds on postprandial glycemia and satiety in healthy individuals: a randomized, controlled, crossover study. **1**:1–5. https://doi.org/https://doi.org/10.1038/ejcn.2016.148.
63. Jacobson, L. & Sapolsky, R. The role of the hippocampus in feedback regulation of the hypothalamic-pituitary-adrenocortical axis. *Endocr. Rev.* **12**, 118–134 (1991).
64. Brureau, A. *et al.* Deregulation of hypothalamic-pituitary-adrenal axis functions in an Alzheimer's disease rat model. *Neurobiol. Aging* **34**, 1426–1439 (2013).
65. Rasmuson, S. *et al.* Increased glucocorticoid production and altered cortisol metabolism in women with mild to moderate Alzheimer's disease. *Biol. Psychiatry* **49**, 547–552 (2001).
66. Pasieka, A. M. & Rafacho, A. Impact of glucocorticoid excess on glucose tolerance: clinical and preclinical evidence. *Metabolites* **6**, 1 (2016).
67. Stalder, M. *et al.* Association of microglia with amyloid plaques in brains of APP23 transgenic mice. *Am. J. Pathol.* **154**, 1673–1684 (1999).
68. López-Picón, F. R. *et al.* Neuroinflammation appears early on PET imaging and then plateaus in a mouse model of Alzheimer disease. *J. Nucl. Med.* **59**, 509–515 (2018).
69. Vegeto, E. *et al.* The endogenous estrogen status regulates microglia reactivity in animal models of neuroinflammation. *Endocrinology* **147**, 2263–2272 (2006).
70. Beilharz, J. E., Maniam, J. & Morris, M. J. Short-term exposure to a diet high in fat and sugar, or liquid sugar, selectively impairs hippocampal-dependent memory, with differential impacts on inflammation. *Behav. Brain Res.* **306**, 1–7 (2016).
71. Teixeira, D. *et al.* The metabolic and neuroinflammatory changes induced by consuming a cafeteria diet are age-dependent. *Nutr. Neurosci.* **22**, 284–294 (2019).
72. Dejager, L., Vandevyver, S., Petta, I. & Libert, C. Dominance of the strongest: inflammatory cytokines versus glucocorticoids. *Cytokine Growth Factor Rev.* **25**, 21–33 (2014).
73. Cerovic, M., Forloni, G. & Balducci, C. Neuroinflammation and the gut microbiota: possible alternative therapeutic targets to counteract Alzheimer's disease?. *Front. Aging Neurosci.* **11**, 1–9 (2019).
74. Lim, G. P. *et al.* A diet enriched with the omega-3 fatty acid docosahexaenoic acid reduces amyloid burden in an aged Alzheimer mouse model. *J. Neurosci.* **25**, 3032–3040 (2005).
75. Amtul, Z., Uhrig, M., Rozmahel, R. F. & Beyreuther, K. Structural insight into the differential effects of omega-3 and omega-6 fatty acids on the production of Aβ peptides and amyloid plaques. *J. Biol. Chem.* **286**, 6100–6107 (2011).
76. Vloeberghs, E. *et al.* Altered ingestive behavior, weight changes, and intact olfactory sense in an APP overexpression model. *Behav. Neurosci.* **122**, 491–497 (2008).
77. Lalonde, R., Dumont, M., Staufenbiel, M. & Strazielle, C. Neurobehavioral characterization of APP23 transgenic mice with the SHIRPA primary screen. *Behav. Brain Res.* **157**, 91–98 (2005).
78. Poehlman, E. T. & Dvorak, R. V. Energy expenditure, energy intake, and weight loss in Alzheimer disease. *Am. J. Clin. Nutr.* **71**, 650–655 (2000).
79. Vuksan, V. *et al.* Salba-chia (*Salvia hispanica* L.) in the treatment of overweight and obese patients with type 2 diabetes: a double-blind randomized controlled trial. *Nutr. Metab. Cardiovasc. Dis.* **27**, 138–146 (2017).

Acknowledgements

We thank Jessica Albrecht and Alexander Haake for excellent technical support.

Author contributions

S.S. contributed to the design of the study, conducted data acquisition, analysis, and interpretation and wrote the manuscript. C.K. contributed to the design of the study, to the acquisition of body weight and glucose tolerance data and revised the manuscript. A.P. and J.R. contributed to the acquisition of glucose tolerance and behavioral data and revised the manuscript. L.S., K.K., B.A. and A.E.C.P. contributed to the performance of histological analyses, to analyses of plasma samples, and to data processing. A.R. supported the design of behavioral experiments and provided behavioral test equipment. S.K. generated the Matlab code used for the analysis of Morris Water Maze data and performed the analysis. S.H. contributed to the design of the study and to the writing process by intensely revising the manuscript. B.S. contributed to the design of the study and revised the manuscript. All authors read and approved the final manuscript.

Funding

Open Access funding enabled and organized by Projekt DEAL. First author S. Schreyer was funded by the Elsa-Neumann-Scholarship of the state Berlin and by the graduation scholarship of Charité Universitätsmedizin Berlin.

Competing interests
The authors declare no competing interests.

Additional information
Supplementary information is available for this paper at https://doi.org/10.1038/s41598-020-75209-z.

Correspondence and requests for materials should be addressed to S.S.

Reprints and permissions information is available at www.nature.com/reprints.

Publisher's note Springer Nature remains neutral with regard to jurisdictional claims in published maps and institutional affiliations.

Version of Record – Study III

Publikation III meiner Arbeit wird hier nicht veröffentlicht, da keine Genehmigung des Verlags vorliegt. Die Publikation kann unter folgender URL eingesehen werden:

https://doi.org/10.1016/j.bbr.2018.03.030

Curriculum vitae

Mein Lebenslauf wird aus datenschutzrechtlichen Gründen in der elektronischen Version meiner Arbeit nicht veröffentlicht.

List of publications

Original Research Articles

Schreyer, S., Berndt, N., Eckstein, J., Mülleder, M., Hemmati-Sadeghi, S., Klein, C., Abuelnor, B., Panzel, A., Meierhofer, D., Spranger, J., Steiner, B. & Brachs, S. (2021) Dietary-challenged mice with Alzheimer-like pathology show increased energy expenditure and reduced adipocyte hypertrophy and steatosis. *Aging* 13, Epub ahead of print.
Impact Factor 4.831 (2020 Journal Citation Report)

Schreyer, S., Klein, C., Pfeffer, A., Rasińska, J., Stahn, L., Knuth, K., Abuelnor, B., Panzel, A. E. C., Rex, A., Koch, S., Hemmati-Sadeghi, S. & Steiner, B. (2020) Chia seeds as a potential cognitive booster in the APP23 Alzheimer's disease model. *Scientific Reports* 10, 18215.
Impact Factor 3.998 (2020 Journal Citation Report)

Bertalan, G., Klein, C., **Schreyer, S.**, Steiner, B., Steiner, B., Kreft, B., Tzschätzsch, H., de Schellenberger AA., Nieminen-Kelhä, M., Braun, J., Guo, J., & Sack, I. (2019). Biomechanical properties of the hypoxic and dying brain quantified by magnetic resonance elastography. *Acta Biomateriala*, 101, 395-402.
Impact Factor 7.242 (2019 Journal Citation Report)

Guo, J., Bertalan, G., Meierhofer, D., Klein, C., **Schreyer, S.**, Steiner, B., Wang, S., da Silva, RV., Infante-Duarte, C., Koch, S., Boehm-Sturm, P. & Sack, I. (2019). Brain maturation is associated with increasing tissue stiffness and decreasing tissue fluidity. *Acta biomaterialia*, 99, 433-442.
Impact Factor 7.242 (2019 Journal Citation Report)

Bertalan, G., Guo, J., Böhm-Sturm, P., **Schreyer, S.**, Steiner, B., Tzschätzsch, H., Braun, J., & Sack, I. (2019). The influence of body temperature on tissue stiffness, blood perfusion, and water diffusion in the mouse brain. *Acta Biomaterialia*, 96, 412-420.
Impact Factor 7.242 (2019 Journal Citation Report)

Klein, C., Jonas, W., Wiedmer, P., **Schreyer, S.**, Akyüz, L., Spranger, J., Hellweg, R. & Steiner, B. (2019). High-fat Diet and Physical Exercise Differentially Modulate Adult Neurogenesis in the Mouse Hypothalamus. *Neuroscience*, *400*, 146-156.
Impact Factor 3.056 (2019 Journal Citation Report)

Pfeffer, A., Munder, T., **Schreyer, S.**, Klein, C., Rasińska, J., Winter, Y., & Steiner, B. (2018). Behavioral and psychological symptoms of dementia (BPSD) and impaired cognition reflect unsuccessful neuronal compensation in the pre-plaque stage and serve as early markers for Alzheimer's disease in the APP23 mouse model. *Behavioural brain research*, *347*, 300-313.
Impact Factor 2.770 (2018 Journal Citation Report)

Michels, B., Zwaka, H., Bartels, R., Lushchak, O., Franke, K., Endres, T., Fendt, M., Song, I., Bakr, M., Budragchaa, T., Westermann, B., Mishra, D., Eschbach, C., **Schreyer, S.**, Lingnau, A., Vahl, C., Hilker, M., Menzel, R., Kähne, T., Leßmann, V., Dityatev, A., Wessjohann, L. & Gerber, B. (2018). Memory enhancement by ferulic acid ester across species. *Science advances* 4(10), eaat6994.
Impact Factor 12.804 (2018 Journal Citation Report)

Munder, T., Pfeffer, A., **Schreyer, S.**, Guo, J., Braun, J., Sack, I., Steiner, B. & Klein, C. (2018). MR elastography detection of early viscoelastic response of the murine hippocampus to amyloid β accumulation and neuronal cell loss due to Alzheimer's disease. *Journal of Magnetic Resonance Imaging*, *47*(1), 105-114.
Impact Factor 3.732 (2018 Journal Citation Report)

Klein, C., **Schreyer, S.**, Kohrs, F. E., Elhamoury, P., Pfeffer, A., Munder, T., & Steiner, B. (2017). Stimulation of adult hippocampal neurogenesis by physical exercise and enriched environment is disturbed in a CADASIL mouse model. *Scientific reports*, *7*, 45372.
Impact Factor 4.122 (2018 Journal Citation Report)

Conference Contributions (Poster Presentation)

Schreyer, S., Klein, C., Rasinska, J., Pfeffer, A., Abuelnor, B., Knuth, K., Rex, A., & Steiner, B. Chia seeds as a possible cognitive booster in Alzheimer's disease.
14th International Conference on Alzheimer's & Parkinson's Diseases, Lisbon, March 2019

Schreyer, S., Klein, C., Rasinska, J., Pfeffer, A., Abuelnor, B., Knuth, K., Rex, A., & Steiner, B. Chia seeds as a possible cognitive booster in Alzheimer's disease.
11th FENS Forum of Neuroscience, Berlin, July 2018

Acknowledgements

I want to thank all the great people supporting me during my demanding but also inspiring time as a PhD student. A tiny piece of this thesis belongs to each of you, as I could have never mastered this challenge all alone.

First things first, I want to thank my supervisor Prof. Dr. Barbara Steiner for the possibility of conducting this thesis in her lab, for providing her support and for sharing her scientific knowledge with me. Moreover, I want to thank Dr. Sebastian Brachs for an exceptional fruitful cooperation, for his great effort and support, for his expertise, and for his faith in my work. Finally, my gratitude goes to the committee of the Elsa-Neumann-Scholarship of the county Berlin and to the Academic Grants' Committee of Charité – Universitätsmedizin Berlin for granting me financial support of my PhD project.

There are no words for appropriately expressing my gratitude towards my dearest lab colleagues – and by now valuable friends – Charlotte Klein, Justyna Rasińska, Laura Stahn, Jessica Albrecht, Aileen Hakus, Shabnam Hemmati-Sadeghi, Anna Pfeffer, Tonia Munder, Friederike Kohrs, Elisabeth Hain, Karlotta Knuth, Basim Abuelnor, and Alina Panzel. Your endless support, your optimism in times of doubt and frustration, the constant provision of great food and alcoholic beverages and the millions of hours, we spent together – working, laughing, crying, drinking – made my time in the lab a time to remember. I miss you every day!

I want to shout out a big and loud “thank you” to all my friends, especially to Jenny, Anne, Julia, Julia, Jessi, Ladina, and Ilana, who always lent an ear at any time, who were always there in good but especially in hard times, who encouraged me by hating the same things and the same people as me – without even knowing them – and who gave me a kick in the pants during motivational crises. Thank you for guarding my back!

I owe my biggest gratitude to my boyfriend Alexander Haake. Not the title but you are the first prize of this thesis – we wouldn’t have met without it. I can never count all the situations, in which both your personal and your scientific advice helped me finding a solution to so many problems. Thank you for distracting me, when I urgently needed a break and thank you for pushing me, when I was frustrated or unmotivated. Your faith in me gave me the strength to finish this challenge. You truly earned your golden name plate with the engraved “Dr.”!

Finally, I want thank my loving and supporting parents Anne and Axel, my dearest “big little” brother Sebastian with his girlfriend Pauline and the most adorable, caring and interested grandparents Eka and Klaus and Eva and Roland for always believing in me and for supporting me in so many ways. The will to make you proud was a major part of my motivation! I love you!

Although the time as a PhD student was one of the most challenging, demanding and sometimes frustrating times of my life so far, I don’t want to miss a second of it. It helped me growing and becoming a different – much stronger, much tougher, much braver, maybe even a tiny little bit wiser – person.

And last but not least: Thank you, my dear little mice, for sacrificing your bodies to the scientific progress.